BK CHANNEL, 5-HT AND SEX IN GASTROINTESTINAL MOTILITY IN HEALTH AND OBESITY

By

Marion France

A DISSERTATION

Submitted to

Michigan State University
in partial fulfillment of the requirements
for the degree of

Neuroscience – Doctor of Philosophy

2015

ABSTRACT

BK CHANNEL, 5-HT AND SEX IN GASTROINTESTINAL MOTILITY
IN HEALTH AND OBESITY

By

Marion France

Highly regulated motor reflexes observed in gastrointestinal (GI) motility promote nutrient digestion and absorption as well as excretion of indigestible material. Motor reflexes are fundamentally regulated by the enteric nervous system (ENS), and can be modulated by 1) smooth muscle tone changes by the activation of large conductance Ca^{2+}-activated K^+ (BK) channels and by 2) intrinsic neuron activation by 5-hydroxytryptamine (5-HT, serotonin). Impairments in the modulation of motor reflexes cause GI motility disorders. Although GI motility disorders are typically not life threatening, the quality of life of affected individuals can be poor. GI motility disorders are common in obesity that affects millions of people in the United States. GI motility dysfunction in obesity may be caused by perturbations in intestinal 5-HT dynamics. 5-HT located in enterochromaffin (EC) cells of the GI mucosa influences GI motility by coordinating the nerve circuits in the ENS. I investigated 1) the role BK channels in normal GI transit in mice and 2) 5-HT signaling in controlling GI transit in male and female mice fed a high fat diet (HFD) to produce diet-induced obesity (DIO). I used complimentary *in vivo* and *in vitro* methods to identify sex differences in small intestinal transit and 5-HT dynamics in obese mice. Overall, I found 1) BK channels are necessary for normal propulsive colonic transit and 2) sex and obesity-related alterations in small intestinal transit and 5-HT signaling. These sex differences in DIO must be considered when designing therapeutic approaches targeting intestinal 5-HT to treat impaired motility in obesity.

ACKNOWLEDGMENTS

For this work, I would first like to thank my advisors, Dr. Greg Swain and Dr. James Galligan. Drs. Swain and Galligan are respected experts in their fields and their valuable advice was indispensable to my dissertation research. Throughout my candidacy, they have taught me to become an independent scientist and I will forever value their guidance in the beginning stages of my career.

I would like to thank Dr. Mark Kadrofske for being a member of my committee. He has also offered much guidance and support through my candidacy. I would like to thank him for his valuable input in interpreting my results, and for helping me put together figures and presentations for my interviews. I would like to thank Dr. Stephen Schneider and Dr. Cheryl Sisk for being members of my committee as well. Dr. Schneider has helped me through my early candidacy and provided valuable input during lab meetings and my proposal oral exam. Dr. Sisk has helped me through my late candidacy by providing valuable advice on sex differences during committee meetings and during office meetings. I thank her for joining my committee so late in my candidacy and being so available for me to meet with her.

I also would like to thank those that helped me to run experiments. I thank Robert Burnett who performed all the HPLC measurements, Amy S. Porter, HT (ASCP) QIHC and Kathleen A. Joseph, HT (ASCP) QIHC at Michigan State University Investigative Histopathology Laboratory for performing the IHC experiments, and Laura Osaer for counting EC cells. I would also like to thank Cathy Tyler L.A.T. for helping me maintain the TPH1 KO colony and for ear punching. I would like to thank Christi Hemming of the MSU Research Technology Support Facility for genotyping. Lastly, I would like to thank Dr. Hui Xu, Dr. Xiaochun Bian and Beth Lockwood for their valuable training and data interpretation.

TABLE OF CONTENTS

LIST OF TABLES

LIST OF FIGURES

KEY TO ABBREVIATIONS

ACh	Acetylcholine
ATP	Adenosine triphosphate
BDD	Boron-doped diamond electrode
BK channel	Large conductance Ca^{2+} activated K^+ channel
BSA	Bovine serum albumin
CA	Continuous amperometry
CD	Control diet
CFM	Carbon fiber microelectrode
CMMCs	Colonic migration motor complexes
CNS	Central nervous system
CV	Cyclic voltammetry
DA	Dopamine
DAT	Dopamine transporter
DIO	Diet-induced obesity
DOPAC	3,4-Dihydroxyphenylacetic acid
DSS	Dextran sulfate sodium
E2	17β-estradiol
EC	Enterochromaffin
EC_{50}	Half maximal effective concentration
ELISA	Enzyme linked immunosorbent assay
E_p^{ox}	Peak oxidation potential
ENS	Enteric nervous system
FITC	Fluorescein isothiocyanate

FSCV	Fast scan cyclic voltammetry
GAPDH	Glyceraldehyde-3-phosphate dehydrogenase
GC	Geometric center
GI	Gastrointestinal
GSH	Glutathione
5-HIAA	5-Hydroxyindole acetic acid
HF	High fat
HFD	High fat diet
5-HT	5-Hydroxytryptamine
5-HTP	5-Hydroxytryptophan
IBD	Inflammatory bowel disorder
IBS	Irritable Bowel Syndrome
ICC	Interstitial cell of Cajal
IL	Interleukin
INFɣ	Interferon ɣ
IPANS	Intrinsic primary afferent neurons
i_p^{ox}	Peak current
KO	Knockout
L-AADC	L-amino acid decarboxylase
LDH	Lactate dehydrogenase
LMMP	Longitudinal muscle-myenteric plexus
MAO_A	Monoamine oxidase A
MMC	Migrating motor complex
MPO	Myeloperoxidase
NE	Norepinephrine
NET	Norepinephrine transporter

NO	Nitric oxide
PVDF	Polyvinylidene difluoride membrane
RyRs	Ryanodine receptors
SERT	Serotonin transporter
SP	Submucosal plexus
SR	Sarcoplasmic reticulum
SSRI	Serotonin selective reuptake inhibitor
STOC	Spontaneous transient outward K^+ current
TNFα	Tumor necrosis factor α
TPH1	Tryptophan hydroxylase 1
TPH2	Tryptophan hydroxylase 2
UC	Ulcerative colitis
VIP	Vasoactive intestinal peptide
VMAT-1	Vesicular monoamine transporter 1
WT	Wild-type

CHAPTER 1

GENERAL INTRODUCTION

1.1 The Enteric Nervous System (ENS)

The division of the autonomic nervous system that contains 200-600 million neurons in the gut wall is called the enteric nervous system (ENS).[1] The remaining divisions of the autonomic nervous system are the sympathetic and parasympathetic divisions. The ENS functions autonomously and enteric neurons are grouped in two main neuronal networks: the myenteric plexus and the submucosal plexus (Figure 1). The myenteric plexus found between the longitudinal and circular muscle layers coordinates complex motor reflexes. The submucosal plexus is found between the circular muscle layer and the muscularis mucosa and controls secretomotor and vasodilator reflexes. The circuitry of the ENS contains excitatory and inhibitory motoneurons, interneurons and intrinsic primary afferent neurons (IPANS).[2] Cell bodies of IPANS are found in both plexuses and send projections into the mucosa within the lamina propria extending to the villus tip.[3] Hence, any luminal nutrient or microbiota cross talk with the ENS involves enteroendocrine cells of the epithelial layer strategically located at the interface of the gut lumen and nerve terminals of IPANs.

1.2 Reflexes of the ENS

The most well characterized reflex of the ENS is the peristaltic reflex. The peristaltic reflex is a propulsive pattern that moves luminal content along the length of the intestine. This reflex involves coordination of a muscle contraction occurring proximal to a luminal stimulus and a muscle relaxation occurring distal to the same stimulus. The reflex pathway involves a chemical or mechanical stimulation of the mucosa that activates the mucosal terminals of IPANS that then activate interneurons located in the myenteric plexus.[4, 5] This reflex is also evoked by distension.[6] Ascending and descending interneurons communicate to excitatory and inhibitory motoneurons, respectively.[7] The main neurotransmitter in interneuron communication with motoneurons is acetylcholine (ACh). ACh acts at neuronal nicotinic receptors on excitatory and inhibitory motoneurons to elicit activation. Activation of excitatory motoneurons releases

ACh into both surrounding muscle layers. ACh acts at smooth muscle muscarinic receptors leading to increased intracellular calcium and thus smooth muscle contraction. Activation of inhibitory motoneurons releases nitric oxide (NO), vasoactive intestinal peptide (VIP) and ATP into the surrounding muscle layers resulting in smooth muscle relaxation. Activation of excitatory and inhibitory motoneurons generates smooth muscle contraction and relaxation, respectively. The coordination of smooth muscle contraction and relaxation produces a luminal pressure gradient that propels luminal content along the length of the intestine in an aboral direction. This concept is illustrated in Figure 2.

The peristaltic reflex occurs during a fed state and during phase II of the migrating motor complex (MMC).[1] Both peristalsis and MMC are classified as motility patterns. The MMC can occur during both the fed and fasted state. During the fasted state (i.e. interdigestive), the MMC cleans the intestine by rapidly moving any undigested material aborally by the action of cyclic muscle contractions. The MMC is characterized by three phases. Phase I, phase II and phase III are described by a quiescent period, a period of irregular contractions and a period of intense contraction burst-like activity, respectively, where phase III is the main propulsive force in moving material aborally.[8] In freely-moving conscious mice, phase III contractions occur every 12-15 min in the stomach[9] similar to that observed in the stomach and duodenum of freely-moving conscious rats.[10]

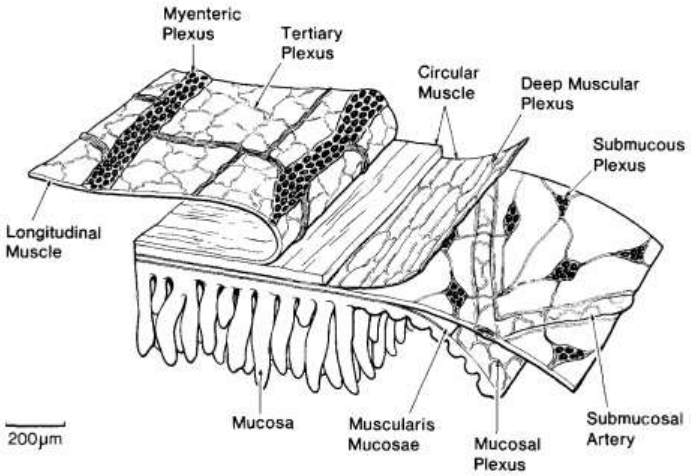

Figure 1. Layers of the intestine. Relevant layers of the intestine include the mucosa, myenteric and submucosal plexuses, and the longitudinal and circular muscle layers. Reprinted from Cell Tissue Research, 188, Furness, J.B. and Costa, M., "Distribution of intrinsic nerve cell bodies and axons which take up aromatic amines and their precursors in the small intestine of the guinea pig," 527-54, Copyright (1978), with permission from Springer.

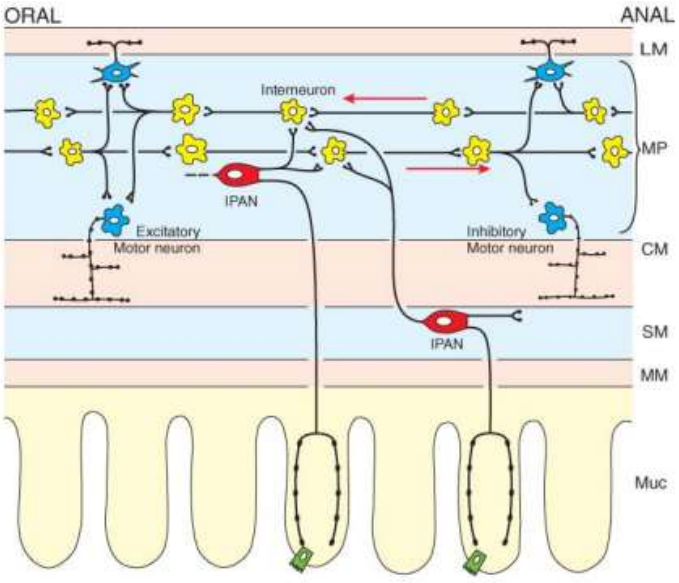

Figure 2. Illustration of ENS. Relevant ENS circuitry contains intrinsic primary afferent neurons (IPANS) with cell bodies contained in the myenteric plexus (MP), interneurons and excitatory and inhibitory motor neurons. Reprinted from Enteric Nervous System Ch.3, Furness, J.B., "Reflex Circuitry of the Enteric Nervous System," pg. 84, Copyright (2007), with permission from John Wiley and Sons.

1.3 BK channels in GI smooth muscle tone

Smooth muscle tone is essential for the intestinal motility patterns and involves multiple regulatory mechanisms. These regulatory mechanisms govern smooth muscle contraction generation and relaxation. For example, activation of muscarinic receptors (e.g., M1 and M3) by the ligand ACh mediates intracellular calcium concentration increases by a Gq-dependent phospholipase C (PLC), inositol trisphosphate (IP_3) pathway. The increase in intracellular calcium elicits smooth muscle cell contraction. On the other hand, other mechanisms govern smooth muscle relaxation. For example, large-conductance Ca^{2+}-activated K^+ (BK) channels expressed in smooth muscle cells[11] generates K^+ efflux from the cell and subsequent smooth muscle relaxation. The pore of BK channels is formed from 4 α-subunits. The α-subunit regulates two mechanisms of BK channel activation 1) mechanisms involving both activation by a change in membrane voltage and intracellular Ca^{2+} and 2) mechanisms involving only membrane voltage changes.[12] Accessory β-subunits found encircling the α-subunits modulate Ca^{2+} sensitivity of the α-subunit. The β1-subunit is smooth muscle specific[13, 14] and contributes to regulation of smooth muscle tone in the intestine.[15]

Ca^{2+}-dependent activation of BK channels involves Ca^{2+} influx through L-type Ca^{2+} channels.[16] In smooth muscle cells, intracellular Ca^{2+} activates ryanodine receptors (RyRs) on the sarcoplasmic reticulum (SR). Activation of RyRs causes Ca^{2+} release from the SER as Ca^{2+} sparks.[11, 17] This increase in intracellular Ca^{2+} activates BK channels and evokes K^+ efflux carried by the BK channel known as spontaneous transient outward K^+ currents (STOCs). STOCs result in membrane hyperpolarization and subsequent closure of L-type Ca^{2+} channels leading to smooth muscle relaxation.[11, 17] BK channels regulate smooth muscle tone in the intestine by the coupling of Ca^{2+} sparks and STOCs. This concept is illustrated in Figure 3.

When the BK channel is dysfunctional, impairments in channel opening and the coupling of Ca^{2+} sparks to STOCs occur. For example, in β1-subunit knockout (KO) mice, a reduction in the open probability of the BK channel occurred in myocytes from the urinary bladder,[18]

arterials[19] and the trachea.[20] A reduction in coupling of Ca^{2+} sparks to STOCs was observed in arterial and colonic myocytes.[15, 19] In colonic smooth muscle cells an uncoupling between Ca^{2+} sparks and STOCs was demonstrated.[20] The functional consequences of BK channel dysfunction have not been studied.

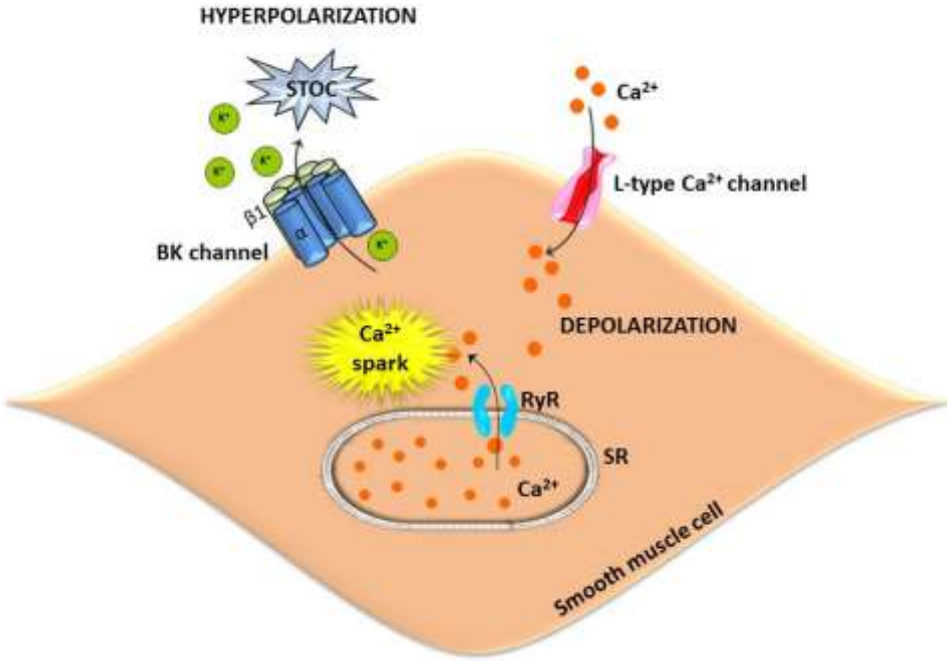

Figure 3. BK channel function in the smooth muscle cell. Smooth muscle tone is regulated by Ca^{2+} influx through L-type Ca^{2+} channels that initiates Ca^{2+} flux from the sarcoplasmic reticulum (SR) as a Ca^{2+} spark. BK channel activation is dependent on membrane depolarization caused by Ca^{2+} influx and β1 sensing of Ca^{2+} sparks. BK channel activation results in K^+ efflux as spontaneous transient outward K^+ currents (STOCs) that cause hyperpolarization and results in smooth muscle cell relaxation.

1.4 Vagovagal reflex controls gastric emptying

Whereas motor reflexes of the intestine are under control of the ENS, motor control of the stomach is extensively regulated by extrinsic inputs of the CNS.[21] Most of the motor control of the stomach is controlled by the parasympathetic system by the vagovagal reflex (Figure 4). Sensory information from the intestine arrives directly to the brainstem at the level of the nucleus of the tractus solitaries (NTS) by way of the afferent vagus nerve whose cell bodies are

contained in the nodose ganglion.[22] In the NTS, GABAergic second order neurons receive information from glutamatergic vagal afferent fibers and send projections to the adjacent dorsal motor nucleus of the vagus (DMV).[23] These second order neurons transmit information to the parasympathetic pre-ganglionic neurons located in the DMV that then provide vagal motor control to the stomach. In the stomach, the cholinergic pre-ganglionic parasympathetic neurons synapse with post-ganglionic neurons. Post-ganglionic neurons can be cholinergic or non-adrenergic, non-cholinergic (NANC). Excitatory cholinergic post-ganglionic neurons promote increased gastric tone, motility and secretion by activation of muscarinic receptors. Inhibitory NANC post-ganglionic neurons inhibit gastric functions by the actions of NO or VIP.

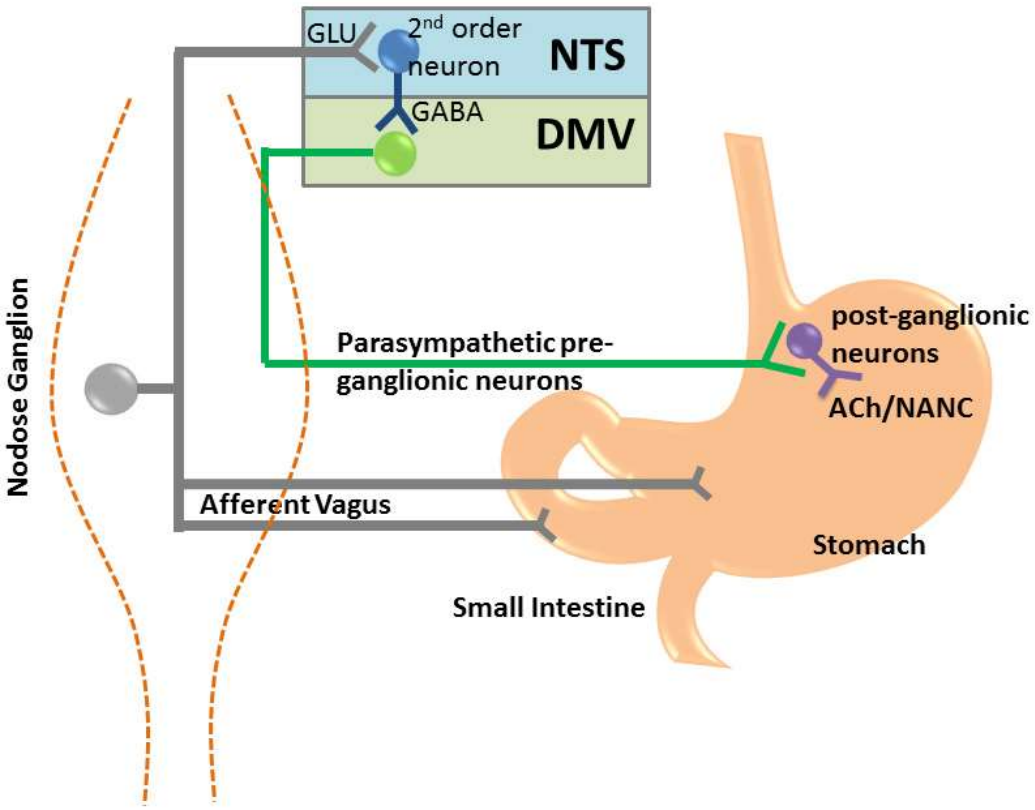

Figure 4. Vagovagal reflex control of gastric emptying. Vagal afferents transmit sensory input from the intestine to the nucleus of the tractus solitaries (NTS). NTS neurons send projections to the dorsal motor nucleus of the vagus (DMV) and DMV parasympathetic pre-ganglionic neurons innervate post-ganglionic neurons in the stomach. Excitatory cholinergic (ACh) outputs increase gastric functions and inhibitory non-adrenergic, non-cholinergic (NANC) outputs inhibit gastric functions.

1.5 Obesity associated GI dysfunction

1.5.1 GI dysfunction in obese humans

Obesity, as defined by a body mass index (BMI) ≥ 30, is highly prevalent in the United States as 35% of adults were obese in 2011-2012.[24] Obesity development is multi-factorial. The idea that obesity was solely a result of poor life choices is changing. The National Institutes of Health attribute obesity to genetic, environmental (e.g. diet), cultural and socioeconomic causes. In addition to the life threatening consequences of obesity, there are non-life threatening consequences that decrease the quality of life. For example, impaired GI motility in obesity causes diarrhea, constipation, irritable bowel syndrome (IBS) and fecal incontinence.[25] In addition, BMI has been linked to diarrhea.[26-29] Alterations in GI motility are observed in gastric emptying, small and large intestinal transit. However, studies demonstrating that motility is altered in obese humans are limited and inconsistent. For example, gastric emptying has been shown to be increased[30] or delayed in obesity.[31] Small intestinal motility in obese humans was increased compared to lean controls after delivery of a radiolabeled liquid test meal.[32] However, in other studies orocecal (i.e. mouth to cecum) transit was delayed[33] or not altered[34] in obese compared to normal weight humans. These inconsistencies are largely caused by differences in methods used to measure motility and measuring small intestinal motility independently of gastric emptying is difficult in human subjects.

1.5.2 Rodent models of obesity

1.5.2.1 Genetic models

Genetic rodent models are used to study the molecular mechanisms of obesity. Genetic rodent models develop obesity and insulin resistance that is driven by monogenetic spontaneous mutations in leptin (*ob/ob)* or the leptin receptor (*db/db*) in mice[35] and mutations in *db/db* in the Zucker-fatty rat.[36] However, genetic rodent models do not fully mimic development of obesity in humans. For example, neither mutation is typically found in humans.[37] In addition,

genetically-derived mouse models develop retinal degeneration and deafness, which are not common symptoms of obesity in humans.[37] A comprehensive review of monogenetic obesity models have been described elsewhere.[38]

1.5.2.2 Diet-induced obesity (DIO) models

Diet-induced obesity (DIO) rodent models better recapitulate obesity development and its consequences in humans. Obesity development in this model involves environmental (e.g. high-fat diet) and polygenetic causes; however the specific genes important in obesity development are unknown. Rats and mice that are genetically predisposed to gain weight on a high fat diet (HFD) are commonly used. Sprague Dawley rats are unique to study DIO because when rats are placed on a high energy diet, some rats develop obesity (DIO-prone) while some rats do not (DIO-resistant).[39] Similar to DIO-prone rats, the C57BL/6J mouse strain effectively gains weight and exhibits hyperphagia after a few weeks fed a HFD.[40-42] However, not all mouse strains develop an obese phenotype (e.g. PWD, WSB)[43] and some sub-strains are more sensitive to DIO (e.g. C57BL/6J vs. C57BL/6NJ).[44]

1.5.2.3 Diet-induced obesity (DIO) diets

In addition to the many types of DIO rodent models, there are many types of obesity generating diets. These diets include Western diets (e.g. cafeteria style), HFD and high sucrose diets. For the Western diets, it is commonplace to add palatable high energy foods (e.g. meat pies, cakes, potatoes) to the normal chow diet.[45] In doing so, other nutrients can become diluted meaning that those rodents fed the Western diet will ingest less protein, vitamins, minerals and fiber than control-fed rodents.[46] It is possible to induce protein deficiencies in the Western diet fed group as well. In addition, rodents have a choice in what they consume (e.g. chow vs. high energy foods) such that the caloric composition of the Western diet ingested cannot be reproduced. The chow diets commonly used are grain/cereal based and so the

composition of the chow diet will change between harvest location and season. Therefore, in a single study, Western and chow diet compositions vary and cannot be adequately replicated. In contrast, control diet (CD) and high fat diets (HFD) using purified ingredients have been manufactured so that the diets are isocaloric. To create the HFD, the amount of calories from the carbohydrate, but not protein, source is reduced to provide for the larger caloric amount from the addition of fat. Using these diets achieves similar caloric intake in each diet group because rodents eat for calories and not for weight of food. This means either rodent on the CD or HFD will be consuming the same amount of protein, vitamins, minerals and fiber. Both differences in the DIO model (e.g. causation and/or strain) and the control/HF diets may be reasons for differences in DIO studies.

1.5.3 Impaired GI function in DIO rodent models

Similar to humans, transit studies in DIO rodent models are limited and inconsistent. As described above, these inconsistencies are likely attributed to species and diet differences. In *ob/ob* mice, gastric emptying was increased, but small intestinal transit was reduced.[47] In DIO rodent models, studies demonstrated that gastric emptying was reduced[48, 49] or increased.[50] Both studies showed no changes in transit. In our studies, we use C57BL/6J mice that are more sensitive to obesity development to understand if gastric emptying and small intestinal transit are altered in both males and females.

1.6 Obesity and intestinal inflammation

Obesity is characterized by a chronic low-grade inflammatory state that it is not associated with infection, autoimmunity or extensive tissue injury.[51] Inflammation in obesity occurs mainly in visceral fat where adipocyte hyperplasia and hypertrophy results in increased proinflammatory cytokine release. Circulating levels of proinflammatory cytokines such as TNFα, IL-1β and IL-6 are elevated in obesity.[52] Visceral fat tangled within the organs in the

abdominal cavity is responsible for cardiovascular and metabolic diseases associated with obesity.[53-55] Inflammation also occurs in the intestine in humans.[56] Similarly, HFD-fed DIO-prone rats exhibited greater myeloperoxidase (MPO) activity in ileal mucosa compared to both CD-fed and HFD-fed DIO-resistant rats, suggesting that changes in MPO activity were obesity-dependent and diet-independent.[57] MPO is a peroxidase enzyme in neutrophils that uses hydrogen peroxide as a main substrate to produce hypochlorous acid (HOCl). MPO oxidation activity is involved in inflammatory pathophysiology and so MPO activity is often used as a marker for inflammation.[58] Likewise, HFD-fed mice exhibited elevated ileal TNFα mRNA levels that positively correlated with both body weight and percent fat.[59] The presence of intestinal inflammation in DIO is likely driven by many factors. For example, the combination of elevated circulating cytokines released from visceral fat, increased intestinal permeability and changes in the gut bacterial (microbiota) composition are involved in intestinal inflammation in DIO. As such, increased intestinal permeability concurrent with decreased tight junction protein expression was observed in DIO mice.[60] In addition, a shift in the microbiota from toward more pathogenic strains increased intestinal permeability and inflammation in HFD-fed rodents[57, 61] and these bacterial-host interactions were necessary for the observed intestinal inflammation.[59] In summary, intestinal inflammation persists in DIO in humans and rodent models.

1.7 Intestinal 5-hydroxytryptamine (5-HT, serotonin)

1.7.1 Role of 5-HT in GI motility

In the epithelial layer of the mucosa, 5-HT is synthesized, stored and released from enterochromaffin (EC) cells. EC cells represent 1-3% of the epithelial cell population[62] and store 90% of the total body 5-HT.[63] Inside the EC cell, the essential amino acid tryptophan is hydroxylated by the rate-limiting and EC cell specific enzyme tryptophan hydroxylase 1 (TPH1)[64] to the precursor 5-hydroxytryptophan (5-HTP). 5-HTP is then decarboxylated by L-amino acid decarboxylase generating 5-HT. 5-HT is then transported into secretory granules by

the vesicular transporter VMAT1. These secretory granules are located both at the basolateral and apical side of the EC cell.[65] 5-HT is released from the EC cell into the lumen or lamina propria following EC cell activation by chemical[66] [67] or mechanical stimuli.[68] 5-HT release is dependent on L-type calcium channels.[67] The importance of 5-HT release into the lumen is unknown; however, the neurotransmitters norepinephrine (NE), epinephrine (EPI) and an indole are chemoattractants for gut bacteria.[69] When 5-HT is released from the EC cell into the lamina propria it acts in a paracrine manner by activating ionotropic 5-HT_3 receptors localized on nerve terminals of IPANS whose cell bodies are located in the myenteric plexus.[70] Activation of IPANS stimulates ascending and descending interneurons that then activate excitatory and inhibitory motoneurons, respectively, causing coordinated smooth muscle contraction and relaxation.[3] The local concentration of 5-HT at its receptor is termed 5-HT availability. 5-HT availability is predominately regulated by the enterocyte serotonin transporter (SERT) localized near adjoining EC cells.[71] Once 5-HT is cleared from the extracellular space, 5-HT is metabolized by enterocyte monoamine oxidase A (MAO_A) to 5-hydroxyindolacetic acid (5-HIAA). This concept is illustrated in Figure 5.

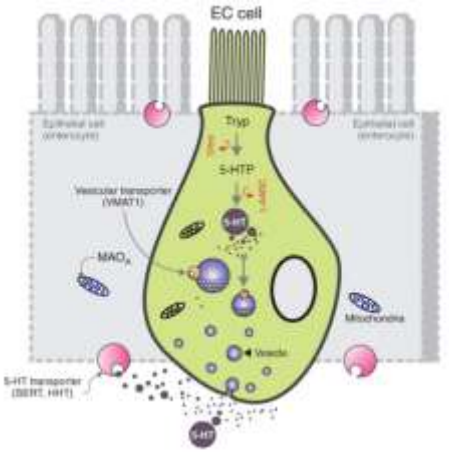

Figure 5. Synthesis, storage and release of 5-HT from EC cells in intestinal epithelial layer. Reprinted from Autonomic Neuroscience: Basic and Clinical, 153, Bertrand, P. and Bertrand, R., Serotonin release and uptake in the gastrointestinal tract, pg. 49, Copyright (2010), with permission from Elsevier

The hypothesis that the peristaltic reflex was initiated by 5-HT released from EC cells in response to pressure was described first by Bülbring and colleagues in the 1950's. Bülbring demonstrated that the rate of peristalsis could be increased by intraluminally applied 5-HT and that 5-HT also was released during stimulated peristalsis in *in vitro* preparations.[72] Similarly, release of 5-HT was increased during *in vivo* stimulated peristalsis.[73] In support of Bülbring's hypothesis, Heredia and colleagues demonstrated that MMCs were absent in tissues where the mucosal layer containing 5-HT was dissected away.[74] Moreover, drugs that target 5-HT_3 receptors (e.g. alosetron and ondansetron) decrease intestinal transit. For example, alosetron reduces transit in irritable bowel syndrome patients.[75] In rodents, alosetron treatment (0.5 mg kg^{-1}) reduced the length of the MMC cycle in conscious rats[76] and decreased the frequency of the MMC in the murine ileum tissues.[77] Likewise, ondansetron abolished MMCs in murine colon tissues.[74]

Not long after Heredia and colleagues' study, Keating and Spencer published results demonstrating that 5-HT was not essential in MMCs.[78] This controversy was driven by differences in dissection technique.[79] Evidence in support of a non-essential role came from Li and colleagues that used a genetic model that lacked the enzyme necessary for EC cell 5-HT production (TPH1).[80] Li et al. demonstrated total transit time, assessed by the first observance of carmine red dye in fecal pellets, gastric emptying and the GC were similar in TPH1 KO and WT littermates. The authors describe neuronal 5-HT as essential for constitutive motility, not mucosal 5-HT. Neal et al. provided evidence that the rate-limiting enzyme for 5-HT synthesis within neurons (tryptophan hydroxylase 2, TPH 2) was localized in longitudinal muscle-myenteric plexus (LMMP) preparations, confirming the identification of serotonergic interneurons previously proposed.[81] Serotonergic interneurons are arranged in descending chains such that 5-HT immunoreactive varicosities appose 5-HT immunoreactive neurons[82] and compromise 1.9% of the total number of myenteric neurons.[83] 5-HT interneurons are involved in descending excitatory reflexes demonstrated by the involvement of neuronal 5-HT in

propagating contractile complexes[82], fast excitatory synaptic responses in the myenteric plexus[84] and myenteric plexus excitatory transmission to the circular muscle.[85] Li and colleagues used TPH2 KO animals and demonstrated that small intestinal transit was much reduced in TPH2 KO animals compared to control littermates.[80] Moreover, a similar reduction in transit was observed in TPH1/TPH2 double KO animals. Regardless, in the same study the authors demonstrate that the myenteric plexus of TPH2 KO tissues contain significantly fewer neurons than WT controls. Hence, it is not clear if reduced motility was a result of the absence of neuronal 5-HT or a reduction in ENS neuron number.

Despite being perhaps nonessential in peristalsis initiation, mucosal 5-HT does play a prominent role in disease. For example, EC cell numbers and mucosal 5-HT content were increased in a rodent model of inflammatory bowel disease (IBD).[86] There are two types of IBD: ulcerative colitis (UC) and Crohn's disease that both are characterized by chronic intestinal inflammation that greatly impairs GI function. IBD is associated with dysfunctional motility and therefore, it may be that mucosal 5-HT plays a prominent role *not* in normal l GI motility, but rather in disorders of GI motility. In agreement, Bertrand and colleagues demonstrated that mucosal 5-HT availability was increased in the small intestine of Western diet fed rats compared to controls.[45] Specifically they found that the small intestine of Western diet fed rats was insensitive to the selective serotonin reuptake inhibitor fluoxetine and contained a greater number of EC cells. Together, the impairment in SERT function and greater EC cell number likely contributed to greater 5-HT availability. Therefore, changes in mucosal 5-HT concentrations in DIO likely lead to changes in small intestinal transit.

1.7.2 Role of 5-HT in GI inflammation

Most peripheral 5-HT is found in the intestinal mucosa. It is not surprising then that evidence supports numerous roles for mucosal derived 5-HT in the cardiovascular system,[87, 88] bone remodeling,[89] liver regeneration,[90] uterine contractions[91] and metabolic effects including

lipid and glucose homeostasis.[92] In addition, 5-HT can modulate the immune system.[93] Dendritic cells express functional 5-HT receptors and stimulation of mature dendritic cells with 5-HT, 5-HT_3, 5-HT_4 and 5-HT_7 receptor agonists increased proinflammatory IL-8 and IL-1β production and release.[94] Macrophages, neutrophils, and eosinophils also express 5-HT receptors.[93] In rodents, mast cells release 5-HT.[95] Furthermore a crosstalk between EC cells and cytokines has been demonstrated. For example, EC cells express a functional receptor for IL-1β and release 5-HT in a dose-dependent manner with addition of IL-1β.[96]

The significance of mucosal 5-HT in intestinal inflammation has been demonstrated in IBD models using TPH1 knockout (KO) mice. Dendritic cell culture supernatant from dextran sulfate sodium (DSS)-induced colitis TPH1 KO mice contained significantly less of the proinflammatory mediator, IL-12p40, compared to WT.[97] Further, exogenous 5-HT addition to naïve dendritic cells obtained from TPH1 KO mice significantly up-regulated IL-12p40 production.[97] Production of IL-12p40 from dendritic cells is critical in inflammatory responses (e.g. IBD) by acting as a chemoattractant for macrophages and an inducer for dendritic cell migration and the proinflammatory mediator INFɣ. Similarly, intestinal IL-12p40 levels were elevated in a DIO mouse model.[98] Thus, it is possible that mucosal 5-HT activates dendritic cells and thereby promotes inflammation in DIO. In addition to mucosal 5-HT activation of dendritic cells, mucosal 5-HT mediates MPO activity. For example, in a model of DSS-induced colitis, TPH1 KO mice exhibited reduced mucosal MPO activity as well as TNFα and IL-1β levels.[99] Further, MPO activity and TNFα and IL-1β levels were upregulated with treatment of 5-HTP (5-hydroxytryptophan; 5-HT precursor). Together these studies suggest mucosal 5-HT in DIO have the propensity to drive intestinal inflammation by accelerating dendritic cell and neutrophil activation.

1.8 Sex differences in obesity and the serotonergic system

To date there are few studies of sex differences in obesity and the intestinal serotonergic system. It is known that more women are severely obese than men.[24] In relation to the serotonergic system, obese women respond to SSRI treatment where obese men have little to no response to SSRI treatment for major depressive disorder.[100] There are sex differences in the response to serotonergic drugs used to treat GI motility and sensation disorders as well. For example, the 5-HT_3 receptor antagonist alosetron reduces diarrhea and visceral pain in women but not men IBS patients.[75] In rodents, a similar sex difference was observed. Bush and colleagues demonstrated that *ex vivo* female mouse ileum was more sensitive to alosetron-dependent decreases in the frequency of the MMC compared to male mouse ileum.[77] In the CNS, it was demonstrated that women respond greater to SSRI treatment compared to men for major depressive disorder.[101] Moreover, rodent studies demonstrated sex differences in 5-HT content in the CNS. For example, numerous studies demonstrate that 5-HT and 5-HIAA concentrations are greater in the brain of female rodents compared to males.[102] It is not known if this is true in the intestine. Overall, studies showing a sex difference in response to drugs that target the serotonergic system for bowel improvements suggest that sex differences in 5-HT GI physiology are present. Therefore, research in this area is crucial.

1.9 Hypothesis and Specific Aims

The goals of the research were 1) to investigate the functional consequences of BK channel β1-subunit absence in the intestine, 2) to investigate how DIO changes GI transit and mucosal 5-HT in the gut in a DIO mouse model (C57BL/6J), and 3) to understand if altered GI motility and inflammation in DIO is dependent upon 5-HT. The central hypothesis was DIO causes GI motility dysfunction and inflammation by disrupting 5-HT availability. The research covered three specific aims as follows:

Specific Aim 1: To determine if BK channels are necessary for normal GI transit

Specific Aim 2: To understand if DIO causes small intestinal dysmotility as a result of altered 5-HT availability

Specific Aim 3: To learn if altered 5-HT availability in DIO activates an intestinal inflammatory response

REFERENCES

REFERENCES

1. Furness JB. The enteric nervous system. Malden, Mass.: Blackwell Pub.,, 2006:xiii, 274 p. ill. (some col.).

2. Furness JB, Callaghan BP, Rivera LR, et al. The enteric nervous system and gastrointestinal innervation: integrated local and central control. Adv Exp Med Biol 2014;817:39-71.

3. Furness JB, Kunze WA, Bertrand PP, et al. Intrinsic primary afferent neurons of the intestine. Prog Neurobiol 1998;54:1-18.

4. Hukuhara T, Miyake T. The intrinsic reflexes in the colon. Jpn J Physiol 1959;9:49-55.

5. Smith TK, Furness JB. Reflex changes in circular muscle activity elicited by stroking the mucosa: an electrophysiological analysis in the isolated guinea-pig ileum. J Auton Nerv Syst 1988;25:205-18.

6. Bayliss WM, Starling EH. The movements and innervation of the small intestine. J Physiol 1899;24:99-143.

7. Bornstein JC, Costa M, Grider JR. Enteric motor and interneuronal circuits controlling motility. Neurogastroenterol Motil 2004;16 Suppl 1:34-8.

8. Takahashi T. Mechanism of interdigestive migrating motor complex. J Neurogastroenterol Motil 2012;18:246-57.

9. Zheng J, Ariga H, Taniguchi H, et al. Ghrelin regulates gastric phase III-like contractions in freely moving conscious mice. Neurogastroenterol Motil 2009;21:78-84.

10. Fujino K, Inui A, Asakawa A, et al. Ghrelin induces fasted motor activity of the gastrointestinal tract in conscious fed rats. J Physiol 2003;550:227-40.

11. Wellman GC, Nelson MT. Signaling between SR and plasmalemma in smooth muscle: sparks and the activation of Ca2+-sensitive ion channels. Cell Calcium 2003;34:211-29.

12. Latorre R, Morera FJ, Zaelzer C. Allosteric interactions and the modular nature of the voltage- and Ca2+-activated (BK) channel. J Physiol 2010;588:3141-8.

13. Knaus HG, Folander K, Garcia-Calvo M, et al. Primary sequence and immunological characterization of beta-subunit of high conductance Ca(2+)-activated K+ channel from smooth muscle. J Biol Chem 1994;269:17274-8.

14. Garcia-Calvo M, Knaus HG, McManus OB, et al. Purification and reconstitution of the high-conductance, calcium-activated potassium channel from tracheal smooth muscle. J Biol Chem 1994;269:676-82.

15. Hagen BM, Bayguinov O, Sanders KM. Beta 1-subunits are required for regulation of coupling between Ca2+ transients and Ca2+-activated K+ (BK) channels by protein kinase C. Am J Physiol Cell Physiol 2003;285:C1270-80.

16. Vandael DH, Marcantoni A, Mahapatra S, et al. Ca(v)1.3 and BK channels for timing and regulating cell firing. Mol Neurobiol 2010;42:185-98.

17. Ohi Y, Yamamura H, Nagano N, et al. Local Ca(2+) transients and distribution of BK channels and ryanodine receptors in smooth muscle cells of guinea-pig vas deferens and urinary bladder. J Physiol 2001;534:313-26.

18. Petkov GV, Bonev AD, Heppner TJ, et al. Beta1-subunit of the Ca2+-activated K+ channel regulates contractile activity of mouse urinary bladder smooth muscle. J Physiol 2001;537:443-52.

19. Brenner R, Perez GJ, Bonev AD, et al. Vasoregulation by the beta1 subunit of the calcium-activated potassium channel. Nature 2000;407:870-6.

20. Semenov I, Wang B, Herlihy JT, et al. BK channel beta1 subunits regulate airway contraction secondary to M2 muscarinic acetylcholine receptor mediated depolarization. J Physiol 2011;589:1803-17.

21. Chang HY, Mashimo H, Goyal RK. Musings on the wanderer: what's new in our understanding of vago-vagal reflex? IV. Current concepts of vagal efferent projections to the gut. Am J Physiol Gastrointest Liver Physiol 2003;284:G357-66.

22. Travagli RA, Hermann GE, Browning KN, et al. Brainstem circuits regulating gastric function. Annu Rev Physiol 2006;68:279-305.

23. Browning KN, Travagli RA. Plasticity of vagal brainstem circuits in the control of gastric function. Neurogastroenterol Motil 2010;22:1154-63.

24. Ogden CL, Carroll MD, Kit BK, et al. Prevalence of Childhood and Adult Obesity in the United States, 2011-2012. Jama-Journal of the American Medical Association 2014;311:806-814.

25. Mushref MA, Srinivasan S. Effect of high fat-diet and obesity on gastrointestinal motility. Ann Transl Med 2013;1:14.

26. Aro P, Ronkainen J, Talley NJ, et al. Body mass index and chronic unexplained gastrointestinal symptoms: an adult endoscopic population based study. Gut 2005;54:1377-83.

27. Delgado-Aros S, Locke GR, 3rd, Camilleri M, et al. Obesity is associated with increased risk of gastrointestinal symptoms: a population-based study. Am J Gastroenterol 2004;99:1801-6.

28. Talley NJ, Quan C, Jones MP, et al. Association of upper and lower gastrointestinal tract symptoms with body mass index in an Australian cohort. Neurogastroenterol Motil 2004;16:413-9.

29. Talley NJ, Howell S, Poulton R. Obesity and chronic gastrointestinal tract symptoms in young adults: a birth cohort study. Am J Gastroenterol 2004;99:1807-14.

30. Tosetti C, Corinaldesi R, Stanghellini V, et al. Gastric emptying of solids in morbid obesity. Int J Obes Relat Metab Disord 1996;20:200-5.

31. Maddox A, Horowitz M, Wishart J, et al. Gastric and oesophageal emptying in obesity. Scand J Gastroenterol 1989;24:593-8.

32. Wisen O, Johansson C. Gastrointestinal function in obesity: motility, secretion, and absorption following a liquid test meal. Metabolism 1992;41:390-5.

33. Basilisco G, Camboni G, Bozzani A, et al. Orocecal transit delay in obese patients. Dig Dis Sci 1989;34:509-12.

34. French SJ, Murray B, Rumsey RD, et al. Preliminary studies on the gastrointestinal responses to fatty meals in obese people. Int J Obes Relat Metab Disord 1993;17:295-300.

35. Coleman DL. Obese and diabetes: two mutant genes causing diabetes-obesity syndromes in mice. Diabetologia 1978;14:141-8.

36. Bray GA. The Zucker-fatty rat: a review. Fed Proc 1977;36:148-53.

37. Carroll L, Voisey J, Van Daal A. Mouse models of obesity. Clinics in Dermatology 2004;22:345-349.

38. Lutz TA, Woods SC. Overview of animal models of obesity. Curr Protoc Pharmacol 2012;Chapter 5:Unit5 61.

39. Levin BE, Dunn-Meynell AA. Defense of body weight against chronic caloric restriction in obesity-prone and -resistant rats. Am J Physiol Regul Integr Comp Physiol 2000;278:R231-7.

40. Surwit RS, Kuhn CM, Cochrane C, et al. Diet-induced type II diabetes in C57BL/6J mice. Diabetes 1988;37:1163-7.

41. Parekh PI, Petro AE, Tiller JM, et al. Reversal of diet-induced obesity and diabetes in C57BL/6J mice. Metabolism 1998;47:1089-96.

42. Petro AE, Cotter J, Cooper DA, et al. Fat, carbohydrate, and calories in the development of diabetes and obesity in the C57BL/6J mouse. Metabolism 2004;53:454-7.

43. Lee KT, Karunakaran S, Ho MM, et al. PWD/PhJ and WSB/EiJ mice are resistant to diet-induced obesity but have abnormal insulin secretion. Endocrinology 2011;152:3005-17.

44. Nicholson A, Reifsnyder PC, Malcolm RD, et al. Diet-induced obesity in two C57BL/6 substrains with intact or mutant nicotinamide nucleotide transhydrogenase (Nnt) gene. Obesity (Silver Spring) 2010;18:1902-5.

45. Bertrand RL, Senadheera S, Markus I, et al. A Western diet increases serotonin availability in rat small intestine. Endocrinology 2011;152:36-47.

46. Ricci MR, Ulman, E. A.,. Laboratory animal diets: a critical part of your in vivo research. Animal Lab News 2005;4:1-6.

47. Kiely JM, Noh JH, Graewin SJ, et al. Altered intestinal motility in leptin-deficient obese mice. J Surg Res 2005;124:98-103.

48. Li J, Ma W, Wang S. Slower gastric emptying in high-fat diet induced obese rats is associated with attenuated plasma ghrelin and elevated plasma leptin and cholecystokinin concentrations. Regul Pept 2011;171:53-7.

49. Di Marzo V, Capasso R, Matias I, et al. The role of endocannabinoids in the regulation of gastric emptying: alterations in mice fed a high-fat diet. Br J Pharmacol 2008;153:1272-1280.

50. Baudry C, Reichardt F, Marchix J, et al. Diet-induced obesity has neuroprotective effects in murine gastric enteric nervous system: involvement of leptin and glial cell line-derived neurotrophic factor. J Physiol 2012;590:533-44.

51. Monteiro R, Azevedo I. Chronic inflammation in obesity and the metabolic syndrome. Mediators Inflamm 2010;2010.

52. Ouchi N, Parker JL, Lugus JJ, et al. Adipokines in inflammation and metabolic disease. Nat Rev Immunol 2011;11:85-97.

53. van den Borst B, Gosker HR, Koster A, et al. The influence of abdominal visceral fat on inflammatory pathways and mortality risk in obstructive lung disease. Am J Clin Nutr 2012;96:516-26.

54. Item F, Konrad D. Visceral fat and metabolic inflammation: the portal theory revisited. Obes Rev 2012;13 Suppl 2:30-9.

55. Otani H. Oxidative stress as pathogenesis of cardiovascular risk associated with metabolic syndrome. Antioxid Redox Signal 2011;15:1911-26.

56. Spagnuolo MI, Cicalese MP, Caiazzo MA, et al. Relationship between severe obesity and gut inflammation in children: what's next? Ital J Pediatr 2010;36:66.

57. de La Serre CB, Ellis CL, Lee J, et al. Propensity to high-fat diet-induced obesity in rats is associated with changes in the gut microbiota and gut inflammation. Am J Physiol Gastrointest Liver Physiol 2010;299:G440-8.

58. Krawisz JE, Sharon P, Stenson WF. Quantitative Assay for Acute Intestinal Inflammation Based on Myeloperoxidase Activity - Assessment of Inflammation in Rat and Hamster Models. Gastroenterology 1984;87:1344-1350.

59. Ding S, Chi MM, Scull BP, et al. High-fat diet: bacteria interactions promote intestinal inflammation which precedes and correlates with obesity and insulin resistance in mouse. PLoS One 2010;5:e12191.

60. Cani PD, Bibiloni R, Knauf C, et al. Changes in gut microbiota control metabolic endotoxemia-induced inflammation in high-fat diet-induced obesity and diabetes in mice. Diabetes 2008;57:1470-81.

61. Lam YY, Ha CW, Campbell CR, et al. Increased gut permeability and microbiota change associate with mesenteric fat inflammation and metabolic dysfunction in diet-induced obese mice. PLoS One 2012;7:e34233.

62. Furness JB, Costa M. Neurons with 5-hydroxytryptamine-like immunoreactivity in the enteric nervous system: their projections in the guinea-pig small intestine. Neuroscience 1982;7:341-9.

63. Erspamer V. Occurrence of indolealkylamines in nature. In: Erspamer V, ed. 5-Hydroxytryptamine and Related Indolealkylamines. Volume 19: Springer Berlin Heidelberg, 1966:132-181.

64. Walther DJ, Peter JU, Bashammakh S, et al. Synthesis of serotonin by a second tryptophan hydroxylase isoform. Science 2003;299:76.

65. Nilsson O, Ahlman H, Geffard M, et al. Bipolarity of duodenal enterochromaffin cells in the rat. Cell Tissue Res 1987;248:49-54.

66. Kidd M, Modlin IM, Gustafsson BI, et al. Luminal regulation of normal and neoplastic human EC cell serotonin release is mediated by bile salts, amines, tastants, and olfactants. Am J Physiol Gastrointest Liver Physiol 2008;295:G260-72.

67. Raghupathi R, Duffield MD, Zelkas L, et al. Identification of unique release kinetics of serotonin from guinea-pig and human enterochromaffin cells. J Physiol 2013;591:5959-75.

68. Chin A, Svejda B, Gustafsson BI, et al. The role of mechanical forces and adenosine in the regulation of intestinal enterochromaffin cell serotonin secretion. Am J Physiol Gastrointest Liver Physiol 2012;302:G397-405.

69. Bansal T, Englert D, Lee J, et al. Differential effects of epinephrine, norepinephrine, and indole on Escherichia coli O157:H7 chemotaxis, colonization, and gene expression. Infect Immun 2007;75:4597-607.

70. Bertrand PP, Kunze WA, Furness JB, et al. The terminals of myenteric intrinsic primary afferent neurons of the guinea-pig ileum are excited by 5-hydroxytryptamine acting at 5-hydroxytryptamine-3 receptors. Neuroscience 2000;101:459-69.

71. Gill RK, Pant N, Saksena S, et al. Function, expression, and characterization of the serotonin transporter in the native human intestine. Am J Physiol Gastrointest Liver Physiol 2008;294:G254-62.

72. Bulbring E, Lin RC. The effect of intraluminal application of 5-hydroxytryptamine and 5-hydroxytryptophan on peristalsis; the local production of 5-HT and its release in relation to intraluminal pressure and propulsive activity. J Physiol 1958;140:381-407.

73. Bulbring E, Crema A. The action of 5-hydroxytryptamine, 5-hydroxytryptophan and reserpine on intestinal peristalsis in anaesthetized guinea-pigs. J Physiol 1959;146:29-53.

74. Heredia DJ, Dickson EJ, Bayguinov PO, et al. Localized release of serotonin (5-hydroxytryptamine) by a fecal pellet regulates migrating motor complexes in murine colon. Gastroenterology 2009;136:1328-38.

75. Viramontes BE, Camilleri M, McKinzie S, et al. Gender-related differences in slowing colonic transit by a 5-HT3 antagonist in subjects with diarrhea-predominant irritable bowel syndrome. Am J Gastroenterol 2001;96:2671-6.

76. Axelsson LG, Wallin B, Gillberg PG, et al. Regulatory role of 5-HT and muscarinic receptor antagonists on the migrating myoelectric complex in rats. Eur J Pharmacol 2003;467:211-8.

77. Bush TG, Spencer NJ, Watters N, et al. Effects of alosetron on spontaneous migrating motor complexes in murine small and large bowel in vitro. Am J Physiol Gastrointest Liver Physiol 2001;281:G974-83.

78. Keating DJ, Spencer NJ. Release of 5-hydroxytryptamine from the mucosa is not required for the generation or propagation of colonic migrating motor complexes. Gastroenterology 2010;138:659-70 670 e1-2.

79. Smith TK, Dickson EJ, Heredia DJ, et al. Controversies involving the role of 5-hydroxytryptamine in generating colonic migrating motor complexes: what is spontaneous? Gastroenterology 2010;138:1213-4; author reply 1214-5.

80. Li Z, Chalazonitis A, Huang YY, et al. Essential roles of enteric neuronal serotonin in gastrointestinal motility and the development/survival of enteric dopaminergic neurons. J Neurosci 2011;31:8998-9009.

81. Gershon MD, Tack J. The serotonin signaling system: from basic understanding to drug development for functional GI disorders. Gastroenterology 2007;132:397-414.

82. Neal KB, Parry LJ, Bornstein JC. Strain-specific genetics, anatomy and function of enteric neural serotonergic pathways in inbred mice. J Physiol 2009;587:567-86.

83. Costa M, Brookes SJ, Steele PA, et al. Neurochemical classification of myenteric neurons in the guinea-pig ileum. Neuroscience 1996;75:949-67.

84. Galligan JJ, LePard KJ, Schneider DA, et al. Multiple mechanisms of fast excitatory synaptic transmission in the enteric nervous system. Journal of the Autonomic Nervous System 2000;81:97-103.

85. Monro RL, Bertrand PP, Bornstein JC. ATP and 5-HT are the principal neurotransmitters in the descending excitatory reflex pathway of the guinea-pig ileum. Neurogastroenterology and Motility 2002;14:255-264.

86. Oshima S, Fujimura M, Fukimiya M. Changes in number of serotonin-containing cells and serotonin levels in the intestinal mucosa of rats with colitis induced by dextran sodium sulfate. Histochem Cell Biol 1999;112:257-63.

87. Cote F, Thevenot E, Fligny C, et al. Disruption of the nonneuronal tph1 gene demonstrates the importance of peripheral serotonin in cardiac function. Proc Natl Acad Sci U S A 2003;100:13525-30.

88. Berger M, Gray JA, Roth BL. The expanded biology of serotonin. Annu Rev Med 2009;60:355-66.

89. Ducy P, Karsenty G. The two faces of serotonin in bone biology. J Cell Biol 2010;191:7-13.

90. Papadimas GK, Tzirogiannis KN, Mykoniatis MG, et al. The emerging role of serotonin in liver regeneration. Swiss Med Wkly 2012;142:w13548.

91. Minosyan TY, Lu R, Eghbali M, et al. Increased 5-HT contractile response in late pregnant rat myometrium is associated with a higher density of 5-HT2A receptors. J Physiol 2007;581:91-7.

92. Sumara G, Sumara O, Kim JK, et al. Gut-derived serotonin is a multifunctional determinant to fasting adaptation. Cell Metab 2012;16:588-600.

93. Baganz NL, Blakely RD. A dialogue between the immune system and brain, spoken in the language of serotonin. ACS Chem Neurosci 2013;4:48-63.

94. Idzko M, Panther E, Stratz C, et al. The serotoninergic receptors of human dendritic cells: identification and coupling to cytokine release. J Immunol 2004;172:6011-9.

95. Tamir H, Theoharides TC, Gershon MD, et al. Serotonin storage pools in basophil leukemia and mast cells: characterization of two types of serotonin binding protein and radioautographic analysis of the intracellular distribution of [3H]serotonin. J Cell Biol 1982;93:638-47.

96. Kidd M, Gustafsson BI, Drozdov I, et al. IL1beta- and LPS-induced serotonin secretion is increased in EC cells derived from Crohn's disease. Neurogastroenterol Motil 2009;21:439-50.

97. Li N, Ghia JE, Wang H, et al. Serotonin activates dendritic cell function in the context of gut inflammation. Am J Pathol 2011;178:662-71.

98. Li H, Lelliott C, Hakansson P, et al. Intestinal, adipose, and liver inflammation in diet-induced obese mice. Metabolism 2008;57:1704-10.

99. Ghia JE, Li N, Wang H, et al. Serotonin has a key role in pathogenesis of experimental colitis. Gastroenterology 2009;137:1649-60.

100. Khan A, Schwartz KA, Kolts RL, et al. BMI, sex, and antidepressant response. J Affect Disord 2007;99:101-6.

101. Khan A, Brodhead AE, Schwartz KA, et al. Sex differences in antidepressant response in recent antidepressant clinical trials. J Clin Psychopharmacol 2005;25:318-24.

102. Rubinow DR, Schmidt PJ, Roca CA. Estrogen-serotonin interactions: implications for affective regulation. Biol Psychiatry 1998;44:839-50.

CHAPTER 2

IMPAIRED PROPULSIVE MOTILITY IN THE DISTAL BUT NOT PROXIMAL COLON OF BK CHANNEL β1-SUBUNIT KNOCKOUT MICE

2.1 ABSTRACT

Large conductance Ca^{2+}-activated K^+ (BK) channels regulate smooth muscle tone. The BK channel β1-subunit increases Ca^{2+} sensitivity of the pore forming α-subunit in smooth muscle. We studied β1-subunit knockout (KO) mice to determine if gastrointestinal (GI) motility was altered in these animals. Colonic and small intestinal longitudinal muscle reactivity to bethanechol and colonic migrating motor complexes (CMMCs) were measured in excised segments hung in organ baths. Gastric emptying and small intestinal transit were measured *in vivo* using a fluorescent marker. Colonic motility was assessed *in vivo* by measuring fecal output and the latency to expulsion of a glass bead inserted into the colon. Bethanechol-induced contractions were larger in the distal colon of β1-subunit KO compared to WT mice; there were no differences in bethanechol reactivity in the duodenum, ileum or proximal colon of WT *vs.* β1-subunit KO mice. There were more retrogradely propagated CMMCs in colon preparations from β1-subunit KO compared to WT mice. GI transit was unaffected by β1-subunit KO. Fecal output was decreased and glass bead expulsion times were increased in β1-subunit KO mice. BK channels play a prominent role in smooth muscle function only in the distal colon of mice. Defects in smooth muscle BK channel function disrupt colonic motility causing constipation.

2.2 INTRODUCTION

Smooth muscle tone is essential for gastrointestinal (GI) motility. Regulatory mechanisms necessary for smooth muscle tone involve those that play a role in muscle contraction and relaxation. One regulatory mechanism involves the function of large-conductance Ca^{2+}-activated K^+ (BK) channels that are expressed in smooth muscle cells[1]. BK channels are also present in many other cell types including neurons,[2] skeletal,[3] cardiac[4] and immune cells.[5] In all cell types, BK channels contain 4 α-subunits composed of several domains that serve to form the channel pore and participate in channel activation.[6] The α-subunit regulates BK channel activation by voltage- and Ca^{2+}-dependent and voltage-dependent mechanisms.[6] In addition to the channel activation regulatory α-subunit, accessory β-subunits modulate Ca^{2+} sensitivity of the α-subunit. There are four β-subunit subtypes (β1-β4) and differ in their location.[7] The β1-subunit is smooth muscle specific[8, 9] and contributes to regulation of smooth muscle tone in the trachea, blood vessels, urinary bladder and intestine.[10-14]

In smooth muscle the activation of BK channels by Ca^{2+}-dependent means requires Ca^{2+} influx through L-type Ca^{2+} channels.[15] In smooth muscle cells, Ca^{2+} activates ryanodine receptors (RyRs) on the smooth endoplasmic reticulum to cause Ca^{2+} sparks.[1, 16] Ca^{2+} sparks initiate spontaneous transient outward K^+ currents (STOCs) carried by BK channels. STOCs cause membrane hyperpolarization that closes L-type Ca^{2+} channels subsequently resulting in smooth muscle relaxation.[1, 16] Together, Ca^{2+} sparks coupled with STOCs regulate smooth muscle tone.

The importance of the β1-subunit in regulating smooth muscle tone has been illustrated by studies using β1-subunit knockout (KO) mice. Myocytes taken from β1-subunit KO mice show a reduction in the open probability of the BK channel in urinary bladder,[13] arterial[12] and tracheal myocytes[10] as well as a reduced coupling of Ca^{2+} sparks and STOCs in arterial and colonic myocytes.[12, 14] In colonic smooth muscle cells from β1-subunit KO mice, Ca^{2+} sparks were normal but STOCs were smaller and less frequent indicative of a separation between Ca^{2+}

sparks and STOCs.[10] Although Ca^{2+} spark-STOC uncoupling occurs in colonic smooth muscle cells of β1-subunit KO mice, the integrative functional consequences of this uncoupling are unknown. In the present study, we tested the hypothesis that the absence of the β1-subunit in mice would disrupt gut motility. To test this hypothesis we evaluated *in vivo* small and colonic motility, small and colonic longitudinal muscle cholinergic reactivity in excised intestinal segments and colonic migrating motor complex (CMMC) in excised colons in β1-subunit KO mice and compared these observations to those in wildtype (WT) mice.

2.3 METHODS AND MATERIALS

2.3.1 Mice

All animal use protocols were approved by the Institutional Animal Care and Use Committee at Michigan State University. Homozygous breeder β1-subunit KO mice were obtained from Dr. Robert Brenner, University of Texas Health Science Center at San Antonio.[10, 12] Homozygous BK β1-subunit KO mice were then bred in house. The β1-subunit KO mice are congenic as a result of inbreeding to the C57BL/6 strain. Wildtype C57BL/6 (WT) mice were from Jackson Laboratories (Bar Harbor, ME) and served as the control. β1-subunit KO mice were weaned at 3 wk. All mice were fed normal diet and were studied at 10–12 wk of age (male, 25–30 g). Mice were euthanized using isoflurane anesthesia followed by cervical dislocation. We have used BK channel β1-subunit KO mice in a number of previously published studies of smooth muscle function *in vitro* and *in vivo*.[11, 17, 18]

2.3.2 Motility studies *in vivo*

Fecal pellet output was evaluated in WT and β1-subunit KO mice. Mice were individually housed and food and water were removed for 1 h between 10 and 11 AM. Fecal pellets were collected from each mouse during this time. Pellets were counted and wet weight was measured. Following, pellets were placed into a 60 ˚C oven overnight and dry weight was then

determined. This protocol was repeated on 3 consecutive days. Fecal pellet wet and dry weight from each animal was averaged over the 3 day period and that average value was used for each mouse. These values were averaged for statistical comparisons.

Colonic motility was assessed *in vivo* by measuring time to expulsion of a bead inserted 2 cm into the colon. A single bead (3 mm) was inserted 2 cm into the distal colon of WT and β1-subunit KO mice that were fasted 12 h prior to experimentation. Expulsion time was then determined for each mouse.[19]

Small intestinal transit was assessed *in vivo*. WT and β1-subunit KO mice were fasted 12 h prior to experimentation. Mice were gavaged with 0.1 mL of 10 mg mL^{-1} FITC-dextran. After 30 min, mice were euthanized. The gastrointestinal tract from the stomach to the ileum was removed. The small intestine was sectioned into 6 segments (5 cm). Segments were flushed with 1.5 mL PBS and the content of each segment was placed in a microfuge tube and quickly centrifuged. FITC fluorescence activity was measured (488 nm excitation) in a 200 µL aliquot of each sample using a plate reader (Fluoroskan Ascent/FL, Thermo Scientific, Rockford, IL). The percentage of total FITC fluorescence in the stomach and each intestinal segment was determined and the geometric center (GC) of the fluorescence distribution was calculated.[20]

2.3.3 *In vitro* studies

2.3.3.1 Cholinergic reactivity of small intestinal and colonic longitudinal muscle

The small intestine and colon of WT and β1-subunit KO mice were dissected into proximal and distal segments. Each segment (~1cm) was suspended in individual jacketed tissue baths (25 mL volume) filled with warmed (37 ˚C), oxygenated (95% O_2, 5% CO_2) Krebs buffer solution of the following composition (millimolar): 117 NaCl, 4.7 KCl, 2.5 $CaCl_2$, 1.2 $MgCl_2$, 1.2 NaH_2PO_4, 25 $NaHCO_3$, and 11 glucose. The tissue was attached to a tissue holder and a force-

displacement transducer (FT03C, Grass Instruments, Inc.) using silk thread. After a 20 minute incubation period, the optimal initial tension in which the tissue displayed the maximum force in response to acetylcholine (ACh, 100 μmol L^{-1}) was determined by increasing passive tension in stepwise increments until the maximum ACh-induced contraction was achieved. Small intestinal and colonic segments were placed under 0.5 g and 0.8 g initial tension, respectively. All tissue segments were allowed to equilibrate for 20 min. The muscarinic cholinergic receptor agonist, bethanechol (0.3-100 μmol L^{-1}) was then tested to determine muscle reactivity in colonic and small intestinal segments. Individual bethanechol concentrations were added at 10 min intervals for 1 min to ensure sufficient time for maximum contraction to occur. Bethanechol was washed out after 1 min. Data were recorded and analyzed using a Powerlab system and Chart software (ADI Instruments, Colorado Springs, CO http://www.adinstruments.com/). After each experiment, tissues were weighed and results are expressed as force (g) per tissue weight (mg).

2.3.3.2 Colonic migrating motor complex (CMMC) studied *in vitro*

Preparation of colonic segments for recordings of the CMMC was performed as described previously.[21] Briefly, the entire colon was removed from euthanized mice and placed into Krebs buffer solution. Luminal contents were gently flushed out with Krebs buffer solution. A stainless-steel rod was inserted into the lumen and the tissue was secured at each end with surgical silk. Metal clips (Fine Science Tools, Foster City, CA USA) were attached to the oral and anal end of the tissue 2 cm apart and connected by surgical silk to separate force transducers. The rod holding the tissue was secured in a bath (30 mL) containing oxygenated Krebs buffer solution (37 ˚C) and stretched to an initial tension of 0.5 g. The tissue was allowed to equilibrate for 1 h during which a regular pattern of propagating contractions was established (CMMC). The CMMC was recorded for an additional hour and a 20 min segment was selected for analysis. During the entire experiment, resting tension was monitored and the Krebs buffer

solution was changed every 20 min. Frequency, amplitude, and duration of CMMCs were measured as described previously.[21] Propagated CMMCs were determined as a complex in which a contraction occurred first at the oral recording site followed by a contraction at the anal site. Contractions propagated between the two recording sites at a velocity of ~2 mm sec^{-1}.[21] Retrogradely propagated contractions (anal to oral) were identified as those complexes in which a contraction occurred first at the anal recording site and after several seconds, a contraction occurred at the oral recording site. Recordings were obtained using 2 Grass Instruments CP122A strain gauge amplifiers. The output of these amplifiers was fed to an analog/digital converter (Minidigi 1A, Molecular Devices, Sunnyvale, CA; http://www.moleculardevices.com/) and Axoscope software 9.2 (Molecular Devices).

2.3.4 Reagents and drugs

All drugs and reagents were obtained from Sigma Aldrich Chemical Company (St. Louis, MO USA).

2.3.5 Statistical analysis

Two group comparisons were made using an unpaired Student's t-test. Comparisons of bethanechol concentration response curves in tissues from WT and β1-subunit KO mice were made using a two way ANOVA and Bonferoni's post hoc test. This was done across all tissues because bethanechol concentration response curves in distal colon preparations did not reach a maximum response at the highest concentration tested of 100 μmol L^{-1}. Therefore, calculation of accurate half maximal effective concentrations (EC_{50}) was not possible. For all comparisons $P < 0.05$ was considered statistically significant. Data are reported as mean ± S.E.M.

2.4 RESULTS

2.4.1 Reduced distal colonic propulsive motility in β1-subunit KO mice *in vivo*

To investigate gut function *in vivo*, fecal pellet output was measured. The number of fecal pellets produced in 1 h was substantially less in β1-subunit KO compared to WT mice (Figure 6A). This result was quantitated by measuring fecal pellet wet and dry weights, which revealed significant reductions from β1-subunit KO compared to WT mice (Figure 6B). Further evidence for reductions in propulsive distal colonic motility in β1-subunit KO mice was obtained in the glass bead expulsion time assay. These studies revealed significantly longer expulsion times in the β1-subunit KO compared to WT mice (Figure 6C).

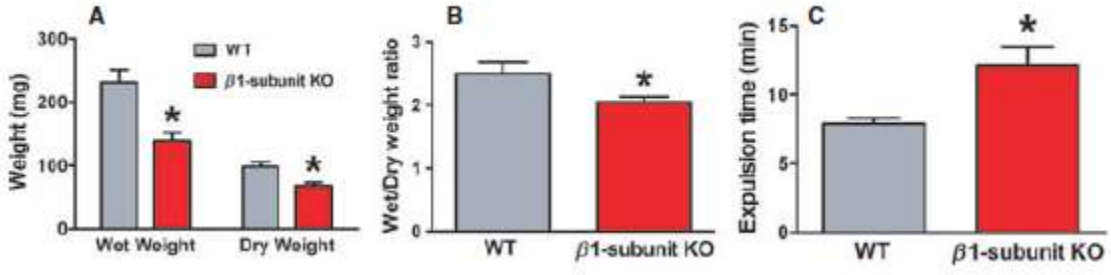

Figure 6. Reduced propulsive colonic motility in β1-subunit knockout (KO) mice. (A) Fecal pellet output was measured over a 1 h period for three consecutive days in each mouse. The 3 day average for each mouse was used as a measure of output for that animal. Fecal pellet wet and dry weight were lower in β1-subunit KO (n = 13) compared to WT (n = 13) mice (*P < 0.05). (B) The fecal pellet wet/dry ratio was also lower for β1-subunit KO compared to WT mice (*P < 0.05). (C) Expulsion time for a glass bead inserted into the rectum was increased in β1-subunit KO (n = 10) compared to WT (n = 7) mice (*P < 0.05). Reprinted from Neurogastroenterology & Motility, 24, France et al., "Impaired propulsive motility in the distal but not proximal colon of BK channel β1subunit knockout mice," e450-e459, Copyright (2012), with permission from John Wiley and Sons.

The results above suggested that impaired BK channel function is associated with reduced propulsive distal colonic motility. We next measured gastric emptying and small intestinal transit to determine if BK channel deficiencies caused reductions in upper GI propulsive motility. FITC-conjugated dextran was administered by gastric gavage and progression of the marker was measured 30 min later. There were no differences in the

progression of the marker (as measured by the geometric center of marker distribution) in WT vs. β1-subunit KO mice (Figure 7).

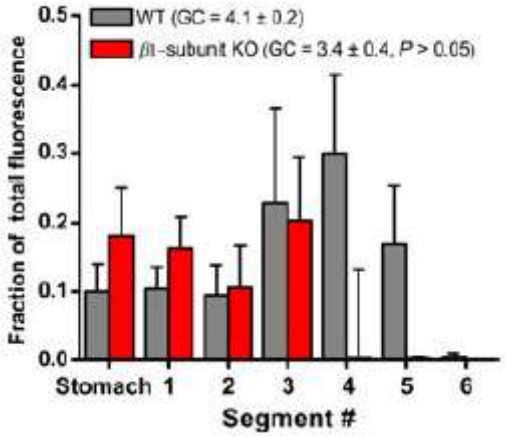

Figure 7. Gastrointestinal transit is not altered in β1-subunit KO mice. Gastrointestinal transit was measured by calculating the geometric center (GC) of the distribution of FITC-dextran in the stomach and six small intestinal segments. There was no difference in the mean GC in β1-subunit KO (*n* = 8) and WT mice (*n* = 8) (*P* > 0.05). Reprinted from Neurogastroenterology & Motility, 24, France et al., "Impaired propulsive motility in the distal but not proximal colon of BK channel β1subunit knockout mice," e450-e459, Copyright (2012), with permission from John Wiley and Sons.

2.4.2 Increased cholinergic reactivity *in vitro* in distal colon of β1-subunit KO mice

Bethanechol, a muscarinic cholinergic receptor agonist, was used to elicit longitudinal muscle contractions of duodenal, ileal, proximal colon and distal colon segments maintained *in vitro.* There were no differences in bethanechol concentration response curves in the duodenum, ileum or proximal colon of β1-subunit KO compared to WT mice (Figure 8A, B, C). However, there was an increase in contraction amplitude in the concentration response curve in the distal colon of β1-subunit KO compared to WT mice (Figure 8D).

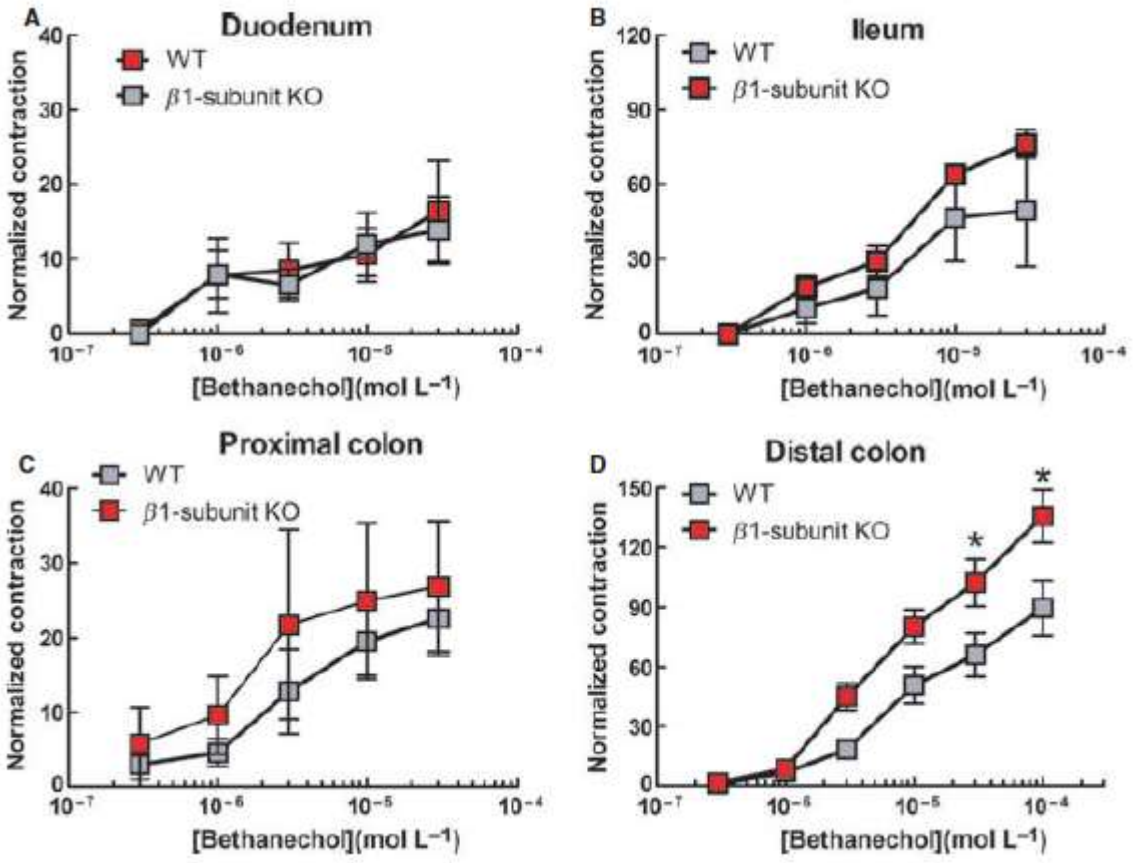

Figure 8. Comparison of in vitro cholinergic reactivity in the small intestine and colon of WT and β1-subunit KO mice. (A, B) Bethanechol-induced contractions of the longitudinal muscle in the duodenum and ileum from WT (*n* = 5) and β1-subunit KO (*n* = 5) mice were similar. (C) Bethanechol induced contractions in the proximal colon of WT (*n* = 7) and β1-subunit KO (*n* = 8) mice were also similar. (D) There was an increase in contraction amplitude in the bethanechol concentration response curve in the distal colon of β1-subunit KO (*n* = 8) compared to WT (*n* = 8) mice (*$P < 0.05$). Reprinted from Neurogastroenterology & Motility, 24, France et al., "Impaired propulsive motility in the distal but not proximal colon of BK channel β1subunit knockout mice," e450-e459, Copyright (2012), with permission from John Wiley and Sons.

2.4.3 Alteration in the CMMC in the distal colon of β1-subunit KO mice

The CMMC is a spontaneous pattern of propagating contractions that occurs in the mouse colon in excised colons (Figure 9A). There were no differences in the amplitude of contractions, frequency of the CMMC or contraction propagation speed when colonic segments from WT and β1-subunit KO mice were compared (data not shown). It was also found that

almost 80% of the CMMCs that began at the oral end of the segment propagated to the distal recording site in segments from both WT and β1-subunit KO mice (Figure 9B). Colonic segments from β1-subunit KO mice exhibited significantly more retrograde (anal to oral) propagating contractions compared to segments from WT mice (Figure 9B).

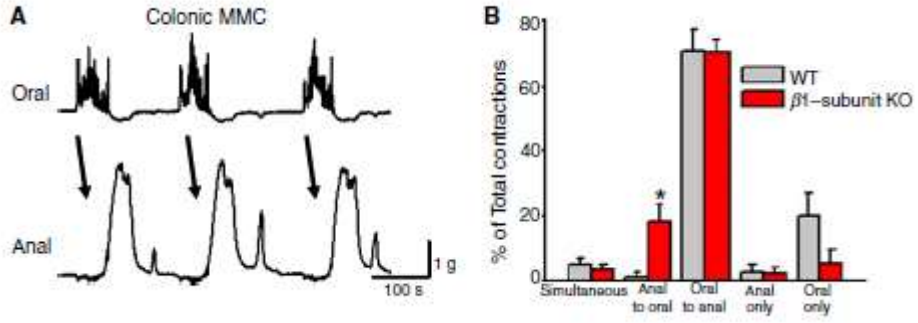

Figure 9. Recordings of colonic migrating motor complex (CMMC) in colonic segments from β1-subunit KO and WT mice. (A) Representative recording of CMMC in the colon from a WT mouse. Recording shows that contractions propagate regularly in an oral to anal direction. (B) Summary of propagation patterns in colon segments from WT (*n* = 7) and β1-subunit KO (*n* = 9) mice. Almost 80% of CMMCs propagate in an oral to anal direction in tissues from both types of mice. However, there was a significant increase in the percentage of retrograde (anal to oral) propagated contractions in colonic segments from β1-subunit KO compared to WT mice (**P* < 0.05). Reprinted from Neurogastroenterology & Motility, 24, France et al., "Impaired propulsive motility in the distal but not proximal colon of BK channel β1subunit knockout mice," e450-e459, Copyright (2012), with permission from John Wiley and Sons.

2.5 DISCUSSION

The results of this study show that compromised BK channel function in the gastrointestinal tract leads to reduced propulsive motility particularly in the distal colon.

2.5.1 BK channels and colonic motility

We assessed colonic motility *in vivo* indirectly by measuring fecal pellet output and glass bead expulsion time. Both techniques are used routinely in mice as it is difficult to make more

direct *in vivo* assessments of colon motility.[19, 22, 23] There are limited studies in which *in vivo* assessments of colon motility have been made. Intracolonic pressure was assessed at a single site in the distal colon using telemetry.[24] However, this technique does not provide propagation information. Although, propagation patterns and intracolonic pressures were determined using miniature pressure transducers, mice were restrained and such results may be confounded by stressor effects. Our results indicate fecal pellet output by β1-subunit KO was reduced compared to WT mice. This could result from decreased propulsive motility or from water absorption changes by colonic epithelial cells. The latter is supported by the reduced fecal pellet wet/dry weight ratio from β1-subunit KO mice suggesting increased colonic water absorption. However, glass bead expulsion time was increased in β1-subunit KO mice compared to WT mice suggesting propulsive colonic motility was reduced. Longer colonic transit times would allow for more water absorption accounting for the reduced fecal pellet wet/dry weight ratio from β1-subunit KO mice. In addition, deletion of the β1-subunit in gastrointestinal smooth muscle would alter contractility and therefore propulsive motility, which is consistent with the known function of the BK channel and β1-subunit in smooth muscle cells.

Our data suggest BK channel function plays a more prominent role in controlling colonic motility than either gastric or small intestinal motility. This conclusion is supported by our data showing gastric emptying and small intestinal propulsion of FITC labeled dextran sulfate were not different in WT vs. β1-subunit KO mice. We measured liquid emptying and propulsion in the stomach and small intestine, respectively. BK channel function would contribute to gastric accommodation and small intestinal tone regulation and this may be more critical for solid emptying and propulsion (as occurs in the distal colon). However, our data from cholinergic reactivity in small and large longitudinal muscle in excised segments indicate BK channel function is more prominent in the distal colon *vs.* the small intestine (see below). It is important to speculate if alterations in distal colonic motility and not in either gastric or small intestinal motility present significant changes to overall transit time. It can be suggested that changes in

distal colonic motility have the ability to alter whole gut transit times since β1-subunit KO mice exhibited reduced fecal pellet output regardless of food intake (data not shown) and gastric and small intestinal motility changes.

2.5.2 Alterations in smooth muscle function in excised distal colon of β1-subunit KO mice

Our *in vivo* data indicate BK channel function is more prominent in the distal colon than in the proximal colon and small intestine. We conducted studies in excised intestinal segments in an effort to identify possible mechanisms responsible for impairment of propulsive colonic motility. Because acetylcholine is an important stimulant of smooth muscle contraction throughout the gut, we investigated cholinergic reactivity in small intestinal and colonic excised segments. We used the muscarinic cholinergic receptor agonist, bethanechol, to minimize activation of enteric neurons that could release modulatory neurotransmitters confounding interpretations of any genotypic differences in cholinergic reactivity. Cholinergic reactivity was similar in small intestinal and proximal colon segments from WT and β1-subunit KO mice. However, cholinergic reactivity was increased significantly in distal colon segments from β1-subunit KO vs. those from WT mice as indicated by the increase in contraction amplitude in the bethanechol concentration response curve. This increase in cholinergic reactivity would be consistent with the known function of BK channels and the β1-subunit in smooth muscle. BK channels are activated by Ca^{2+} released from intracellular stores and the β1-subunit modulates channel function by increasing Ca^{2+} sensitivity.[7, 10, 16] Absence of the β1-subunit would reduce Ca^{2+} sensitivity and therefore reduce channel opening. As a result, reductions in outward K^+ currents would increase smooth muscle excitability. Therefore, the increase in smooth muscle excitability as a result of β1-subunit absence would increase reactivity to drugs that cause muscle contraction such as bethanechol.

BK channel function may be more prominent in the distal colon compared to the small intestine or proximal colon because of the different functional roles of these tissues. The distal colon is primarily a storage organ while the small intestine and proximal colon function to absorb nutrients and water from the gut lumen. Hence, the need for smooth muscle relaxation (which would be facilitated by BK channel activity) is less critical in the small intestine and proximal colon compared to the distal colon.

2.5.3 CMMCs are disrupted in the distal colon of β1-subunit KO mice

In the colon, fecal material is propelled by giant migrating contractions that occur periodically and move colonic content along the length of the colon. The CMMC in the mouse colon is the human equivalent of these giant migrating contractions and the CMMC occurs spontaneously in the excised mouse colon. This provides an opportunity for detailed studies of the mechanisms responsible for these propulsive contractions. The CMMC occurs in regular intervals with contractions that begin at the oral end of colonic segments and propagate to the anal end in > 80% of cases. We found that contractions occurred at the anal end of the segment before a contraction at the oral end more often in segments from β1- subunit KO compared to WT mice. This disruption in the normal propagation pattern could be a result of the increase in smooth muscle excitability described above in tissues from β1- subunit KO mice. Disruption of oral to anal propagation would also be responsible for reduced fecal pellet output and prolonged glass bead expulsion time detected in our *in vivo* studies. Hagen et al. studied the electrophysiological properties of colon smooth muscle cells from β1-subunit KO mice.[14] Although they did not study integrative colonic function, they did report that colons of β1-subunit KO mice had loose fecal material that was not formed into pellets typically seen in the colon from WT mice. These observations differ from our own data where we found that β1-subunit KO mice produce hard dry fecal pellets that might have been caused by reduced propulsive

colonic motility. The previous study did not provide any specific data on this issue so it is difficult to compare the data from the previous work with our study.

2.5.4 Conclusions

The β1-subunit of the BK channel is smooth muscle specific and regulates Ca^{2+} sensitivity of the pore forming α-subunit. Knockout of the gene encoding the β1-subunit in mice causes impaired colonic propulsive motility with little effect on upper GI motility.

Slow transit constipation can occur in different segments of the colon. Our data suggest that the β1-subunit KO mouse may be a model of segmental slow transit constipation in humans in which colonic dysmotility affects the left-side (descending colon). Slow transit constipation is associated with altered propulsive pressure waves at least in a subset of patients. In addition, there are neuronal, myogenic and interstitial cell of Cajal (ICC) based alterations associated with slow transit constipation in humans.[25-27] These changes include loss of ICC and myenteric nerve fibers containing substance P and VIP.[28] Myogenic deficiencies in human slow transit constipation have been identified using histopathological assessments but it is also possible that functional changes not revealed by histology could be responsible for impaired muscle function. Altered function or expression of ion channels in smooth muscle could disrupt propulsive motility patterns. Our data suggest that impaired BK channel function would result in slow transit constipation. These data also suggest that the β1-subunit KO mouse may be a suitable animal model for testing prokinetic drugs that could be used for treatment of slow transit constipation affecting the left-side.

REFERENCES

REFERENCES

1. Wellman GC, Nelson MT. Signaling between SR and plasmalemma in smooth muscle: sparks and the activation of Ca2+-sensitive ion channels. Cell Calcium 2003;34:211-29.

2. Salkoff L, Butler A, Ferreira G, et al. High-conductance potassium channels of the SLO family. Nat Rev Neurosci 2006;7:921-31.

3. Tricarico D, Mele A, Conte Camerino D. Phenotype-dependent functional and pharmacological properties of BK channels in skeletal muscle: effects of microgravity. Neurobiol Dis 2005;20:296-302.

4. Ko JH, Ibrahim MA, Park WS, et al. Cloning of large-conductance Ca(2+)-activated K(+) channel alpha-subunits in mouse cardiomyocytes. Biochem Biophys Res Commun 2009;389:74-9.

5. Essin K, Gollasch M, Rolle S, et al. BK channels in innate immune functions of neutrophils and macrophages. Blood 2009;113:1326-31.

6. Latorre R, Morera FJ, Zaelzer C. Allosteric interactions and the modular nature of the voltage- and Ca2+-activated (BK) channel. J Physiol 2010;588:3141-8.

7. Sweet TB, Cox DH. Measuring the influence of the BKCa {beta}1 subunit on Ca2+ binding to the BKCa channel. J Gen Physiol 2009;133:139-50.

8. Knaus HG, Folander K, Garcia-Calvo M, et al. Primary sequence and immunological characterization of beta-subunit of high conductance Ca(2+)-activated K+ channel from smooth muscle. J Biol Chem 1994;269:17274-8.

9. Garcia-Calvo M, Knaus HG, McManus OB, et al. Purification and reconstitution of the high-conductance, calcium-activated potassium channel from tracheal smooth muscle. J Biol Chem 1994;269:676-82.

10. Semenov I, Wang B, Herlihy JT, et al. BK channel beta1 subunits regulate airway contraction secondary to M2 muscarinic acetylcholine receptor mediated depolarization. J Physiol 2011;589:1803-17.

11. Xu H, Kandlikar SS, Westcott EB, et al. Requirement for functional BK channels in maintaining oscillation in venomotor tone revealed by species differences in expression of the beta1 accessory subunits. J Cardiovasc Pharmacol 2012;59:29-36.

12. Brenner R, Perez GJ, Bonev AD, et al. Vasoregulation by the beta1 subunit of the calcium-activated potassium channel. Nature 2000;407:870-6.

13. Petkov GV, Bonev AD, Heppner TJ, et al. Beta1-subunit of the Ca2+-activated K+ channel regulates contractile activity of mouse urinary bladder smooth muscle. J Physiol 2001;537:443-52.

14. Hagen BM, Bayguinov O, Sanders KM. Beta 1-subunits are required for regulation of coupling between Ca2+ transients and Ca2+-activated K+ (BK) channels by protein kinase C. Am J Physiol Cell Physiol 2003;285:C1270-80.

15. Vandael DH, Marcantoni A, Mahapatra S, et al. Ca(v)1.3 and BK channels for timing and regulating cell firing. Mol Neurobiol 2010;42:185-98.

16. Ohi Y, Yamamura H, Nagano N, et al. Local Ca(2+) transients and distribution of BK channels and ryanodine receptors in smooth muscle cells of guinea-pig vas deferens and urinary bladder. J Physiol 2001;534:313-26.

17. Xu H, Garver H, Galligan JJ, et al. Large-conductance Ca2+-activated K+ channel beta1-subunit knockout mice are not hypertensive. Am J Physiol Heart Circ Physiol 2011;300:H476-85.

18. Xu H, Wang Y, Garver H, et al. Vascular BK channel deficiency exacerbates organ damage and mortality in endotoxemic mice. J Cardiovasc Pharmacol 2012;59:207-14.

19. Raffa RB, Mathiasen JR, Jacoby HI. Colonic bead expulsion time in normal and mu-opioid receptor deficient (CXBK) mice following central (ICV) administration of mu- and delta-opioid agonists. Life Sci 1987;41:2229-34.

20. Miller MS, Galligan JJ, Burks TF. Accurate measurement of intestinal transit in the rat. J Pharmacol Methods 1981;6:211-7.

21. Devries MP, Vessalo M, Galligan JJ. Deletion of P2X2 and P2X3 receptor subunits does not alter motility of the mouse colon. Front Neurosci 2010;4:22.

22. Stengel A, Goebel-Stengel M, Wang L, et al. Central somatostatin receptor 1 activation reverses acute stress-related alterations of gastric and colonic motor function in mice. Neurogastroenterol Motil 2011;23:e223-36.

23. Fichna J, Dicay M, Hirota SA, et al. Differential effects of salvinorin A on endotoxin-induced hypermotility and neurogenic ion transport in mouse ileum. Neurogastroenterol Motil 2011;23:583-e212.

24. Hoogerwerf WA, Shahinian VB, Cornelissen G, et al. Rhythmic changes in colonic motility are regulated by period genes. Am J Physiol Gastrointest Liver Physiol 2010;298:G143-50.

25. Kashyap P, Gomez-Pinilla PJ, Pozo MJ, et al. Immunoreactivity for Ano1 detects depletion of Kit-positive interstitial cells of Cajal in patients with slow transit constipation. Neurogastroenterol Motil 2011;23:760-5.

26. Knowles CH, Farrugia G. Gastrointestinal neuromuscular pathology in chronic constipation. Best Pract Res Clin Gastroenterol 2011;25:43-57.

27. Dinning PG, Zarate N, Hunt LM, et al. Pancolonic spatiotemporal mapping reveals regional deficiencies in, and disorganization of colonic propagating pressure waves in severe constipation. Neurogastroenterol Motil 2010;22:e340-9.

28. King SK, Sutcliffe JR, Ong SY, et al. Substance P and vasoactive intestinal peptide are reduced in right transverse colon in pediatric slow-transit constipation. Neurogastroenterol Motil 2010;22:883-92, e234.

CHAPTER 3

SEX-RELATED DIFFERENCES IN SMALL INTESTINAL TRANSIT AND 5-HT DYNAMICS IN HIGH-FAT DIET-INDUCED OBESITY IN MICE

3.1 ABSTRACT

Obesity alters gastrointestinal (GI) motility and 5-hydroxytryptamine (5-HT, serotonin) signaling. Extracellular 5-HT depends on release from mucosal enterochromaffin (EC) cells and uptake by the serotonin transporter (SERT). We assessed gastric emptying, small intestinal transit and 5-HT signaling in both male and female mice fed either control diet (CD, 10 kcal % fat) or a high-fat diet (HFD, 60 kcal % fat) to induce obesity. Gastric emptying and transit were accelerated in male HFD and female CD compared to male CD. The 5-HT_3 receptor blocker, alosetron, increased gastric emptying in male CD and decreased transit in female CD. 5-HT-induced jejunal muscle contractions were similar in all mice. In contrast to male CD, continuous amperometric measurements showed that 5-HT uptake was insensitive to fluoxetine, yet sensitive to cocaine and the dopamine transporter (DAT) blocker GBR 12909, in male HFD jejunum. DAT-immunoreactivity was present in the mucosa and protein levels were greater in male HFD compared to CD jejunum. Extracellular 5-HT and tissue 5-HIAA (a 5-HT metabolite) were similar in male HFD compared to CD. Jejunal 5-HT uptake was fluoxetine sensitive in female HFD compared to CD. Greater SERT protein, decreased extracellular 5-HT and greater tissue 5-HIAA were observed in female HFD compared to CD. Tissue 5-HT and EC cell numbers were similar in CD and HFD mucosa in both sexes; however, female 5-HT and EC cell numbers were increased compared to males. HFD did not alter plasma sex hormone levels in all mice. Overall, obesity effects intestinal 5-HT and transit in a sex-dependent manner.

3.2 INTRODUCTION

Obesity, as defined by a body mass index (BMI) ≥ 30, is highly prevalent worldwide as the World Health Organization (WHO) estimated 13% of the world's population was obese in 2014 (http://www.who.int/mediacentre/factsheets/fs311/en/). Generally, more women are more severely obese than men.[1] A common adverse outcome associated with obesity is altered gastrointestinal (GI) motility. Normal GI motility promotes digestion and absorption of nutrients as well as excretion of indigestible material. Impaired GI motility, causes diarrhea, constipation, irritable bowel syndrome (IBS) and or fecal incontinence all of which decrease the quality of life of affected patients.[2] For example, a positive association between BMI and diarrhea has been reported.[3-6] Indeed, small intestinal transit in obese humans was found to be faster compared to lean controls after delivery of a radiolabeled liquid test meal.[7] However, studies demonstrating that transit is altered in obese humans are limited and inconsistent. These inconsistencies are largely caused by differences in methods used to measure motility and measuring small intestinal transit independently of gastric emptying is difficult in human subjects. For example, orocecal (i.e. mouth to cecum) transit is delayed[8] or not altered[9] in obese compared to normal weight humans. Despite this, changes in small intestinal motility can lead to adverse GI outcomes in obesity.

Certain drugs used to treat diarrhea decrease GI motility by targeting 5-HT signaling. For example, alosetron antagonizes the 5-HT_3 receptor and is prescribed for diarrhea-predominant irritable bowel syndrome (IBS-D) in women. 5-HT contributes to the control of intestinal motility by modulating enteric nervous system (ENS) function.[10, 11] The ENS is a division of the autonomic nervous system found in the gut wall that autonomously controls motor reflexes. The circuitry of the ENS contains excitatory and inhibitory motoneurons, interneurons and intrinsic primary afferent neurons (IPANS). 5-HT stimulates the mucosal terminals of IPANS[12] leading to activation of interneurons with cell bodies localized within the myenteric plexus. Ascending and descending interneurons then activate excitatory and inhibitory

motoneurons, respectively to cause coordinated smooth muscle contraction and relaxation.[13] 5-HT is synthesized in mucosal enterochromaffin (EC) cells from tryptophan by the rate-limiting and EC cell specific enzyme tryptophan hydroxylase 1 (TPH1). 5-HT is stored in secretory granules until its release into the lumen or lamina propria following EC cell activation by chemical[14, 15] or mechanical stimuli.[16] When 5-HT is released from the EC cell, it acts in a paracrine manner by activating 5-HT_3 receptors localized on nerve terminals of IPANS. Extracellular 5-HT levels are predominately regulated by the serotonin transporter (SERT) localized on enterocytes near EC cells.[17] 5-HT transported into the enterocyte is metabolized by monoamine oxidase A (MAO_A) to 5-hydroxyindolacetic acid (5-HIAA).

Shifts in intestinal 5-HT levels caused by changes in 5-HT synthesis, release or uptake are associated with intestinal dysmotility.[18, 19] In obesity, increased 5-HT levels, attributed to an increase in EC cell number and impaired SERT function, occur in the small intestine of a diet-induced obesity (DIO) rat model.[20] In DIO rodent models, small intestinal motility is increased[21] possibly due to abnormal 5-HT levels. We hypothesized that increased small intestinal motility in a DIO mouse model is caused by altered 5-HT signaling and that there are sex-dependent differences in the intestinal 5-HT system in obesity. In our studies we determined: 1) if a high-fat diet (HFD) in a DIO mouse (C57BL/6J) model causes changes in GI transit and if transit can be decreased by targeting the 5-HT system *in vivo,* 2) if intestinal serotonergic receptor activation and components regulating 5-HT concentration are altered in DIO, and 3) if changes in plasma sex hormone levels can account for any observed difference.

3.3 METHODS AND MATERIALS

3.3.1 Mice and diets

All animal use protocols were approved by the Institutional Animal Care and Use Committee at Michigan State University. Male and female C57BL/6J mice were purchased from Jackson Laboratories (Bar Harbor, ME, USA) at 14 weeks of age. These mice had received either a

control diet (CD, 10 kcal % as fat, D12450B) or a HFD (60 kcal % as fat, D12492) (Research Diets, Inc., New Brunswick, NJ, USA) after weaning at ca. 4-5 weeks of age. These diets are isocaloric per weight and have identical levels of protein, minerals and fiber. Upon arrival to our animal facility, the mice remained on either a CD or HFD for an additional 3 weeks before use in our studies. Mice were housed in individual cages and allowed food and water *ad libitum* on a 12 h light/dark cycle. Mice were studied at 17-19 wk of age (ca. 13-15 wk on diets). Mice were euthanized using isoflurane anesthesia followed by cervical dislocation. Both body weight and abdominal fat pad weights were measured at the time of sacrifice. For all studies, a segment of the jejunum was excised just distal to the ligament of Treitz and placed in oxygenated (95% O_2, 5% CO_2) Krebs buffer (pH 7.4).

3.3.2 Reagents and drugs

The Krebs buffer used in the measurements consisted of the following composition (mmol L^{-1}): 117 NaCl, 4.7 KCl, 2.5 $CaCl_2$, 1.2 $MgCl_2$, 1.2 NaH_2PO_4, 25 $NaHCO_3$, and 11 glucose. All drugs and reagents were obtained from Sigma Aldrich (St. Louis, MO, USA). For continuous amperometry (CA) and organ bath studies, drugs were stored as aliquots at -20 ˚C and were freshly prepared in Krebs buffer for each experiment. Alosetron was dissolved in sterile saline solution. Fluorescein isothiocyanate (FITC)-dextran (70 kDa) was freshly prepared for each experiment in tap water.

3.3.3 *In vivo* GI transit

GI transit was assessed by measuring the distribution of a fluorescent marker along the length of the small intestine after an ingestion period. Mice were fasted 12 h prior to gastric gavage of FITC-dextran (0.1 mL of 10 mg mL^{-1}) given between 8-9 AM the following day. After 30 min, mice were euthanized and the stomach and small intestine were removed. The small intestine was cut into 6 segments (5 cm in length) with the duodenum as segment #1 and the most distal

ileum as segment #6. Each segment was flushed with 1.5 mL of phosphate buffered saline (PBS). PBS containing luminal content was then centrifuged (14,000 RPM for 10 min). The fluorescence of the supernatant from each segment was measured (485 nm excitation; 510 nm emission) on a plate reader (Fluoroskan Ascent/FL, Thermo Scientific, Rockford, IL). The fraction of FITC of each segment was calculated and this was used to calculate the geometric center (GC) value. The GC value does not include gastric emptying. The GC value is a weighted mean that includes the marker distribution and the distance traveled. The GC value was calculated using the following equation: [22]

$$\mathrm{GC} = \Sigma(\text{fraction of FITC per segment}) * (\text{segment number})$$

Gastric emptying was calculated as [(Total fluorescence – fluorescence in stomach)/(Total fluorescence)] x100.

The 5-HT_3 receptor antagonist alosetron (0.1 mg kg^{-1}) or saline was administered by intraperitoneal (i.p.) injection 30 min prior to gastric gavage of FITC-dextran. Following 30 min, the intestine was removed and the GC value and gastric emptying was calculated as described above.

3.3.4 Estrous cycle and sex hormone assays

The stage of the estrous cycle was identified in females used in the *in vivo* transit and longitudinal muscle contraction studies. Vaginal cytology using wet smears was performed to identify estrous cycle stage each day at 9 AM two weeks prior to sacrifice in order to establish regular cyclers and continuing until sacrifice in order to sacrifice mice in the correct stage.[23-25] All *in vivo* transit studies were performed during metestrus. This stage of the estrous cycle was chosen because 1) estradiol, the main estrogen, and progesterone modulate small intestinal motility in rats[26] and 2) estradiol and progesterone levels are not elevated or reduced during metestrus as compared to estrus and diestrus in the mouse.[27]

Sex hormones were measured in plasma. Briefly, blood was collected by cardiac puncture and centrifuged (4 ˚C) at 14,000 RPM for 10 min. Serum was removed and stored at -80 ˚C until analysis. Estradiol levels were measured in female plasma using a commercial estradiol enzyme-linked immunosorbent assay (ELISA) kit (CalBiotech, Spring Valley, CA) as this assay yielded the best overall performance compared to other commercially available kits.[28] Progesterone levels were measured in female plasma and testosterone levels were measured in male plasma using commercially available ELISA kits (BioVendor, Asheville, NC; CalBiotech, Spring Valley, CA, respectively). All assays were performed according to the manufacturer's instructions and measured using an Infinite M1000 Pro Microplate Reader (Tecan, Männedorf, Schweiz). Analysis was performed using a four parameter logistic curve (SigmaPlot 11.0, Systat Software, Inc., San Jose, CA, USA).

3.3.5 5-HT_3 reactivity of small intestinal longitudinal muscle in jejunal segments

5-HT_3 receptor function was determined by measuring the reactivity of jejunal longitudinal muscle to 5-HT in the presence of the 5-HT_3 antagonist, ondansetron. The jejunum of CD-fed and HFD-fed mice was excised and cut into 4 segments (ca. 1 cm in length) for each animal. Segments were hung in individual organ baths (20 mL) filled with warm oxygenated (37 °C, 95% O_2 +5% CO_2) Krebs buffer by attaching one end to a glass tissue holder and the other to an isomeric force-displacement transducer (FT03C, Grass Instruments, Inc.) with silk suture thread (LOOK 4-0 SP116). Tissues were placed under 1.0 g of tension and allowed to equilibrate for 20 min. Each organ bath was randomly assigned a drug treatment for the remainder of the experiment. The drug treatments used were: methysergide (1 μmol L^{-1}), a 5-HT_1, 5-HT_2, 5-HT_5 and 5-HT_7 receptor antagonist; 5-HT_3 receptor antagonist, ondansetron (0.1 μmol L^{-1}) + methysergide (1 μmol L^{-1}); and no treatment (i.e. 5-HT dose response curve without any antagonist). Methysergide was used to isolate 5-HT_3 receptors and methysergide addition

alone served as the control. Each drug treatment was added to a bath for 10 min prior to the first 5-HT dose. The 5-HT was applied at different doses (0.01 – 10 μmol L^{-1}) in 10 min intervals. Each 5-HT dose was added for 1 min to achieve maximum contraction followed by 2 rinses with Krebs buffer for washout. After the washouts, each drug treatment was added to the bath again for 10 min prior to the next 5-HT dose. Maximum longitudinal muscle contraction to acetylcholine (ACh; 100 μmol L^{-1}; 1 min) was measured before and after the 5-HT dose-response curve to normalize all 5-HT responses to ACh. The maximum ACh (average of ACh before and after) and 5-HT (for all doses) response (g) per tissue weight (g) was calculated and used to find the percent ACh response. Data are expressed as a percent of the maximum ACh response. Data were collected and analyzed using a Powerlab system and Chart software, respectively (ADI Instruments, Colorado Springs, CO).

3.3.6 HPLC measurements of 5-HT and 5-HIAA levels

Mucosal whole tissue levels of 5-HT and 5-HIAA and extracellular 5-HT levels were measured using HPLC with electrochemical detection. For whole tissue levels, segments of jejunum were removed and placed in Krebs buffer. Segments were cut along the mesenteric border and the mucosa was rinsed with Krebs buffer. The mucosal surface (~2 cm) was removed using a sharp scalpel and placed into a tissue homogenizer (2 mL) filled with ice cold 0.1 M perchloric acid (0.5 mL). The sample was then centrifuged (4 ˚C) at 14,000 RPM for 10 min. Supernatant was removed and stored at -80 ˚C until analysis. Protein analysis was performed using a DC™ Protein Assay kit (Bio–Rad Laboratories, Hercules, CA). For extracellular 5-HT levels, a Hamilton syringe was used to sample the Krebs buffer (150 μL) near to the mucosa surface (~500 μm away) using a micromanipulator in jejunal preparations used for CA experiments. Extracellular fluid was quickly mixed with 50 μL of ice cold 0.1 M perchloric acid and then centrifuged (4 ˚C) at 14,000 RPM for 10 min. The supernatant was then removed for HPLC analysis. Supernatant (20 μL) samples from whole tissue and extracellular fluid were injected

using an autosampler (ESA 542, Thermo-Fisher) maintained at 35 ˚C onto a ESA guard column (70-1972) in-line with a Thermo MD column (150 mm x 3.2 mm, 3 µm particle size) for separation. Detection was accomplished using an ESA 5011A analytical cell set to a potential of +200 mV. The mobile phase consisted of the following composition (mmol L^{-1}): 90 sodium phosphate, 50 citrate, 1.94 sodium octyl sulfate, 0.05 EDTA and 10 % acetonitrile and flowed at a rate of 0.6 mL min^{-1} (ESA 582). Results are presented as ng per mg protein and nmol L^{-1} for whole tissue and extracellular analyte levels, respectively.

3.3.7 Western blotting

Western blotting was performed on jejunal mucosal scrapes. Segments of jejunum (~1 cm) were removed, placed in Krebs buffer and cut along the mesenteric border. The mucosa was rinsed with Krebs buffer, removed using a sharp scalpel, flash-frozen in liquid nitrogen and stored at -80˚C until further analysis. For the analysis, mucosal scrapes were lysed using a mortar and pestle in Lysis buffer (62.5 mM Tris pH 6.8, 20% SDS, 5 mM EDTA, 10 mM NaF, 1 mM Na_3VO_4) containing a commercially available protease inhibitor cocktail (#P8340, Sigma-Aldrich). Tissue samples were sonicated and centrifuged (14,000 RPM for 12 min at room temperature). The supernatant was removed to measure total protein using a DC™ Protein Assay kit (Bio-Rad, Hercules, CA). The remaining pellet was resuspended with 1:1 Laemmli buffer (#1610737, Bio-Rad, Hercules, CA) containing β-mercaptoethanol (5% vol/vol; M6250; Sigma-Aldrich), boiled at 95-100 ˚C (5 min), aliquoted and frozen at -20 ^{o}C until further analysis. Protein (30 µg) separation was accomplished using a 4% SDS-PAGE stacking gel on top of a 10% SDS-PAGE running gel at 30 V for 30 min then increasing to 100 V for 1.5 h. After separation, protein was transferred to a polyvinylidene difluoride (PVDF) membrane (# IPVH00010, pore size 0.45 µm, EMD Millipore, Billerica, MA) overnight at 30 V. The following morning, membranes were blocked with 5-10% w/v non-fat dry milk in T-TBS (1% Tween-20, 20 mM Tris pH 7.5, 200 mM NaCl) for 1 h at room temperature. Membranes were then incubated

with primary antibodies for 2 h at room temperature. For SERT detection, a goat anti-SERT primary antibody (sc 1458, Santa Cruz, CA) was used at 1:800 dilution. For DAT detection a rabbit anti-DAT primary antibody (AB 2231, EMD Millipore, MA) was used at 1:2000 dilution. For LDH detection a rabbit anti-LDH primary antibody (SC 33781, Santa Cruz, CA) was used at 1:30,000 and 1:40,000 dilution for SERT and DAT, respectively. Next, membranes were washed 3 times for 10 min with T-TBS and incubated with horseradish-peroxidase-conjugated secondary antibodies for 1 h at room temperature and finally washed 3 times for 10 min with T-TBS. The secondary antibody used for SERT was donkey anti-goat (sc 2056, Santa Cruz, CA) at a 1:2000 dilution. Lactate dehydrogenase (LDH) protein levels were determined to control for loading, transfer and developing. For LDH detection, a rabbit anti-LDH primary antibody (SC 33781, Santa Cruz, CA) was used at 1:30,000 dilution. The secondary antibody for DAT and LDH was donkey anti-rabbit (sc 2313, Santa Cruz, CA) at a 1:8000 and 1:30,000 dilution, respectively. A pre-stained protein ladder (#26616, Thermo Fisher Scientific Inc., Waltham, MA, USA) was used to determine apparent molecular weights. Immunoreactivity was detected using an enhanced chemiluminescence kit (#RPN2232, GE Healthcare, Buckinghamsire, UK). Densitometry was used to measure protein levels normalized to LDH and images were analyzed using ImageJ 1.48v software (http://imagej.nih.gov/ij).

3.3.8 SERT mRNA expression

Quantitative real-time PCR (qRT-PCR) was used to quantify mRNA encoding SERT in jejunal mucosal scrapes. Segments of jejunum (~1 cm) were removed and cut along the mesenteric border. The mucosa was rinsed with Krebs buffer, removed using a sharp scalpel, flash-frozen in liquid nitrogen and stored at -80 ˚C until further analysis. Tissue digestion and RNA isolation were performed using MELT^{TM} Total Nucleic Acid Isolation System Kit according to the manufacturer's instructions (AM 1983, Ambion, Carlsbad, CA). Nucleic acid concentration and purity was determined using Nanodrop 2000c (Thermo Fisher Scientific, Wilmington, Delaware

USA). Samples of cDNA were generated by reverse transcription using a High Capacity RNA-to-cDNA kit according to the manufacturer's instructions (4387406; Applied Biosystems, Carlsbad, CA). Resultant cDNA was used for qRT-PCR and was performed using TaqMan reagents on a 7500 FAST Real-time PCR System (Applied Biosystems, Carlsbad, CA). Amplifications were performed in a final volume of 20 μL prepared with TaqMan Fast Advanced master mix according to manufactures instructions (4444556, Applied Biosystems). cDNA synthesis reactions were ran with samples that did not contain reverse transcriptase as a control for genomic DNA contamination. Samples and controls were run in triplicate with TaqMan Gene Expression assays (Rn01462137_m1 for SERT, Rn01775763_g1 for GAPDH, Life Technologies). Measurements were analyzed using the $\Delta\Delta C_T$ method. SERT mRNA levels were expressed as a fold change and normalized to glyceraldehyde 3-phosphate dehydrogenase (GAPDH). GAPDH is a housekeeping gene that was found not to be altered from an obesity-causing diet.[20]

3.3.9 Immunohistochemistry and quantification of EC cells

Segments of jejunum were cut along the mesenteric border, stretched gently (~1 cm^2) and pinned with the mucosal surface facing upwards in a Sylgard® lined Petri dish. The segment was gently washed with Krebs buffer and fixed with 10% neutral buffered formalin (pH 6.9 - 7.1) overnight (4 ˚C). 10% neutral buffered formalin-fixed specimens were embedded in paraffin and sectioned on a rotary microtome at 4-5 m. Sections were placed on slides (4 sections per slide with 40 μm between each section) coated with 2% 3-Aminopropyltriethoxysilane and dried overnight (56 C). Slides were subsequently deparaffinized in xylene and hydrated through descending grades of ethyl alcohol to distilled water. To adjust pH, slides were placed in Tris Buffered Saline (TBS, pH 7.4) (Scytek Labs, Logan, UT) for 5 min. Following TBS, slides underwent heat induced epitope retrieval utilizing Citrate Plus (pH 6.0) (Scytek Labs, Logan, UT) for 30 min in a vegetable steamer at 100°C followed by 10 min at room temperature and then underwent several changes of distilled water. Endogenous enzyme activity was blocked

with a 3% hydrogen peroxide/methanol solution (1:4) for 30 min followed by tap and distilled water rinses. Following, standard avidin-biotin complex (ABC) staining protocol was performed at room temperature on a DAKO Autostainer. All staining steps were followed by rinses in TBS with Tween 20 (Scytek Labs, Logan, UT). Blocking for non-specific protein was accomplished using normal goat serum (Vector Labs, Burlingame, CA) for 30 minutes. Sections were then incubated with avidin-biotin blocking system for 15 min (Avidin D, Vector Labs, Burlingame, CA; d-Biotin, Sigma, St. Louis, MO). Primary antibody slides were incubated for 1 h with either polyclonal rabbit anti-5-HT diluted at 1:40,000 (S5545, Sigma, St. Louis, MO) or rabbit anti-DAT (Ab2231, Millipore) diluted at 1:1350 in normal antibody diluent (NAD) (Scytek Labs, Logan, UT). Next, slides were incubated for 30 min in biotinylated goat anti-rabbit IgG prepared in NAD (11.5 g/ml) and then incubated for 30 min in Ready-to-use Vector Elite Peroxidase Reagent (Vector Labs, Burlingame, CA). Reaction development was performed by incubating slides for 15 min in Vector® NovaRED™ peroxidase chromogen (Vector Labs, Burlingame, CA) followed by counterstain in Gill Hematoxylin (Thermo Fisher, Kalamazoo, MI) for 15 s, differentiation, dehydration, clearing and finally mounting with synthetic mounting media.

Sections were viewed using a Nikon microscope and images were acquired using SPOT Advanced software (Spot Imaging Solutions, Sterling Heights, MI, USA). The number of intact villi and the number of 5-HT positive cells located in the epithelium (crypt-villus axis) in intact villi was counted in the four sections of one slide (4 sections per 1 animal) by a blinded observer. The ratio of the total number of 5-HT positive cells located in the epithelium of the crypt-villus axis in intact villi to the total number of intact villi was calculated for individual sections. This ratio was averaged over the four sections and that average was used for each animal. The number of EC cells is expressed per 10 villus-crypt axes.

3.3.10 Boron-doped diamond microelectrode

Details of the preparation and characterization of the diamond microelectrodes have been reported elsewhere.[29-32] After growth, the diamond-coated wire was cut in the center producing two conically-shaped diamond microelectrodes. The cut end of each wire was connected to a copper wire using a dab of super glue to enhance the mechanical strength and then with conducting silver epoxy for electrical connection. The end of the diamond-coated wire was then sealed by carefully melting the end of a polypropylene pipette tip using the heating coil of a micropipette puller. The resulting exposed diamond microelectrode was conical in shape with a tip diameter of about 10 μm and an exposed length of 300-700 μm. In this preparation, the exposed length is difficult to reproducibly control. Cyclic voltammetry was then used to determine which microelectrodes are suitable for the *in vitro* continuous amperometry (CA) measurements. This was done with several aqueous redox systems, including a 10 μmol L^{-1} 5-HT standard solution, using a CH Instruments electrochemical workstation (Model 600D, Austin, TX). All measurements were made in a single-compartment glass electrochemical cell. A Pt wire served as the counter electrode and a commercial, no-leak, Ag/AgCl electrode (3 M KCl) was used as the reference. The cyclic voltammetric peak oxidation potential (E_p^{ox}) and peak current (i_p^{ox}) for 5-HT (10 μmol L^{-1}) prepared in Krebs buffer (pH 7.4) were measured before and after the CA measurements to assess the stability of the microelectrode response. The cyclic voltammetric E_p^{ox} was also used to determine the fixed potential to use for detection in the CA measurements. For most diamond microelectrodes, there was very little change in either the E_p^{ox} or i_p^{ox} for the 5-HT standard solution after CA measurements (data not shown). This confirmed the excellent response stability of diamond in this complex biological environment.

3.3.11 Continuous amperometric (CA) measurements of 5-HT uptake

A segment of jejunum was cut along the mesenteric border (~ 1 cm^2), stretched gently and pinned (stainless steel, 0.2 mm diameter, 26002-20, Fine Science Tools, Foster City, CA)

with the mucosal surface facing upwards in a Sylgard® lined flow bath (~ 6 mL). Oxygenated Krebs buffer solution, kept at room temperature, flowed over the tissue at a rate of 2 mL min^{-1} using a peristaltic pump (Minipuls 2, Gilson, Middleton, WI). Precise positioning of the diamond microelectrode was accomplished using a micromanipulator (MM33, Fine Scientific Tools, Foster City). Villi and diamond microelectrode positioning were visualized using an upright microscope (Model SMZ1000, Nikon, USA). Experiments commenced after a 30 min equilibration period. Measurements were made in a Faraday cage to minimize electrical noise.

For the CA experiments, 5-HT detection was accomplished at +0.8 V vs. Ag/AgCl (3 M KCl) using a ChemClamp potentiostat (Dagan Corp., Minneapolis, MN, USA). The analog current from the potentiostat was captured and digitally converted with an e-corder hardware unit (eDAQ Inc., Colorado Springs, CO, USA) at a sampling rate of 200 points s^{-1}. The current was low-pass filtered (1 kHz filter) prior to digitization. Current recordings were generated on-line using Chart software. A home-made Ag/AgCl electrode served as the counter and reference in a two-electrode measurement configuration. The reference electrode was positioned in the flow bath somewhat removed from the position of the working electrode and tissue. CA measurements consisted of current approach curves in which the electrode distance in relation to the mucosal surface was decreased in a step-wise fashion. Electrode distances used were 750, 500, 250, 100, 50 and 10 µm away from the mucosal surface. In order to determine electrode distance from the mucosal surface, the electrode was first positioned such that it gently touched the villus, then it was retracted to a distance of 2000 µm that served as the distance for background current measurements. The background current was measured at 2000 µm as at this distance the current was unaffected by 5-HT release due to dilution effects. When the background current was stable, the recording of current-approach curves commenced. For each current measurement, the electrode was positioned at a calibrated distance for ca. 40 - 60 s. Within this time window, a stable current was reached. The current magnitude at each electrode distance was recorded by averaging the current over the last 20 -

30 s of the period and subtracting from this the average background current measured at the 2000 μm distance. The natural log (*ln*) of the current at each electrode distance was plotted as a function of the distance. A linear fit of the data was performed and the slope was determined in order to assess 5-HT uptake as previously described.[33, 34] Fluoxetine (1 μmol L^{-1}), a selective 5-HT reuptake inhibitor (SSRI), cocaine (10 μmol L^{-1}), a SERT, norepinephrine (NET) and dopamine transport (DAT) inhibitor, and GBR 12909 (0.1 μmol L^{-1}), a DAT inhibitor, were used to assess SERT and DAT function. Fluoxetine, cocaine and GBR 12909 are not electroactive at the potential used for detecting 5-HT (data not shown). A solution containing any of the drugs used was flowed across the tissue for 5 min before a current approach curve was recorded. The drug was also present during the measurement. Measurements were made before (Krebs buffer) during application and after washout (20 min) of the drug. All drugs evoked a reversible increase in the 5-HT oxidation current due to an increase in the 5-HT extracellular concentration. In our studies, SERT function was assessed by comparing the slope of the *ln* current (pA) vs. the electrode distance plots (μm) with and without drug addition.[34] A decrease in the slope indicated reduced 5-HT uptake.[34]

3.3.12 Statistical analysis

All data analysis was performed using GraphPad Prism software (GraphPad Software, Inc., La Jolla, CA). Two group comparisons were made using an unpaired Student's *t*-test for parametric data. For data not normally distributed, a log transformation of the data or a Mann-Whitney test was performed. For CA experiments, comparisons between measurements made in Krebs buffer and measurements made in the presence of a drug were made using a paired Student's *t*-test. For all fraction of fluorescence vs. intestinal segment number plots, comparisons were made using a two-way ANOVA. For all comparisons, $P < 0.05$ was considered statistically significant. Data are reported as mean $\pm$ S.E.M.

3.4 RESULTS

3.4.1 Male and female C57BL/6J mice developed DIO on HFD

Male and female C57BL/6J mice on a HFD (60 kcal %) diet developed an obese phenotype compared to mice placed on a CD (10 kcal %). Male (Figure 10A) and female (Figure 10B) mice fed a HFD developed greater body weights compared to controls at 11-15 weeks spent on the diets (n = 4-10, $P < 0.05$). In addition, we determined the abdominal fat pad weight encompassing the fat pads surrounding the reproductive organs and retroperitoneal fat pads as an index of obesity. Both HFD-fed male (Figure 10C) and female (Figure 10D) mice had greater abdominal fat pad weights at the time of sacrifice (13-15 weeks on diets) compared to CD-fed mice (n = 8; $P < 0.05$).

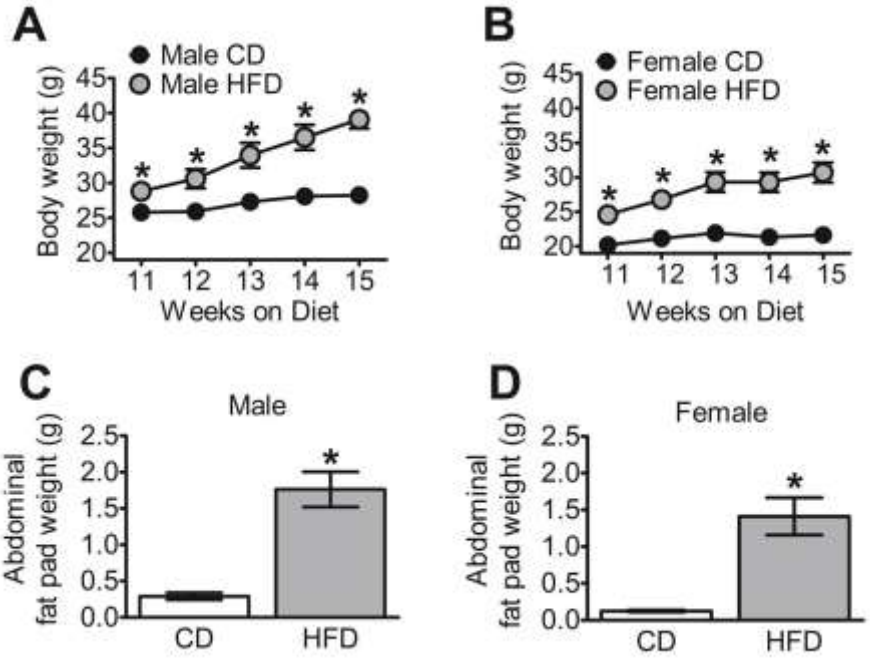

Figure 10. Male and female mice (C57BL/6J) developed DIO with time when fed a HFD. HFD-fed (60 kcal %) male and female body weights measured at a number of weeks spent on the diet (11-15 weeks; A and B, respectively) and abdominal fat pad weights at time of sacrifice (13-15 weeks on diet; C and D, respectively) were greater compared to their respective CD-fed (10 kcal %) mice. Data are mean ± SEM. *$P < 0.05$, N = 4–10.

3.4.2 Gastric emptying and small intestinal transit were altered in HFD-fed mice

In HFD-fed males, gastric emptying was increased compared to CD-fed males (n = 7 – 8, P < 0.05, Figure 11A). Gastric emptying was similar between CD-fed and HFD-fed females (n = 8, Figure 11A). The GC value was increased in HFD-fed compared to CD-fed males (n = 7 – 8, P < 0.05, Figure 11B). HFD-fed and CD-fed female mice had similar GC values (n = 8, P > 0.05, Figure 11B). In CD-fed mice, females had a greater GC value compared to males (P < 0.05, Figure 11B). HFD increase intestinal permeability,[35] however, we found no detectable fluorescence in the plasma from either HFD-fed or CD-fed male or female mice (data not shown). Therefore, differences in marker progression or intensity were not due to leakage from the gut lumen. To visualize patterns of FITC-dextran distribution along the small intestine, we plotted the fraction of fluorescence intensity as a function of the intestinal segment number. In HFD-fed males, a large fraction of marker was found in a more distal segment compared to CD-fed males demonstrating that transit was increased in HFD-fed males (P < 0.05, Figure 11C). In addition, the transit pattern was bimodal in HFD-fed males. In HFD-fed females, the fraction of fluorescence vs. intestinal segment number was different from CD-fed females. FITC-dextran was distributed equally among the middle portion of the small intestine in HFD-fed females whereas the greater majority of fluorescence was found in segment #4 in CD-fed females (P < 0.05, Figure 11D). Although there was no significant change in the GC value, HFD-fed females had altered transit of FITC-dextran compared to CD-fed females.

3.4.3 Sex specific effect of alosetron on GI transit

Alosetron increased gastric emptying in CD-fed males compared to saline-treated CD-fed mice (n = 8, P < 0.05, Figure 12A). Alosetron treatment did not change gastric emptying in HFD-fed males and females as well as CD-fed females compared to respective saline-treated mice (n = 6 - 8, Figure 12A). Alosetron treatment decreased the GC value in CD-fed females compared to saline-treated mice (n = 6 - 8, P < 0.05, Figure 12B). In HFD-fed females, HFD-fed

males and CD-fed males, alosetron did not change the GC value compared to their respective saline-treated mice (n = 6 - 8, P > 0.05, Figure 12B). The fraction of fluorescence as a function of segment number plot showed that alosetron treatment in either CD-fed (Figure 12C) or HFD-fed (Figure 12D) males did not change the marker distribution. However, when the alosetron-treated HFD-fed male curve was overlaid with saline-treated CD-fed male curve (Figure 12E), it was apparent that the marker was no longer present in the more distal segment #5 and the bimodal distribution was eliminated as compared to the plot in Figure 11C. This suggests that

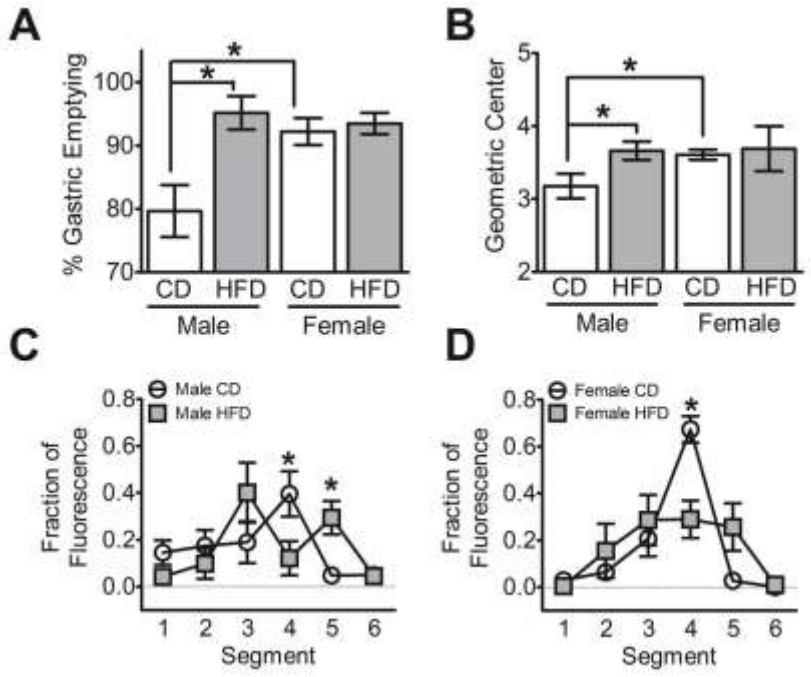

Figure 11. ***In vivo*** **gastric emptying and small intestinal transit was increased in male HFD-fed mice.** Gastric emptying and small intestinal transit were assessed 30 min after gastric gavage of FITC-dextran. (A) Gastric emptying was increased in HFD-fed male and CD-fed female compared to CD-fed male mice. (B) The GC value was greater in HFD-fed compared to CD-fed males and in CD-fed females compared to CD-fed males, indicating increased transit in these groups. (C) Fraction of fluorescence as a function of segment number describes FITC-dextran distribution along the length of the intestine where HFD-fed males displayed increased transit compared to CD-fed males. (D) HFD-fed females presented a flattened distribution of fluorescence where FITC-dextran was present in equal amounts within the middle portion of the small intestine compared to CD-fed females where the greater majority of FITC-dextran was found in segment 4 with little in other segments. Data are mean ± SEM. *P < 0.05, N = 7-8.

small intestinal transit was modestly reduced by alosetron in HFD-fed males although the GC did not detect this difference. The curve of the fraction of fluorescence versus segment number plot was leftward shifted in alosetron-treated CD-fed females compared to saline-treated CD-fed females (Figure 12F) demonstrating that transit was slower. This was similar for alosetron-treated HFD-fed females (Figure 12G) even though the GC measurement did not detect this difference (P = 0.17). When the plots of the fraction of fluorescence versus segment number of alosetron-treated HFD-fed females were overlaid with that of saline-treated CD-fed females, the curves overlapped (Figure 12H) suggesting that alosetron normalized marker distribution in HFD-fed females.

3.4.4 5-HT_3 receptor was unchanged in HFD-fed mice

To determine if 5-HT_3 receptor signaling is different in HFD-fed female or male mice compared to CD-fed mice, we measured 5-HT concentration response curves (0.01-10 μmol L^{-1}) for longitudinal muscle contraction in jejunal segments in the absence and presence of the 5-HT_3 receptor antagonist ondansetron (0.1 μmol L^{-1}). Irrespective of diet, blocking 5-HT_3 receptors caused a significant reduction of the 5-HT induced contractions when non-5-HT_3 receptors were blocked with methysergide (P < 0.05) in male (Figure 13A) and female (Figure 13B) jejunum. Ondansetron produced a selective reduction in contractions caused by higher 5-HT concentrations (1-10 μmol L^{-1}) while methysergide inhibited contractions caused by lower concentrations of 5-HT (< 1 μmol L^{-1}). Interestingly, 5-HT induced contractions in female CD-fed jejunum, but not female HFD-fed jejunum, were insensitive to methysergide. 5-HT (0.3 μmol L^{-1}) produced a greater muscle contraction in the jejunum from male CD-fed compared to female CD-fed mice. 5-HT (3 μmol L^{-1}) produced a greater muscle contraction in the jejunum from female HF-fed compared to CD-fed mice (P = 0.051).

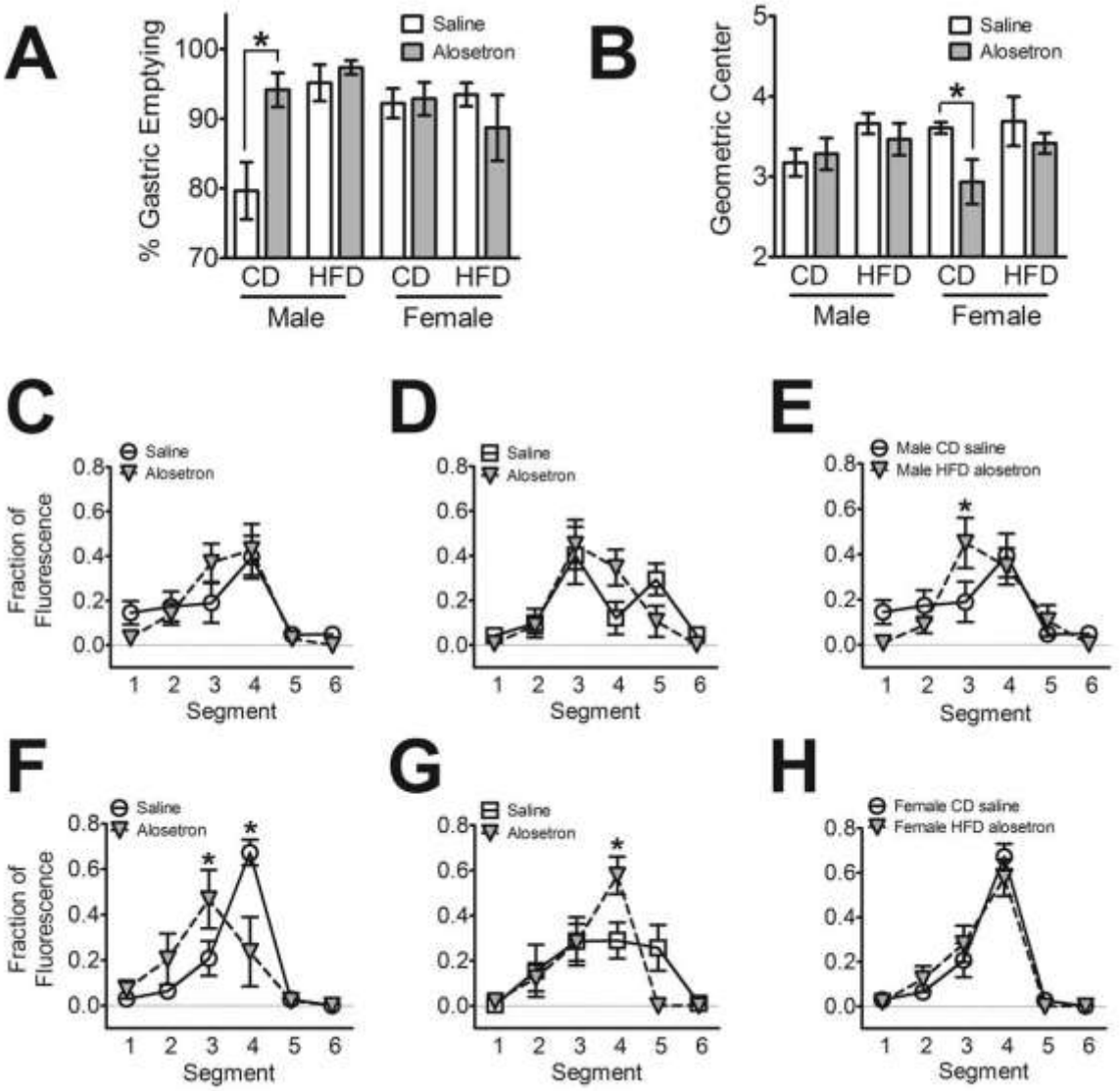

Figure 12. Alosetron, a 5-HT$_3$ receptor antagonist, changed gastric emptying and GC in CD-fed mice. Following 30 min after intraperitoneal (i.p.) administration of alosetron (0.1 mg kg^{-1}), mice were gavaged with FITC-dextran. Gastric emptying and the GC value were measured after an additional 30 min. (A) Alosetron treatment increased gastric emptying in CD-fed males compared to saline-treated mice. (B) The GC value was decreased in alosetron-treated CD-fed females compared to saline-treated controls indicating transit was reduced when blocking 5-HT$_3$ receptors. Alosetron did not alter the distribution of FITC-dextran along the length of the small intestine in either CD-fed (C) or HFD-fed (D) males. (E) Alosetron-treated HFD-fed males share a similar pattern of FITC-dextran distribution along the small intestine as saline-treated CD-fed males. Alosetron-treated CD-fed (F) and HFD-fed (G) females show a leftward shift of the fraction of fluorescence along the small intestine compared to saline-treated CD-fed and HFD-fed females, respectively. (H) The pattern of FITC-dextran distribution in alosetron-treated HFD-fed females overlies that of saline-treated CD-fed females. Data are mean ± SEM. *P < 0.05, N = 6 - 8

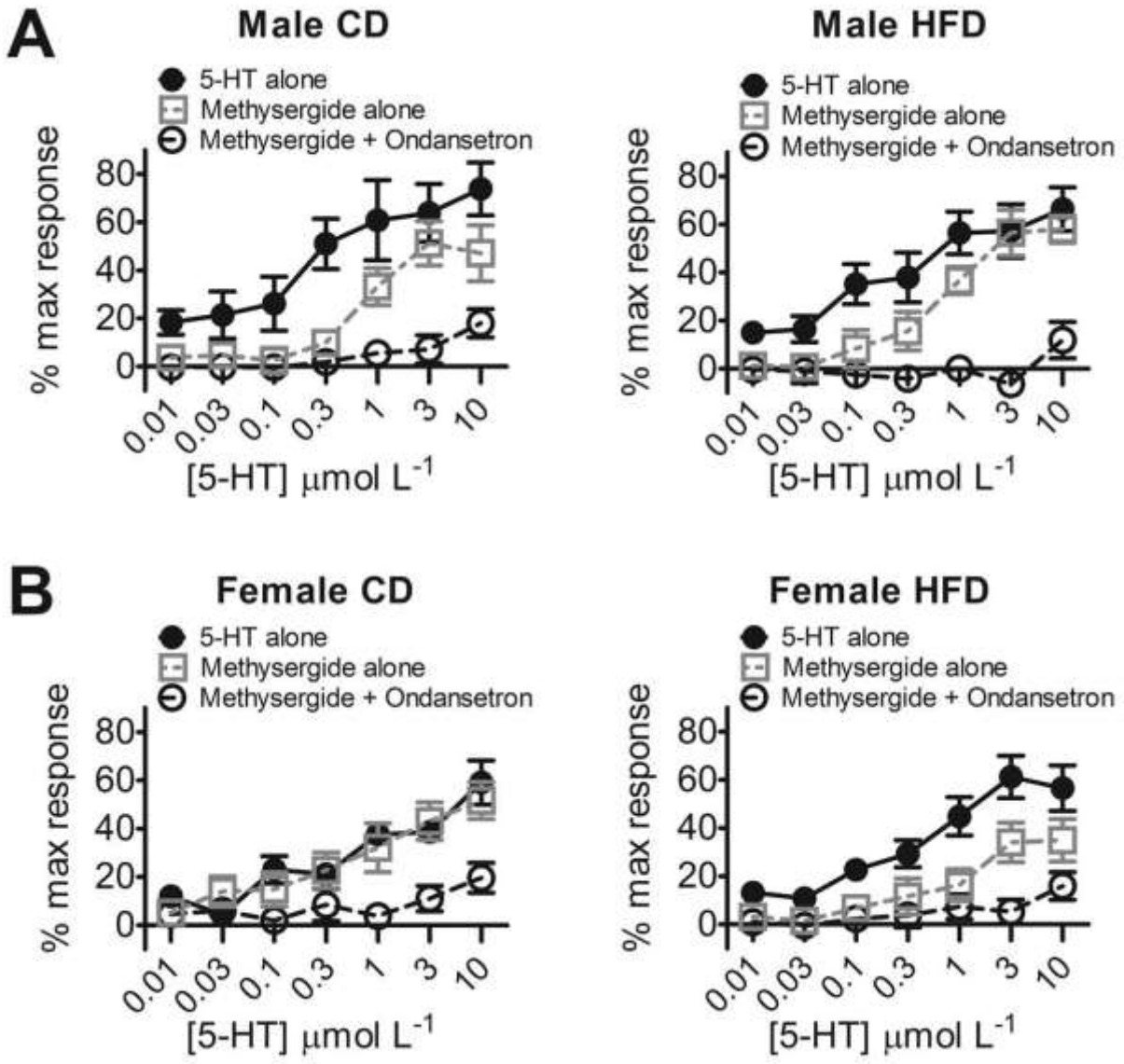

Figure 13. Jejunal 5-HT$_3$ receptor function is similar in HFD-fed and CD-fed mice. 5-HT (0.01-10 μmol L^{-1}) generated longitudinal muscle contractions in jejunal segments (black circles). The 5-HT$_3$ receptor antagonist ondansetron (0.1 μmol L^{-1}) in the presence of methysergide (1 μmol L^{-1}) (black open circles) produced a similar inhibition of 5-HT-induced contractions at the greatest 5-HT doses in HFD-fed and CD-fed jejunal segments in both males (A) and females (B). Methysergide was used as a control to block non-target 5-HT receptors (grey open squares). Measurements are expressed as a percentage of maximum contraction by ACh (100 μmol L^{-1}). Data are mean ± SEM, *n* = 6-8.

3.4.5 HFD altered 5-HT uptake in males

A schematic of the diamond microelectrode and the mucosal preparation used in CA measurements is shown in Figure 14A. Figure 14B shows a representative voltammogram of 5-HT (10 μmol L^{-1}) prepared in Krebs buffer against the voltammogram of Krebs buffer alone. Electrode potential was scanned from -0.2 to 1 V at a rate of 0.1 V s^{-1}. The peak oxidation potential (E_p^{ox}) of 5-HT is ca. 0.65 V. At this voltage, 5-HT molecules from nearby EC cells are oxidized at a mass-transport controlled rate.

Current-approach curves were generated at +0.80 V, based on the E_p^{ox} (Figure 14B). The current increased as the electrode was positioned closer to the mucosal surface (750-10 μm). Figure 14C shows current approach curves made before (Krebs buffer, pH = 7.4), during application and after washout of fluoxetine (1 μmol L^{-1}, 5 min). Two consecutive current approach curves (only one of which is shown) were made under control conditions where only Krebs buffer flowed over the tissue. Fluoxetine (1 μmol L^{-1}) applied for 5 min caused in increase in the oxidation current at all electrode distances. Two consecutive curves were made in the presence of fluoxetine and both traces were reproducible in terms of the current magnitudes. Fluoxetine was washed from the tissue (20 min) and oxidation currents returned to Krebs buffer only levels. Current magnitudes were plotted as a function of tissue-electrode distance (Figure 14D) and the best-fit line to the *ln* current vs. electrode distance plot (Figure 14E) was used to obtain the slope, a measure of 5-HT uptake.

Fluoxetine decreased 5-HT uptake (i.e. slope) in jejunal tissues from male CD-fed (n = 9, P < 0.05), but not HFD-fed mice (n = 9, P > 0.05, Figure 15A). In jejunal tissues from female CD-fed and HFD-fed mice, fluoxetine decreased 5-HT uptake (n = 6, P < 0.05, Figure 15A). These findings indicate that SERT function was impaired in the jejunum from male HFD-fed mice, but unchanged in female HFD-fed mice.

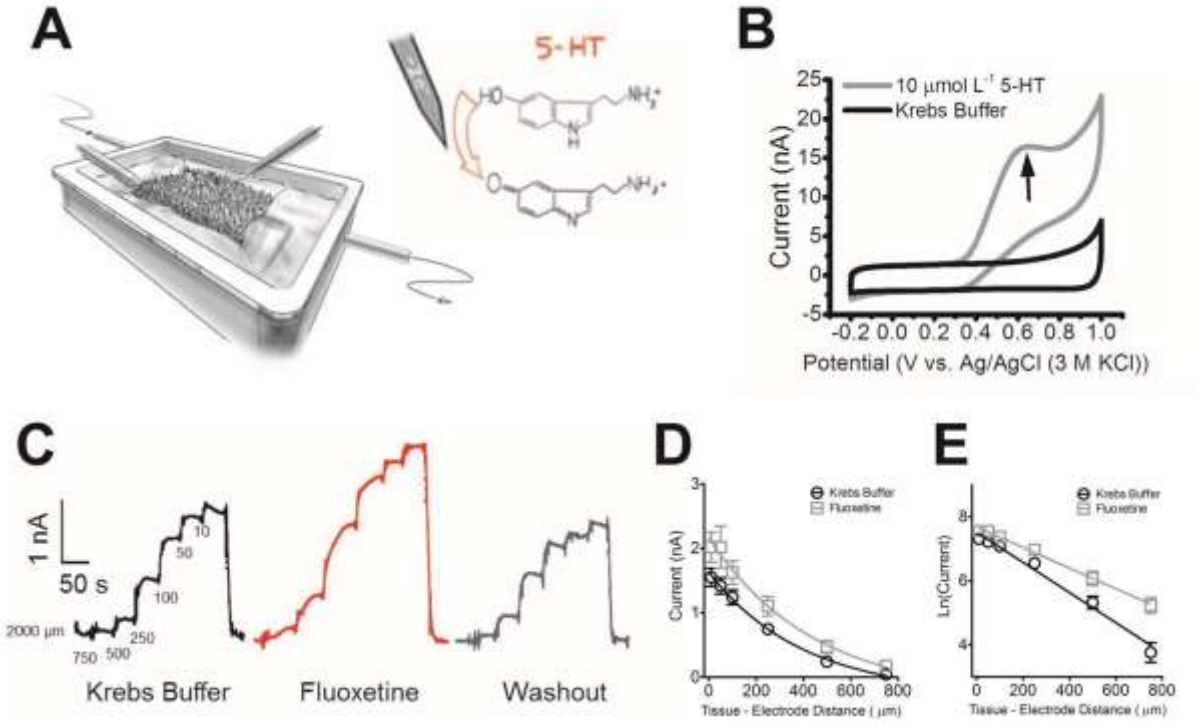

Figure 14. Continuous amperometry (CA) method for 5-HT uptake in jejunal tissues. (A) Schematic showing the flow bath housing the jejunal preparation and diamond microelectrode position at the mucosal surface. (B) Representative cyclic voltammogram of 5-HT (10 µmol L^{-1}) made in Krebs buffer (grey line) and in Krebs buffer alone (black line). The E_p^{ox} of 5-HT is ca. +0.65 V (black arrow). Scan rate was 0.1 V s^{-1}. (C) Current approach curves made from current measurements obtained at varying electrode distances (750 – 10 µm) before (Krebs buffer; pH = 7.4), during and after (washout) application of the SSRI, fluoxetine (1 µmol L^{-1}; 5 min), to determine if increases in current magnitude at each electrode distance were fluoxetine-dependent. Fluoxetine produced a reversible increase in 5-HT oxidation currents. (D) Current vs. tissue-electrode distance plots in which the current magnitude plotted against a specific tissue-electrode distance was calculated from the difference in current magnitude from an individual tissue-electrode distance and the current measured within the bulk media (2000 µm). (E) Representative natural log (ln) of the current magnitude (pA) pictured in (D) was plotted against tissue-electrode distances with measurements made in Krebs buffer (black squares) and in the presence of fluoxetine (grey squares). The slope is a measure of 5-HT uptake and fluoxetine reduces the slope (i.e. reduces 5-HT uptake). Data are mean ± S.E.M.

3.4.6 HFD altered extracellular 5-HT levels and SERT expression in females

To investigate further how a HFD altered intestinal serotonergic dynamics, we measured extracellular 5-HT near to the mucosa surface, mucosal SERT protein, mucosal SERT mRNA levels and whole-tissue 5-HIAA levels in the jejunum. Extracellular 5-HT levels were found to be similar between male CD-fed and HFD-fed mice (*n* = 15, Figure 15B). Extracellular 5-HT

levels were reduced in female HFD-fed compared to CD-fed mice (n = 10, P < 0.05, Figure 15B). Extracellular 5-HT levels were greater in tissues from female CD-fed compared to male CD-fed mice (P < 0.05).

Whole tissue 5-HIAA levels were similar in jejunal mucosal scrapes from male HFD-fed and CD-fed mice (n = 15, Figure 15C). Whole tissue 5-HIAA levels were greater in female HFD-fed compared to CD-fed jejunal mucosa, although this did not reach significance (P = 0.058, Figure 15C). Regardless of diet, whole tissue 5-HIAA levels were greater in females compared to males (P < 0.05, Figure 15C).

Western blotting for SERT protein levels in jejunal mucosal scrapes revealed a single band at the apparent molecular weight of ca. 100 kDa and a LDH band at 35 kDa (Figure 15D). The 100 kDa SERT band was absent in secondary antibody only controls (data not shown) and was absent in SERT knock-out (KO) rat small intestine compared to wildtype (WT) controls (data not shown). In male jejunal mucosa, the ratio of SERT to LDH was similar between CD-fed and HFD-fed (n = 8, Figure 15E), but jejunal mucosa from female HFD-fed mice had greater SERT protein levels compared to tissues from female CD-fed mice (n = 8, P <0.05, Figure 15E).

To determine if the increase in SERT protein levels in HFD-fed females was dependent on an increase in SERT gene expression, we determined SERT mRNA levels. Expression of SERT mRNA levels were similar between jejunal mucosa from female HFD-fed and CD-fed mice (n = 8, P > 0.05, Figure 15F).

3.4.7 HFD does not alter EC cell number or mucosal 5-HT levels

We measured the number of 5-HT positive cells within the epithelial layer (i.e. EC cells) along the crypt-villus axis (per 10 villi) in the jejunum of mice (Figure 16A) to distinguish between 5-HT positive mast cells[36] located in the lamina propria in stained paraffin-embedded sections. EC cell number was similar in HFD-fed and CD-fed male jejunum and HFD-fed and

CD-fed female jejunum (n = 10 for each, P > 0.05, Figure 16B). Control-fed female compared to control-fed male jejunum had more EC cells (P < 0.05, Figure 16B).

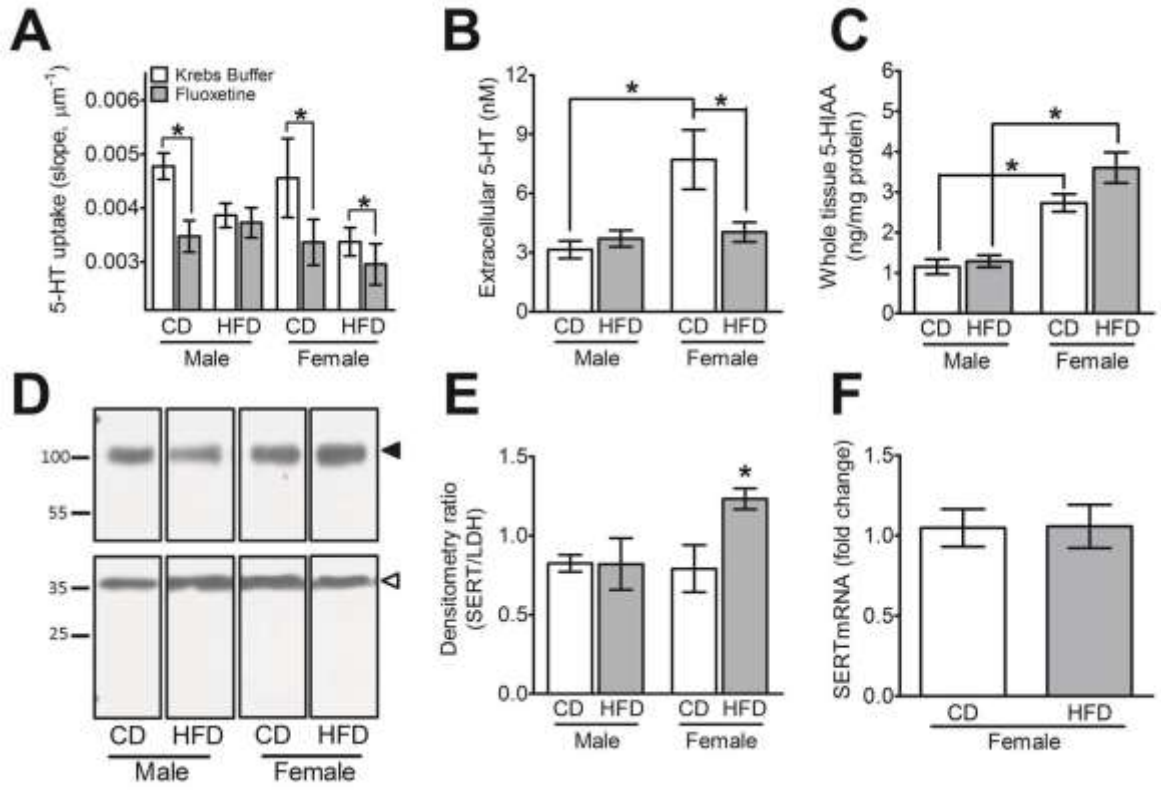

Figure 15. Jejunal SERT function and expression are altered in HFD-fed mice. (A) Continuous amperometric measurements in the presence of fluoxetine (1 µmol L^{-1}) reduced 5-HT uptake (slope) in CD-fed, but not HFD-fed male jejunal tissues (n = 8) compared to measurements made in Krebs buffer (control conditions). (B) Extracellular 5-HT levels sampled using a Hamilton syringe approximately 500 µm from the mucosa and measured using HPLC were reduced in HFD-fed compared to CD-fed female jejunum (n = 10 for each) and increased in CD-fed female compared to CD-fed male jejunum (n = 15). Extracellular 5-HT levels in CD-fed and HFD-fed male jejunum (n = 15) were similar. (C) Whole tissue 5-HIAA levels in jejunal mucosal scrapes measured using HPLC were similar in HFD-fed compared to CD-fed males (n = 15) and were slightly greater in HFD-fed compared to CD-fed females (n = 10), although not significant (P = 0.058). (D) Representative Western blot showing SERT protein levels in jejunal mucosal scrapes from female and male CD-fed and HFD-fed mice. SERT protein was found at the apparent MW of approximately 100 kDa (closed arrow) and LDH at 35 kDa (open arrow). (E) The densitometry ratio of SERT protein to LDH was increased in HFD-fed compared to CD-fed females where SERT/LDH was not altered in HFD-fed compared to CD-fed males (n = 8 for each). (F) SERT mRNA expressed as a fold change where SERT was normalized to GAPDH was similar in CD-fed and HFD-fed female jejunal mucosal scrapes (n = 8). Data are mean ± SEM, *P < 0.05.

Whole-tissue 5-HT levels in jejunal mucosal scrapes were similar in HFD-fed and CD-fed male jejunum (n = 15, P > 0.05, Figure 16D) and HFD-fed and CD-fed female jejunum (n = 10, P > 0.05, Figure 16C). Whole-tissue 5-HT levels were greater in females compared to males regardless of diet (P < 0.05).

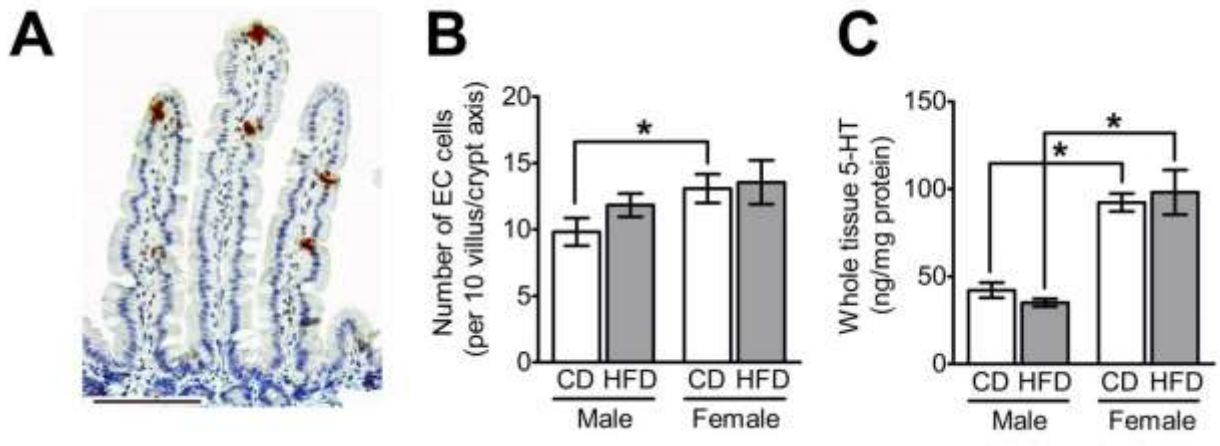

Figure 16. Mucosal 5-HT levels in the jejunum are sex-dependent, but diet-independent. (A) Representative image of EC cells within the epithelial layer along the crypt-villus axis of the jejunal mucosa. The EC cells were identified (red) by immunohistologic staining using anti-5-HT antibody of thin (4-5 um) sections from paraffin-embedded jejunum. Scale bar is 100 µm. (B) The number EC cells was unchanged with respect to diets, but were greater in CD-fed females compared to CD-fed males (n = 10). (C) Whole tissue 5-HT levels in jejunal mucosal scrapes measured using HPLC with electrochemical detection were unchanged with respect to diets in either males (n = 15) or females (n = 10), but were greater in females compared to males independent of diet. Data are mean ± SEM, *P < 0.05.

3.4.8 5-HT is cleared by DAT in HFD-fed male jejunum

To determine if other monoamine transporters compensate for the SERT dysfunction in the male HFD-fed jejunum, we used cocaine (10 µmol L^{-1}) in our CA experiments. Cocaine decreased 5-HT uptake (i.e. slope) in jejunal tissues from male CD-fed mice (cocaine = 0.0031 ± 0.0003 μm^{-1} vs. Krebs buffer = 0.0045 ± 0.0005 μm^{-1}, respectively, n = 7, P < 0.05). Cocaine blocked 5-HT uptake in tissues from male CD-fed mice to a similar extent as fluoxetine as determined by the percentage change in the slope from Krebs buffer (-28.9 ± 4.1%, n = 9 vs. -

29.6 ± 5.2%, n = 7, respectively) confirming that SERT was mainly responsible for clearing 5-HT. In tissues obtained from male HFD-fed mice, cocaine reduced slightly 5-HT uptake (cocaine = 0.0027 ± 0.0002 μm^{-1} vs. Krebs buffer = 0.0031 ± 0.0002 μm^{-1}, n = 13, $P < 0.05$). The DAT antagonist GBR 12909 (0.1 $\mu mol\ L^{-1}$) did not change 5-HT uptake in tissues from male CD-fed mice (n = 5, Figure 17A). Conversely, GBR 12909 reduced 5-HT uptake in jejunal tissues obtained from male HFD-fed mice (n = 5, $P < 0.05$).

We next determined if DAT protein levels were increased in HFD-fed male jejunum mucosa using Western blot. The anti-DAT antibody revealed two predominant bands at the apparent molecular weights of ca. 60 and 100 kDa (Figure 17B). These bands were absent in secondary antibody only controls (Figure 17C). Mucosal scrapes did not include the muscularis propria containing the myenteric plexus nor the submucosal plexus as determined by histologic examination of hematoxylin and eosin stained paraffin-embedded sections (data not shown). The ratio of DAT/LDH was greater for the 100 kDa band and for the 60+100 kDa combined (n = 7, P <0.05, Figure 17D), but not the 60 kDa band alone in HFD-fed males.

Using the same anti-DAT antibody, immunohistochemistry analysis revealed DAT-immunoreactivity in paraffin-embedded sections of jejunal mucosa in the lamina propria and concentrated at the apical side of enterocytes (Figure 17E). As a positive control, DAT-immunoreactivity was observed in the myenteric and submucosal plexuses (Figure 17G). DAT-immunoreactivity was absent in sections stained in the absence of primary antibody (Figures 17F and 17H).

3.4.9 HFD did not change plasma sex hormone levels in males or females

Estradiol and progesterone levels in HFD-fed and CD-fed females were similar (n = 10 for each, $P > 0.05$, Figure 18A, B). Similarly, testosterone levels in HFD-fed and CD-fed males were similar (n = 8 for each, $P > 0.05$, Figure 18C).

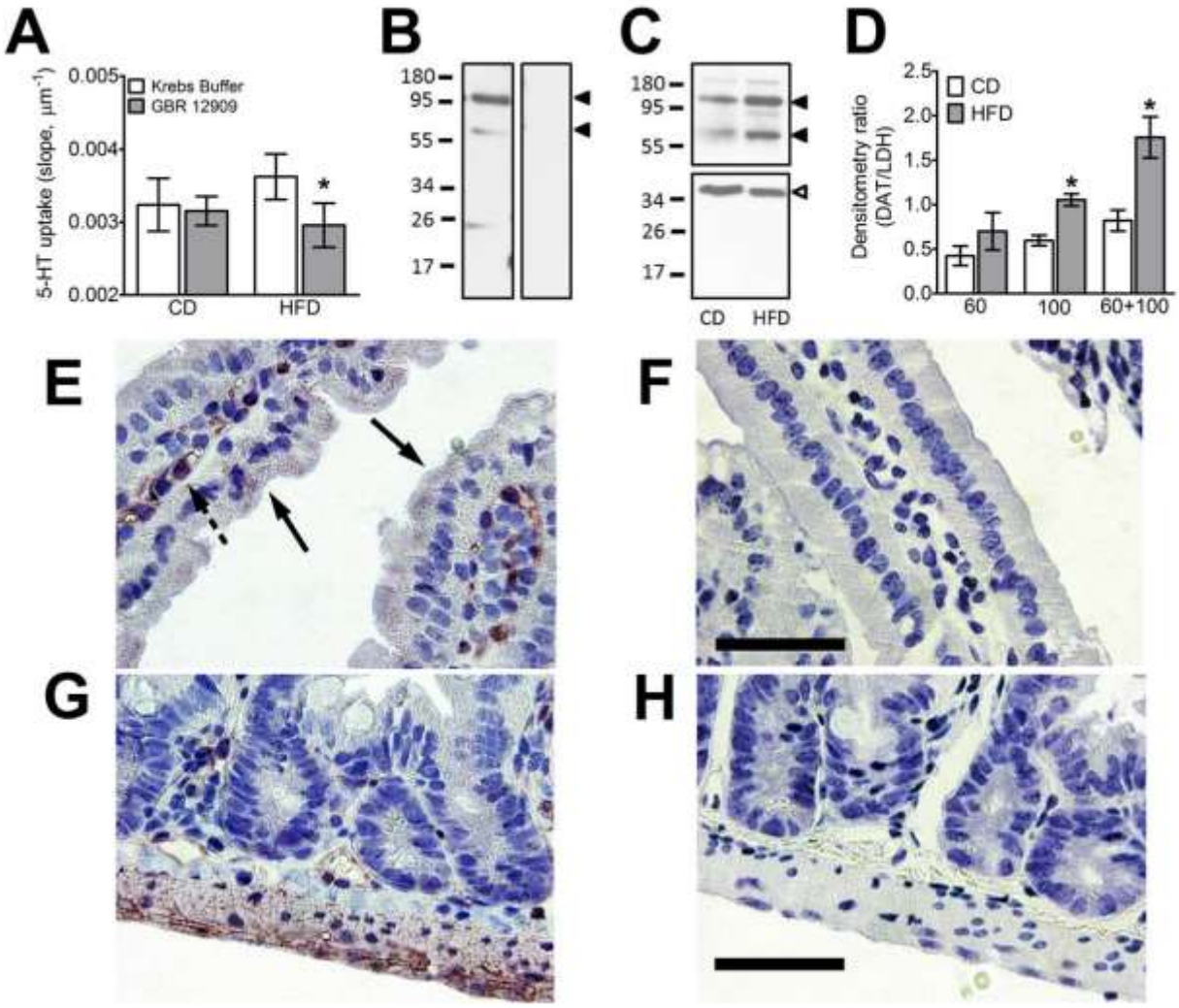

Figure 17 DAT is present in the jejunal mucosa and clears 5-HT in HFD-fed male jejunum. (A) In CA measurements, DAT blocker GBR 12909 reduced 5-HT uptake compared to measurements made in Krebs buffer in HFD-fed male jejunal tissues, but not in CD-fed male jejunal tissues (*n* = 5). (B) By Western blot analysis, the anti-DAT antibody was specific and identified two predominant bands at ca. 60 and 100 kDa (black arrowheads) in mucosal scrapes from the jejunum (left panel: primary and secondary antibody together; right panel: secondary antibody alone). (C) Representative Western blot comparing DAT protein levels between CD-fed and HFD-fed male jejunal mucosa. LDH is shown at ca. 35 kDa (open arrowhead). (D) The DAT/LDH ratio was increased in HFD-fed males compared to CD-fed males for the 100 kDa band and when both the 60 and 100 kDa bands are combined but not for the 60 kDa band alone (*n* = 8 each). (E) DAT-immunoreactivity in thin paraffin-embedded sections was observed in enterocytes (solid arrow) and in the lamina propria (dotted arrow). (G) As a positive control, DAT-immunoreactivity is shown in the myenteric and submucosal plexus. DAT-immunoreactivity was absent in secondary only controls (F, H). Scale bar is 50 µm. Data are mean ± SEM, **P* < 0.05.

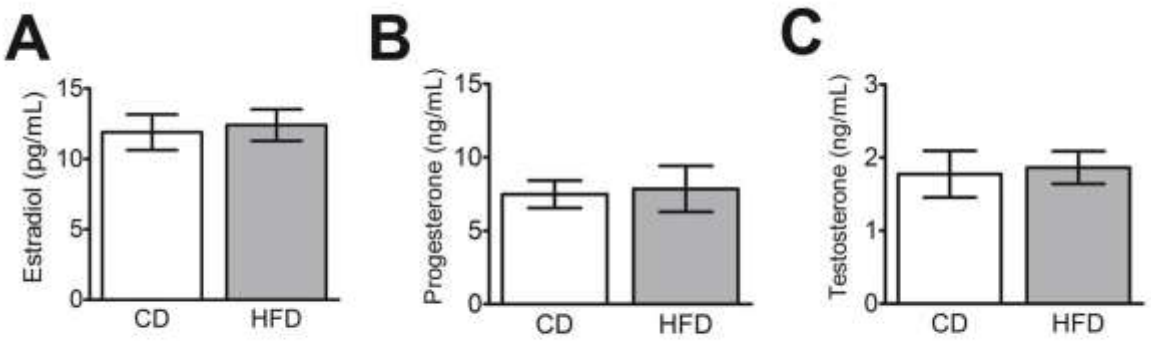

Figure 18. HFD does not alter total plasma sex hormone levels in female and male mice. (A, B) Plasma estradiol and progesterone levels from un-staged CD-fed and HFD-fed females were similar (*n* = 10). (C) Plasma testosterone levels in CD-fed and HFD-fed males were similar (*n* = 10). All sex hormones were measured in plasma using commercially available ELISAs. Data are mean ± SEM.

3.5 DISCUSSION

3.5.1 Sex-dependent differences in SERT in HFD-fed mice

We studied sex-related and diet-induced differences in intestinal 5-HT dynamics. SERT is the key regulator of extracellular 5-HT. We determined if changes in SERT function were present in the jejunum from CD-fed and HFD-fed male and female mice using CA. Impaired SERT function was demonstrated previously using CA with a carbon fiber microelectrode where 5-HT oxidation currents recorded in ileum preparations from Western Diet-fed male rats were fluoxetine-insensitive.[20] We found that 5-HT uptake was fluoxetine-insensitive in the jejunum from male HFD-fed, but not female HFD-fed mice. Our results suggest that SERT function is impaired in the jejunum of male HFD-fed mice, but remains functional in the jejunum of female HFD-fed mice. Our results are consistent with evidence that SERT function in the central nervous system is likely altered in obese human patients. For example, obese patients required a greater number of weeks to respond to antidepressant treatment[37] and greater body weight was found to be a predictor for fluoxetine resistance in patients with major depressive

disorder.[38] Intestinal SERT function in obese humans has not been studied. There is evidence in human studies for sex differences in responses to SSRI treatment in obesity. For example, obese women respond to such treatment where obese men have little to no response to SSRI treatment for major depressive disorder.[39] Overall, we found sex differences in SERT function where SERT is dysfunctional in HFD-fed male, but not HFD-fed female jejunum.

In male HFD-fed mice, impaired SERT function would decrease the amount of 5-HT cleared thereby raising local extracellular 5-HT levels. Moreover, if less 5-HT was cleared by SERT, less 5-HT would be metabolized into 5-HIAA in the enterocyte. We demonstrated that both steady state extracellular 5-HT and whole tissue 5-HIAA levels were similar in tissues from male HFD-fed and CD-fed mice. These results suggest that a compensatory mechanism may clear 5-HT when SERT function is impaired. Possible compensatory mechanisms include other monoamine transporters that exhibit low affinity for 5-HT. For example, both NET and DAT are capable of clearing 5-HT in adrenergic and dopaminergic central neurons, respectively in MAO_A knockout mice that have high extracellular 5-HT levels.[40] We found that cocaine, a non-selective monoamine blocker,[41] reduced 5-HT uptake in the jejunum of male HFD-fed compared to CD-fed mice consistent with the presence of other compensatory reuptake. As DAT is expressed throughout the intestine,[42, 43] we determined that DAT functions to clear 5-HT. In CA studies, blocking DAT with GBR 12909 reduced 5-HT uptake in the HFD-fed male jejunum, indicating that DAT clears 5-HT when SERT is dysfunctional.

We found the decrease in SERT function was not due to decreased SERT expression because jejunal protein and mRNA levels in the mucosa were similar in male HFD-fed compared to CD-fed mice. The calculated MW for SERT is 70 kDa, but the antibody used in this study identifies a single band at 100 kDa in extracts from the jejunal mucosal scrapings. Using the same antibody, a single band of similar size is also found in the wild type rat ileum and colon but absent in the SERT knockout (*SLC6A4*$^{-/-}$) rat (J. Jakupovic, unpublished observations). The increase in the apparent molecular weight of SERT is likely due to post-

translational modifications, including protein glycosylation and phosphorylation.[44] SERT glycosylation may be important for function, stabilization, trafficking and orientation in the plasma membrane.[45] In addition, SERT may be phosphorylated (e.g. by PKC/PKG), internalized and sequestered in endosomes/secretory granules.[46] Future studies could be aimed at assessing diet-induced changes in SERT localization. It is also possible that in HFD-fed male jejunum SERT remains present at the plasma membrane, but is inactive independent of changes in localization. For example, the inflammatory cytokines interferon gamma (IFNɣ) and tumor necrosis factor alpha (TNFα) decreased SERT function in a human intestinal epithelial cell line.[47] Overall, these previous studies by other investigators provide reasonable explanations for alterations in SERT function in the HFD-diet males without a reduction in total protein levels.

We determined if GBR 12909-sensitive 5-HT uptake in the jejunum from male HFD-fed mice was due to an increase in DAT protein expression. Western blot studies revealed that the jejunal mucosa from male HFD-fed mice had greater DAT protein levels at the apparent molecular weight of approximately 100 kDa, but not 60 kDa, compared to CD-fed males. The calculated MW for DAT is 68.8 kDa. It is possible that the higher molecular weight DAT may arise from glycosylation, although we did not determine this in our study. The band we report was similar to that observed in bovine nasal mucosa[48] and to that reported in the rodent myenteric and submucosal plexuses.[43] It has been demonstrated that dopamine (DA) is present both in gastric[49] and duodenal[50] luminal fluid and has been proposed to play a protective role against mucosal injury as DA receptor agonists aid in healing upper GI ulcers.[51] Consistent with this, DAT-immunoreactivity was present in epithelial cells of duodenal mucosa in rodents.[52] In our studies, DAT-immunoreactivity was found in epithelial cells concentrated at the apical surface, in strands found in the lamina propria and within the myenteric and submucosal plexuses. Based on our CA studies, it is likely that this higher MW DAT is located on epithelial cells and is necessary for 5-HT uptake we observed in our CA studies. Our studies

provide evidence that functional DAT is present and that levels are increased in the jejunal mucosal layer of male HFD-fed mice.

SERT function was unchanged in female HFD-fed mice as 5-HT uptake was fluoxetine-sensitive in the jejunum from these mice. Functional SERT in the female HFD-fed jejunum would result in similar extracellular 5-HT levels compared to CD-fed females. However, extracellular 5-HT levels were reduced in HFD-fed compared to CD-fed females. This result suggests that more 5-HT was cleared in HFD-fed females. In agreement, whole tissue 5-HIAA levels were greater in the jejunum from female HFD-fed compared to CD-fed mice. We also found greater SERT protein levels in the jejunum of HFD-fed compared to CD-fed female mice. Thus, it is likely there is greater SERT availability at the plasma membrane in HFD-fed female jejunum that functions to clear more 5-HT. Increased SERT protein was not dependent on changes in the steady state SERT mRNA expression. Alternatively, SERT may not be internalized in HFD-fed females. These data are the first to establish HFD-induced changes in intestinal 5-HT uptake in females.

3.5.2 HFD does not change mucosal 5-HT or 5-HT_3 receptor function

The number of EC cells and mucosal 5-HT levels were similar in HFD-fed and CD-fed mice in both sexes. This suggests that 5-HT synthesis is unaffected by HFD. This result is in contrast with a previous report where the number of EC cells was greater in the ileum of rats fed a Western diet.[20] These inconsistencies may be due to differences in species, diet composition (CD and HFD), time spent on diet, and region of small intestine. For example, not all mouse strains develop an obese phenotype when placed on a HFD[53] while other substrains are more sensitive to changes caused by a HFD (e.g. C57BL/6J versus C57BL/6NJ).[54] In addition, we used isocaloric CD and HFD whereas other HFD consist of added fat to the regular chow diet.

Our studies revealed similar reductions in 5-HT-induced muscle contractions by blocking 5-HT_3 receptors in CD-fed and HFD-fed jejunum in males and females. These results suggest

that 5-HT_3 receptor function remains unchanged in mice fed a HFD. This results agrees with a previous study demonstrating 5-HT_3 receptor mRNA levels were unchanged by HF feeding in mouse nodose ganglia.[55] We observed that 5-HT_3 receptor blockade reduced 5-HT-induced contractions at higher doses of 5-HT. It has been described previously that 5-HT_3 receptor activation is responsible in mediating muscle contraction at micromolar concentrations of 5-HT.[56, 57] We observed increased sensitivity to 5-HT-dependent increases in jejunal longitudinal muscle contractions in HFD-fed compared to CD-fed female jejunum suggesting that HFD-fed females are more sensitive to 5-HT acting at 5-HT_3 receptors. Likewise, low concentrations of 5-HT (≤ 0.3 μmol L^{-1}) produced greater muscle contractions in the jejunum of male CD-fed compared to female CD-fed mice suggesting females are less sensitive to lower concentrations of 5-HT. Interestingly, we found that the CD-fed female jejunum is not affected by methysergide treatment while the HFD-fed female jejunum is sensitive to methysergide block. In addition, we did not find a change in the 5-HT dose response curve when comparing CD-fed and HFD-fed female jejunum. Thus, it is likely there is a gain of function in non-5-HT_3 receptors in HFD-fed females.

3.5.3 HFD alters GI transit

HFD increased gastric emptying and small intestinal transit in male mice. Likewise, CD-fed female mice had increased gastric emptying and small intestinal transit compared to CD-fed male mice. Overall, female CD-fed mice have increased GI transit compared to males. The GC value was similar between CD-fed and HDF-fed females, yet it is apparent that transit is altered in HFD-fed females based on the pattern of FITC-dextran distribution. Since transit was altered in HFD-fed females and gastric emptying was similar to CD-fed females, our results suggest that only small intestinal transit is altered by a HFD in females. We assessed small intestinal transit by calculating the GC value and by comparing the pattern of FITC-dextran distribution in the fluorescence vs. intestinal segment number plots. The pattern of FITC-dextran pattern is

most likely influenced by the interdigestive migrating motor complex (MMC) that occurs during fasting.[58] In our studies, mice were fasted overnight prior to transit studies. The MMC is a well-organized motility pattern that functions to clean the intestine by rapidly moving any undigested material aborally by the action of cyclic muscle contractions.[59] Therefore any differences in the transit patterns may be due to changes in the MMC; however, we did not directly study MMCs. Intestinal MMCs in mice have not been studied to date.

Increased transit in male HFD-fed mice may be a result of increased extracellular 5-HT levels due to impaired SERT function. Indeed, DAT clears 5-HT in HFD-fed males in a compensatory manner, as revealed by our CA experiments and direct measurements of extracellular 5-HT levels using our microsampling technique. For DAT to clear 5-HT, 5-HT must reach a threshold concentration as DAT has low affinity for 5-HT.[60] This threshold concentration for DAT to remove 5-HT is not clearly defined,[60] nevertheless, before DAT clears 5-HT the local 5-HT concentration is increased in HFD-fed males and likely leads to greater activation of 5-HT_3 receptors. This change in 5-HT concentration may not be great enough to cause an increase in 5-HT_3 receptor expression and is consistent with our data showing that ondansetron response is similar in males and females, regardless of diet. An increase in 5-HT_3 receptor activation would increase muscle contractions and ultimately increase small intestinal transit.

In females, the lack of a detectable difference in transit described by the GC value may be dependent on estrous cycle. Transit was assessed in metestrus, where estrogen and progesterone levels are not exaggerated at either extreme. Since estrogen and progesterone modulate transit in females rats,[26] it is quite possible that transit may be different between HFD-fed and CD-fed females in another stage of the estrous cycle. Moreover, obesity can alter female cyclicity in rodents[61] and thus change plasma sex hormone levels. However, we found no differences in plasma sex hormone levels suggesting that a HFD does not change steady state plasma sex hormone levels. Despite no detectable changes in steady state levels, it is possible that HFD-fed females are less responsive to sex hormones. For example, in a DIO

mouse model very similar to ours, the authors found similar plasma hormone levels in HFD-fed and CD-fed female mice, but HFD-fed mice responded less to estrogen-dependent effects in mammary gland development.[62]

Increased transit in CD-fed females compared to males could result from greater 5-HT concentrations. Females have greater whole tissue 5-HT levels compared to males regardless of diet. This increase does not appear to be related to differences in EC cell number as cell numbers in HFD-fed females were not different from those in HFD-fed males. Thus, it is likely females produce greater amounts of 5-HT. In CD-fed females, greater whole tissue 5-HT levels translated to greater extracellular 5-HT levels, possibility caused from greater 5-HT release. Based on our results, females have 2-3X the 5-HT concentration as males. The increase in 5-HT concentration would most likely result in greater or more frequent 5-HT_3 receptor activation and ultimately greater muscle contraction generation and faster transit.

Alosetron treatment increased gastric emptying, but did not change either the GC or FITC-dextran distribution plot in male CD-fed mice. Increased gastric emptying by alosetron likely occurred by blocking the glucose-dependent 5-HT activation of vagal afferent 5-HT_3 receptors that decrease gastric emptying by a vagovagal reflex.[63] The source of glucose from our studies likely comes from FITC-dextran that would be metabolized to glucose by intestinal dextranases. Our results demonstrate different effects of alosetron on gastric emptying and small intestinal transit in CD-fed males by blocking 5-HT_3 receptors located on vagal afferents and myenteric IPANS that influence gastric emptying and transit, respectively. Gastric emptying is regulated by extrinsic inputs from the CNS that are modulated by vagal afferent activation.[64] The lack of alosetron treatment in small intestinal transit in males may be sex related since alosetron decreased the GC in CD-fed female mice. Alosetron sensitivity observed only in females mimics what is seen in human subjects where alosetron improves IBS symptoms in women patients.[65] Bush and colleagues demonstrated that *ex vivo* female mouse ileum was more sensitive to alosetron-dependent decreases in MMC frequency compared to male mouse

ileum.[66] In HFD-fed females, despite similar GC values between saline and alosetron-treated groups, the fraction of fluorescence vs. segment number plot revealed that alosetron treatment eliminated the disruption in transit. The fraction of fluorescence vs. segment number plot of HFD-fed alosetron–treated females overlaid perfectly with the saline-treated CD-fed females. This suggests that the HFD-induced alteration in transit is dependent upon 5-HT_3 receptors in female mice. Together, alosetron may be helpful in treating obesity related intestinal dysmotility in females, but not males.

3.5.4 Conclusions

A key finding of this study is the how differently DIO affects 5-HT signaling and motility in male and female mice. Our study is the first to offer a comprehensive study of the intestinal 5-HT system in female mice. In striking contrast to impaired SERT function in HFD-fed males, SERT remained functional in HFD-fed females. In addition, we demonstrated that alosetron treatment was suitable in HFD-fed females to reduce transit. Regardless of diet, females presented greater mucosal whole tissue 5-HT levels. Greater 5-HT levels may account for increased transit compared to males and offer an avenue for explanations in sex differences in alosetron effects.

REFERENCES

REFERENCES

1. Ogden CL, Carroll MD, Kit BK, et al. Prevalence of Childhood and Adult Obesity in the United States, 2011-2012. Jama-Journal of the American Medical Association 2014;311:806-814.

2. Mushref MA, Srinivasan S. Effect of high fat-diet and obesity on gastrointestinal motility. Ann Transl Med 2013;1:14.

3. Aro P, Ronkainen J, Talley NJ, et al. Body mass index and chronic unexplained gastrointestinal symptoms: an adult endoscopic population based study. Gut 2005;54:1377-83.

4. Delgado-Aros S, Locke GR, 3rd, Camilleri M, et al. Obesity is associated with increased risk of gastrointestinal symptoms: a population-based study. Am J Gastroenterol 2004;99:1801-6.

5. Talley NJ, Quan C, Jones MP, et al. Association of upper and lower gastrointestinal tract symptoms with body mass index in an Australian cohort. Neurogastroenterol Motil 2004;16:413-9.

6. Talley NJ, Howell S, Poulton R. Obesity and chronic gastrointestinal tract symptoms in young adults: a birth cohort study. Am J Gastroenterol 2004;99:1807-14.

7. Wisen O, Johansson C. Gastrointestinal function in obesity: motility, secretion, and absorption following a liquid test meal. Metabolism 1992;41:390-5.

8. Basilisco G, Camboni G, Bozzani A, et al. Orocecal transit delay in obese patients. Dig Dis Sci 1989;34:509-12.

9. French SJ, Murray B, Rumsey RD, et al. Preliminary studies on the gastrointestinal responses to fatty meals in obese people. Int J Obes Relat Metab Disord 1993;17:295-300.

10. Jin JG, Foxx-Orenstein AE, Grider JR. Propulsion in guinea pig colon induced by 5-hydroxytryptamine (HT) via 5-HT4 and 5-HT3 receptors. J Pharmacol Exp Ther 1999;288:93-7.

11. Heredia DJ, Dickson EJ, Bayguinov PO, et al. Localized release of serotonin (5-hydroxytryptamine) by a fecal pellet regulates migrating motor complexes in murine colon. Gastroenterology 2009;136:1328-38.

12. Bertrand PP, Kunze WA, Furness JB, et al. The terminals of myenteric intrinsic primary afferent neurons of the guinea-pig ileum are excited by 5-hydroxytryptamine acting at 5-hydroxytryptamine-3 receptors. Neuroscience 2000;101:459-69.

13. Furness JB, Callaghan BP, Rivera LR, et al. The enteric nervous system and gastrointestinal innervation: integrated local and central control. Adv Exp Med Biol 2014;817:39-71.

14. Kidd M, Modlin IM, Gustafsson BI, et al. Luminal regulation of normal and neoplastic human EC cell serotonin release is mediated by bile salts, amines, tastants, and olfactants. Am J Physiol Gastrointest Liver Physiol 2008;295:G260-72.

15. Raghupathi R, Duffield MD, Zelkas L, et al. Identification of unique release kinetics of serotonin from guinea-pig and human enterochromaffin cells. J Physiol 2013;591:5959-75.

16. Chin A, Svejda B, Gustafsson BI, et al. The role of mechanical forces and adenosine in the regulation of intestinal enterochromaffin cell serotonin secretion. Am J Physiol Gastrointest Liver Physiol 2012;302:G397-405.

17. Gill RK, Pant N, Saksena S, et al. Function, expression, and characterization of the serotonin transporter in the native human intestine. Am J Physiol Gastrointest Liver Physiol 2008;294:G254-62.

18. Spiller R. Serotonin and GI clinical disorders. Neuropharmacology 2008;55:1072-80.

19. Coates MD, Mahoney CR, Linden DR, et al. Molecular defects in mucosal serotonin content and decreased serotonin reuptake transporter in ulcerative colitis and irritable bowel syndrome. Gastroenterology 2004;126:1657-64.

20. Bertrand RL, Senadheera S, Markus I, et al. A Western diet increases serotonin availability in rat small intestine. Endocrinology 2011;152:36-47.

21. Izzo AA, Piscitelli F, Capasso R, et al. Peripheral endocannabinoid dysregulation in obesity: relation to intestinal motility and energy processing induced by food deprivation and re-feeding. Br J Pharmacol 2009;158:451-461.

22. Miller MS, Galligan JJ, Burks TF. Accurate measurement of intestinal transit in the rat. J Pharmacol Methods 1981;6:211-7.

23. McLean AC, Valenzuela N, Fai S, et al. Performing vaginal lavage, crystal violet staining, and vaginal cytological evaluation for mouse estrous cycle staging identification. J Vis Exp 2012:e4389.

24. Byers SL, Wiles MV, Dunn SL, et al. Mouse estrous cycle identification tool and images. PLoS One 2012;7:e35538.

25. Caligioni CS. Assessing reproductive status/stages in mice. Curr Protoc Neurosci 2009;Appendix 4:Appendix 4I.

26. Chen TS, Doong ML, Chang FY, et al. Effects of sex steroid hormones on gastric emptying and gastrointestinal transit in rats. Am J Physiol 1995;268:G171-6.

27. Wood GA, Fata JE, Watson KL, et al. Circulating hormones and estrous stage predict cellular and stromal remodeling in murine uterus. Reproduction 2007;133:1035-44.

28. Haisenleder DJ, Schoenfelder AH, Marcinko ES, et al. Estimation of estradiol in mouse serum samples: evaluation of commercial estradiol immunoassays. Endocrinology 2011;152:4443-7.

29. Patel BA, Bian X, Quaiserova-Mocko V, et al. In vitro continuous amperometric monitoring of 5-hydroxytryptamine release from enterochromaffin cells of the guinea pig ileum. Analyst 2007;132:41-7.

30. Bian X, Patel B, Dai X, et al. High mucosal serotonin availability in neonatal guinea pig ileum is associated with low serotonin transporter expression. Gastroenterology 2007;132:2438-47.

31. Zhao H, Bian X, Galligan JJ, et al. Electrochemical measurements of serotonin (5-HT) release from the guinea pig mucosa using continuous amperometry with a boron-doped diamond microelectrode. Diam Relat Mater 2010;19:182-185.

32. Park J, Show Y, Quaiserova V, et al. Diamond microelectrodes for use in biological environments. Journal of Electroanalytical Chemistry 2005;583:56-68.

33. Marcelli G, Patel BA. Theoretical modelling to understand the neurotransmission mechanism in the gastrointestinal tract. Conf Proc IEEE Eng Med Biol Soc 2008;2008:5548-51.

34. Marcelli G, Patel BA. Understanding changes in uptake and release of serotonin from gastrointestinal tissue using a novel electroanalytical approach. Analyst 2010;135:2340-7.

35. Cani PD, Bibiloni R, Knauf C, et al. Changes in gut microbiota control metabolic endotoxemia-induced inflammation in high-fat diet-induced obesity and diabetes in mice. Diabetes 2008;57:1470-81.

36. Theoharides TC, Bondy PK, Tsakalos ND, et al. Differential release of serotonin and histamine from mast cells. Nature 1982;297:229-31.

37. Kloiber S, Ising M, Reppermund S, et al. Overweight and obesity affect treatment response in major depression. Biol Psychiatry 2007;62:321-6.

38. Papakostas GI, Petersen T, Iosifescu DV, et al. Obesity among outpatients with major depressive disorder. Int J Neuropsychopharmacol 2005;8:59-63.

39. Khan A, Schwartz KA, Kolts RL, et al. BMI, sex, and antidepressant response. J Affect Disord 2007;99:101-6.

40. Cases O, Lebrand C, Giros B, et al. Plasma membrane transporters of serotonin, dopamine, and norepinephrine mediate serotonin accumulation in atypical locations in the developing brain of monoamine oxidase A knock-outs. J Neurosci 1998;18:6914-27.

41. Torres GE, Gainetdinov RR, Caron MG. Plasma membrane monoamine transporters: structure, regulation and function. Nat Rev Neurosci 2003;4:13-25.

42. Chen JJ, Li Z, Pan H, et al. Maintenance of serotonin in the intestinal mucosa and ganglia of mice that lack the high-affinity serotonin transporter: Abnormal intestinal motility and the expression of cation transporters. J Neurosci 2001;21:6348-61.

43. Li ZS, Pham TD, Tamir H, et al. Enteric dopaminergic neurons: definition, developmental lineage, and effects of extrinsic denervation. J Neurosci 2004;24:1330-9.

44. Chamba A, Holder MJ, Barnes NM, et al. Characterisation of the endogenous human peripheral serotonin transporter SLC6A4 reveals surface expression without N-glycosylation. J Neuroimmunol 2008;204:75-84.

45. Rasmussen TN, Plenge P, Bay T, et al. A single nucleotide polymorphism in the human serotonin transporter introduces a new site for N-linked glycosylation. Neuropharmacology 2009;57:287-94

46. Blakely RD, Ramamoorthy S, Schroeter S, et al. Regulated phosphorylation and trafficking of antidepressant-sensitive serotonin transporter proteins. Biol Psychiatry 1998;44:169-78.

47. Foley KF, Pantano C, Ciolino A, et al. IFN-gamma and TNF-alpha decrease serotonin transporter function and expression in Caco2 cells. Am J Physiol Gastrointest Liver Physiol 2007;292:G779-84.

48. Chemuturi NV, Haraldsson JE, Prisinzano T, et al. Role of dopamine transporter (DAT) in dopamine transport across the nasal mucosa. Life Sci 2006;79:1391-8.

49. Mezey E, Eisenhofer G, Hansson S, et al. Non-neuronal dopamine in the gastrointestinal system. Clin Exp Pharmacol Physiol Suppl 1999;26:S14-22.

50. Mezey E, Eisenhofer G, Harta G, et al. A novel nonneuronal catecholaminergic system: exocrine pancreas synthesizes and releases dopamine. Proc Natl Acad Sci U S A 1996;93:10377-82.

51. Sikiric P, Rotkvic I, Mise S, et al. Dopamine agonists prevent duodenal ulcer relapse. A comparative study with famotidine and cimetidine. Dig Dis Sci 1991;36:905-10.

52. Tian YM, Chen X, Luo DZ, et al. Alteration of dopaminergic markers in gastrointestinal tract of different rodent models of Parkinson's disease. Neuroscience 2008;153:634-44.

53. Lee KT, Karunakaran S, Ho MM, et al. PWD/PhJ and WSB/EiJ mice are resistant to diet-induced obesity but have abnormal insulin secretion. Endocrinology 2011;152:3005-17.

54. Nicholson A, Reifsnyder PC, Malcolm RD, et al. Diet-induced obesity in two C57BL/6 substrains with intact or mutant nicotinamide nucleotide transhydrogenase (Nnt) gene. Obesity (Silver Spring) 2010;18:1902-5.

55. Nefti W, Chaumontet C, Fromentin G, et al. A high-fat diet attenuates the central response to within-meal satiation signals and modifies the receptor expression of vagal afferents in mice. Am J Physiol Regul Integr Comp Physiol 2009;296:R1681-6.

56. Buchheit KH, Engel G, Mutschler E, et al. Study of the contractile effect of 5-hydroxytryptamine (5-HT) in the isolated longitudinal muscle strip from guinea-pig ileum. Evidence for two distinct release mechanisms. Naunyn Schmiedebergs Arch Pharmacol 1985;329:36-41.

57. Kilbinger H, Wolf D. Effects of 5-HT4 receptor stimulation on basal and electrically evoked release of acetylcholine from guinea-pig myenteric plexus. Naunyn Schmiedebergs Arch Pharmacol 1992;345:270-5.

58. Romanski KW. Migrating motor complex in biological sciences: characterization, animal models and disturbances. Indian J Exp Biol 2009;47:229-44.

59. Takahashi T. Mechanism of interdigestive migrating motor complex. J Neurogastroenterol Motil 2012;18:246-57.

60. Daws LC. Unfaithful neurotransmitter transporters: focus on serotonin uptake and implications for antidepressant efficacy. Pharmacol Ther 2009;121:89-99.

61. Balasubramanian P, Jagannathan L, Mahaley RE, et al. High fat diet affects reproductive functions in female diet-induced obese and dietary resistant rats. J Neuroendocrinol 2012;24:748-55.

62. Olson LK, Tan Y, Zhao Y, et al. Pubertal exposure to high fat diet causes mouse strain-dependent alterations in mammary gland development and estrogen responsiveness. Int J Obes (Lond) 2010;34:1415-26.

63. Raybould HE, Glatzle J, Robin C, et al. Expression of 5-HT3 receptors by extrinsic duodenal afferents contribute to intestinal inhibition of gastric emptying. Am J Physiol Gastrointest Liver Physiol 2003;284:G367-72.

64. Chang HY, Mashimo H, Goyal RK. Musings on the wanderer: what's new in our understanding of vago-vagal reflex? IV. Current concepts of vagal efferent projections to the gut. Am J Physiol Gastrointest Liver Physiol 2003;284:G357-66.

65. Viramontes BE, Camilleri M, McKinzie S, et al. Gender-related differences in slowing colonic transit by a 5-HT3 antagonist in subjects with diarrhea-predominant irritable bowel syndrome. Am J Gastroenterol 2001;96:2671-6.

66. Bush TG, Spencer NJ, Watters N, et al. Effects of alosetron on spontaneous migrating motor complexes in murine small and large bowel in vitro. Am J Physiol Gastrointest Liver Physiol 2001;281:G974-83.

CHAPTER 4

ALTERED TRANSIT IN HIGH FAT DIET-INDUCED OBESITY IS NOT DEPENDENT ON MUCOSAL 5-HT OR NEURONAL 5-HT LOSS

4.1 ABSTRACT

Gastrointestinal (GI) transit and the intestinal immune system are modulated by 5-hydroxytryptamine (5-HT, serotonin) found in the gut mucosa and in the enteric nervous system (ENS). Alterations in 5-HT signaling in high-fat (HF) diet-induced obesity (DIO) likely occur and contribute to GI transit dysfunction and intestinal inflammation observed in DIO. It is predicted that modulation of GI transit and intestinal inflammation by mucosal 5-HT is functionally dominant since neuronal 5-HT is susceptible to neuropathy from DIO-dependent intestinal inflammation. I studied gastric emptying and small intestinal transit in male and female tryptophan hydroxylase 1 (TPH1) knockout (KO) and wild-type (WT) littermate mice fed a control diet (CD, 10 kcal % fat) or a high fat diet (HFD, 60 kcal % fat) for 13-15 weeks. Intestinal inflammation and serotonergic neuropathy were assessed in WT mice by measuring TNFα protein in the gut mucosa, quantifying mast cells in the lamina propria and measuring total neuronal 5-HT and 5-hydroxyindole acetic acid (5-HIAA) levels in the gut wall. Gastric emptying was increased in female HFD-fed WT and CD-fed TPH1 KO mice compared to female CD-fed WT mice. Transit was greater in male compared to female HFD-fed TPH1 KO mice. Gastric emptying and GC were not different between CD-fed WT and TPH1 KO mice. TNFα protein levels were under the limit of detection (L.O.D) for mucosal tissues from all mice. The number of mast cells was greater in female HFD-fed WT mice compared to male HFD-fed and female CD-fed WT mice. There were no DIO-dependent changes in gut wall whole tissue 5-HT and 5-HIAA levels in all mice. In conclusion, 1) mucosal 5-HT is important in regulating gastric emptying in female mice, 2) mucosal 5-HT is not essential in small intestinal transit in CD-fed mice, but may modulate transit in HFD-fed male mice and 3) neuronal 5-HT is largely unaffected by a HFD in either males or females. Overall, DIO-dependent impairments in transit do not appear dependent on mucosal 5-HT or neuronal 5-HT loss.

4.2 INTRODUCTION

Most (90%) of the total body 5-hydroxytryptamine (5-HT, serotonin) is located in enterochromaffin (EC) cells in the gastrointestinal mucosa.[1] The importance of 5-HT release from EC cells in initiating peristalsis was first described by Bülbring and colleagues in the 1950's.[2, 3] Today, the initiation of peristalsis is described by the following pathway: 5-HT released from EC cells, in response to either mechanical or chemical activation[4, 5], acts at 5-HT receptors located on nerve terminals of intrinsic primary afferent neurons (IPANs) whose cell bodies are in the myenteric plexus.[6] The myenteric plexus is the nerve network in the enteric nervous system (ENS) responsible for coordinating motor reflexes. IPANs relay sensory information from the gut lumen to the myenteric plexus to generate coordinated smooth muscle contractions and relaxations that are essential in propulsive motility.[7] The importance of mucosal 5-HT in modulating propulsive reflexes has been demonstrated *ex vivo* in rodents[8, 9] and *in vivo* using a 5-HT_3 receptor antagonist in humans.[10] Recently, Li and colleagues[11] demonstrated that mucosal 5-HT was not necessary for the initiation of peristalsis and that peristalsis persists without mucosal 5-HT using a tryptophan hydroxylase 1 knockout (KO) mouse (TPH1 KO). TPH1 is essential for 5-HT synthesis in EC cells that are localized exclusively within the mucosa.[12] The authors concluded that mucosal 5-HT was not necessary for essential motility. Therefore, 5-HT may not be necessary for constitutive motility, but is necessary in motility regulation.

Mucosal 5-HT plays a prominent role in diseases associated with dysfunctional motility. For example, EC cell numbers and mucosal 5-HT content were increased in a rodent model of inflammatory bowel disease (IBD).[13] IBD is defined by two types: ulcerative colitis (UC) and Crohn's disease. Both are characterized by chronic intestinal inflammation that greatly impairs GI function. Similar to intestinal diseases characterized by intestinal dysmotility, impaired GI motility in obesity causes diarrhea, constipation, irritable bowel syndrome (IBS) and fecal

incontinence.[14] Therefore, mucosal 5-HT may play a prominent role in dysfunctional GI motility in DIO.

Obesity is characterized by a chronic low-grade inflammatory state driven by visceral adipocyte hyperplasia and hypertrophy that generates an increase in the levels of released proinflammatory cytokines. For example, elevated circulating levels of proinflammatory cytokines, such as TNFα, IL-1β and IL-6, are present in obesity.[15] Concurrent with visceral fat inflammation, intestinal inflammation occurs in obese humans.[16] Intestinal inflammation is likely driven by visceral fat-generated proinflammatory cytokines given the close proximity of these organs and by an increase in intestinal permeability.[17, 18] In rodents, HF fed mice exhibited elevated ileal TNFα mRNA levels that positively correlated with both body weight and percent fat.[19] In summary, intestinal inflammation persists in obese humans and rodent models.

A likely candidate driving intestinal inflammation in DIO is mucosal 5-HT. Dendritic cells, that drive innate inflammation, are present in the intestinal mucosa[20] and are functional in DIO.[21] Dendritic cells express functional 5-HT receptors and stimulation of mature dendritic cells with 5-HT, 5-HT_3, 5-HT_4 and 5-HT_7 receptor agonists increases proinflammatory IL-8 and IL-1β production and release.[22] On the other hand, activation of a functional IL-1β expressed by EC cells by IL-1β application to isolated EC cells *in vitro* caused release of 5-HT.[23] With genetic elimination of mucosal 5-HT in TPH1 KO mice, TNFα and IL-1β levels were much reduced compared to WT mice in a model of stimulated intestinal inflammation by dextran sulfate sodium (DSS).[24] Further, treatment of 5-HTP (5-hydroxytryptophan; 5-HT precursor) in TPH1 KO mice normalized TNFα and IL-1β levels to control levels in DSS-induced intestinal inflammation.[24] Together these studies suggest that mucosal 5-HT in DIO has the propensity to drive intestinal inflammation.

In addition to mucosal 5-HT, a second depot of gut-derived 5-HT is found within the myenteric plexus.[25] Neal et al. provided evidence that the rate-limiting enzyme for 5-HT synthesis within neurons (tryptophan hydroxylase 2, TPH2) was localized in longitudinal muscle-

myenteric plexus (LMMP) preparations, confirming the identification of serotonergic interneurons previously proposed.[26] Serotonergic interneurons are arranged in descending chains such that 5-HT immunoreactive varicosities appose 5-HT immunoreactive neurons[25] and compromise 1.9% of the total number of myenteric neurons.[27] Neuronal 5-HT plays a critical role in GI motility; genetic deletion of TPH2 slowed both small and large intestinal transit.[11] These results suggest that neuronal 5-HT is important in the descending excitatory pathway and coincides with previous reports demonstrating that 5-HT mediates propagating contractile complexes,[25] fast excitatory synaptic responses in the myenteric plexus[28] and myenteric plexus excitatory transmission to the circular muscle.[29]

During inflammation, neutrophils infiltrate the myenteric plexus and reside in close proximity to myenteric neurons.[30] Neutrophil infiltration has been linked to myenteric neuropathy.[31] Neutrophils house myeloperoxidase (MPO) and neuronal 5-HT may act as a substrate for MPO. MPO, using hydrogen peroxide, can convert 5-HT into a free radical that is then converted by a superoxide mechanism to tryptamine-4,5-dione.[32] Tryptamine-4,5-dione has been demonstrated to be neurotoxic *in vitro*.[33] It is suggested that tryptamine-4,5-dione exerts its neurotoxic effects by alkylating thiol and amine groups on proteins such as the anti-oxidant glutathione (GSH)[32] and mitochondrial respiratory enzymes[34] rendering them inactive. Tryptamine-4,5-dione is unstable[35] and reactions between tryptamine-4,5-dione and cellular proteins are rapid, thus its detection is unlikely. Given this evidence, serotonergic interneurons may be susceptible to neuropathy during inflammation. This prediction is similar to inflammation effects on nitric oxide (NO)-containing motoneurons localized in the myenteric plexus. NO inhibitory motoneurons are susceptible to damage from inflammation-generated oxygen radicals occurring by the peroxynitrite formation from reactions between NO and free oxygen radicals.[36] Peroxynitrite formation can lead to cell death and is evident in DIO.[37] It is likely then that DIO-dependent inflammation leads to serotonergic interneuron loss in DIO.

The hypothesis of this study was that dysfunctional GI transit and intestinal inflammation are dependent on mucosal 5-HT, but not neuronal 5-HT due to serotonergic neuropathy. For this study I measured I) transit in male and female wild type (WT) and TPH1 KO DIO mice, 2) TNFα in mucosal scrapes from these mice, and 3) and whole tissue levels of 5-HT and 5-HIAA in the myenteric and submucosal plexus (e.g. whole mount preparation) of DIO WT mice.

4.3 METHODS AND MATERIALS

4.3.1 Mice and diets

All animal use protocols were approved by the Institutional Animal Care and Use Committee at Michigan State University. Homozygous breeder TPH1 KO mice were obtained from Dr. Michael Bader, Max-Delbrück-Center for Molecular Medicine (MDC) at Berlin, Germany.[12, 38] Homozygous TPH1 KO mice were then bred with C57BL/6J WT mice from Jackson Laboratories (Bar Harbor, ME, USA) in house to produce heterozygotes. The colony was maintained by breeding heterozygous mice. Male and female WT and TPH1 KO littermates were used for the studies. Littermates were housed in cages (max. 5 per cage) and allowed food and water *ad libitum* on a 12 h light dark cycle. Mice were placed on either control diet (CD, 10% kcal fat, D12450B) or HF diet (HFD, 60% kcal fat, D12492) at weaning (4-6 weeks). For neuronal 5-HT studies, DIO male and female C57BL/6J mice, placed on diets at weaning, were purchased from Jackson Laboratories (Bar Harbor, ME, USA) at 14 weeks of age. Once mice arrived at our facility, they remained on either CD (10% kcal% fat, D12450B) or HFD (60% kcal% fat, D12492) (Research Diets, Inc., New Brunswick, NJ, USA) for an additional three weeks before use in our studies. Mice were housed in individual cages, allowed food and water *ad libitum* on a 12 h light/dark cycle. Mice were studied at 17-19 wk of age (13-15 wk spent on diets) for all experiments. All mice were euthanized using isoflurane anesthesia followed by cervical dislocation. Both body weight and abdominal fat pad weights were measured at the time of sacrifice. For inflammation studies, a segment of the jejunum was excised just distal to

the ligament of Treitz and placed in oxygenated (95% O_2, 5% CO_2) Krebs buffer (pH 7.4). Eight groups of animals were studied. The groups were the following: male WT CD, male WT HFD, male TPH1 CD, male TPH1 HFD, female WT CD, female WT HFD, female TPH1 CD, and female TPH1 HFD.

4.3.2 Reagents and drugs

Krebs buffer (mmol L^{-1}): 117 NaCl, 4.7 KCl, 2.5 $CaCl_2$, 1.2 $MgCl_2$, 1.2 NaH_2PO_4, 25 $NaHCO_3$, and 11 glucose, was used for all solution preparations All drugs and reagents were obtained from Sigma Aldrich (St. Louis, MO, USA).

4.3.3 *In vivo* GI transit

GI transit was assessed by measuring the distribution of a fluorescent marker along the length of the small intestine. Mice were fasted 12 h prior to gastric gavage of FITC-dextran (0.1 mL of 10 mg mL^{-1}) given between the hours of 8-9 AM the following day. After 30 min, mice were euthanized and the stomach and small intestine were removed. The small intestine was cut into 6 segments (5 cm) with the duodenum as segment #1 and the most distal ileum as segment #6. Each segment was flushed with 1.5 mL of PBS. PBS containing luminal content was then centrifuged (14,000 RPM for 10 min). The fluorescence of the supernatant from each segment was measured (485 nm excitation; 510 nm emission) on a plate reader (Fluoroskan Ascent/FL, Thermo Scientific, Rockford, IL). The fraction of FITC of each segment was calculated and this was used to calculate the geometric center (GC) value. The GC value is a weighted mean that includes the marker distribution and the distance traveled. The GC value was calculated using the following equation:[39]

$$\mathrm{GC} = \Sigma(\text{fraction of FITC per segment}) * (\text{segment number})$$

Gastric emptying was calculated as [(Total fluorescence – fluorescence in stomach)/(Total fluorescence)] x 100.

4.3.4 Staging female estrous cycle

The stage of estrous cycle was identified for females undergoing *in vivo* transit studies. Vaginal cytology using wet smears was performed to identify estrous cycle stage each day at 9 AM two weeks prior to sacrifice in order to establish regular cyclers and continuing until sacrifice in order to sacrifice mice in the correct stage.[40-42] All *in vivo* motility studies were performed during metestrus. This stage of the estrous cycle was chosen because I) estradiol, the main estrogen, and progesterone modulate small intestinal motility in rats[43] and II) estradiol and progesterone levels are not elevated nor reduced during metestrus as compared to estrus and diestrus in the mouse.[44]

4.3.5 TNFα in intestinal mucosa

A segment of jejunum was removed and pinned in a Sylgard®-lined petri dish containing Krebs buffer with the mucosa facing upwards. The mucosal surface was scraped off using a sharp scalpel from a segment of jejunum (ca. 1 cm^2). The mucosal scrape was placed in foil and then flash frozen in liquid nitrogen. Samples were stored at -80 ˚C until all samples were obtained. For tissue processing, tissues were weighed and then put into a 2 mL vial containing ceramic beads (1.4 mm) and 300-400 µL of lysis buffer kept on ice. The lysis buffer composition was 20 mM Tris, 150 mM NaCl, 1 mM EDTA, 0.1% SDS, 0.5% sodium deoxycholate, 1% Triton X-100, and 1% protease inhibitors. Tissue was homogenized using an Omni bead ruptor homogenizer (Omni International, Kennesaw, GA) for 45 s at 4 ˚C. Vials were centrifuged at 14,000 RPM for 10 min at 4 ˚C. All liquid was removed and centrifuged again. Supernatant was removed and protein analysis was performed using DC™ Protein Assay (Bio–Rad Laboratories, Hercules, CA). Samples were then stored at -80 ˚C until further analysis. TNFα levels were measured in mucosal samples using an enzyme-linked immunosorbent assay (ELISA) according to the

manufactures instructions (Mouse TNF alpha ELISA Ready-SET-Go!®, #88-7324, eBioscience, Inc., San Diego, CA).

4.3.6 HPLC measurements of 5-HT and 5-HIAA levels in whole mount preparations

Whole mount tissue levels of 5-HT and 5-HIAA were measured using HPLC with electrochemical detection. For whole mount preparations, segments of jejunum were removed and placed in Krebs buffer. Segments were cut along the mesenteric border and the mucosa was rinsed with Krebs buffer. The mucosal surface (~2 cm) was removed using a sharp scalpel. The resulting whole mount preparation containing the muscularis mucosa, submucosal plexus, submucosa, circular muscle layer, myenteric plexus, longitudinal muscle and serosa (LMMP/SP) was placed into a tissue homogenizer (2 mL) filled with ice cold 0.1 M perchloric acid (0.5 mL). The sample was then centrifuged (4 ˚C) at 14,000 RPM for 10 min. Supernatant was removed and stored at -80 ˚C until analysis. Protein analysis was performed using a DC™ Protein Assay kit (Bio–Rad Laboratories, Hercules, CA). Supernatant (20 µL) samples from whole tissue and extracellular fluid were injected using an autosampler (ESA 542, Thermo-Fisher) maintained at 35 ˚C onto a ESA guard column (70-1972) in-line with a Thermo MD column (150 mm x 3.2 mm, 3 µm particle size) for separation and detected using a ESA 5011A analytical cell set to a potential of + 200 mV. The mobile phase consisted of the following composition (mmol L^{-1}): 90 sodium phosphate, 50 citrate, 1.94 sodium octyl sulfate, 0.05 EDTA and 10 % acetonitrile and flowed at a rate of 0.6 mL min^{-1} (ESA 582). Representative retention times for 5-HT and 5-HIAA were around 15 and 5 min, respectively. Results are presented as ng per mg protein.

4.3.7 Immunohistochemistry and quantification of 5-HT positive cells in lamina propria

Segments of jejunum were cut along the mesenteric border, stretched gently (~ 1 cm^2) and pinned with the mucosal surface facing upwards in a Sylgard® lined Petri dish. The segment

was gently washed with Krebs buffer and fixed with 10% neutral buffered formalin overnight (4 ˚C). Further specimen treatment was performed by Michigan State University Investigative Histopathology Laboratory. Briefly, 10% neutral buffered formalin-fixed specimens were processed, embedded in paraffin and sectioned on a rotary microtome at 4-5 μm. Sections were placed on slides (4 sections per slide with 40 μm between each section), coated with 2% 3-Aminopropyltriethoxysilane and dried overnight (56 °C). Slides were subsequently deparaffinized in xylene and hydrated through descending grades of ethyl alcohol to distilled water. To adjust pH, slides were placed in Tris Buffered Saline (TBS; pH 7.4) (Scytek Labs, Logan, UT) for 5 min. Following TBS, slides underwent heat induced epitope retrieval utilizing Citrate Plus (pH 6.0) (Scytek Labs, Logan, UT) for 30 min in a vegetable steamer at 100°C followed by 10 min at room temperature and then underwent several changes of distilled water. Endogenous enzyme activity was blocked with a 3% hydrogen peroxide/ methanol bath (1:4) for 30 minutes followed by tap and distilled water rinses. Following, standard avidin-biotin complex (ABC) staining protocol was performed at room temperature on a DAKO Autostainer. All staining steps were followed by rinses in TBS with Tween 20 (Scytek Labs, Logan, UT). Blocking for non-specific protein was accomplished using normal goat serum (Vector Labs, Burlingame, CA) for 30 minutes. Sections were then incubated with avidin-biotin blocking system for 15 minutes (Avidin D, Vector Labs, Burlingame, CA; d-Biotin, Sigma, St. Louis, MO). Primary antibody slides were incubated for 1 h with polyclonal rabbit anti-serotonin diluted at 1:40,000 (S5545, Sigma, St. Louis, MO) in normal antibody diluent (NAD) (Scytek Labs, Logan, UT). Following, slides were incubated for 30 min in biotinylated goat anti-rabbit IgG prepared in NAD (11.5 μg/ml) and then incubated for 30 min in Ready-to-use Vector Elite Peroxidase Reagent (Vector Labs, Burlingame, CA). Reaction development was performed by incubating slides for 15 min in Vector® NovaRED™ peroxidase chromogen (Vector Labs, Burlingame, CA) followed by counterstain in Gill Hematoxylin (Thermo Fisher, Kalamazoo, MI) for 15 s,

differentiation, dehydration, clearing and finally mounting with synthetic mounting media. Sections were viewed using a Nikon microscope and images were acquired using SPOT Advanced software (Spot Imaging Solutions, Sterling Heights, MI, USA). The number of intact villi and the number of 5-HT positive cells located in the lamina propria in intact villi was counted in the four sections of one slide (4 sections per 1 animal) by a blinded observer. The 5-HT positive cells in the lamina propria were assigned as mast cells. The ratio of the total number of 5-HT positive cells located in the lamina propria in intact villi to the total number of intact villi was calculated for individual sections. This ratio was averaged over the four sections and that average was used for each animal. The number of mast cells is expressed per 10 villus-crypt axis.

4.3.8 Immunohistochemistry in whole mount intestinal tissues

Neuronal 5-HT was visualized in the myenteric plexus in whole mount preparations. For whole mount preparations, segments of jejunum were removed and placed in Krebs buffer with nifedipine to minimize muscle movement (1 μmol L^{-1}). Segments were cut along the mesenteric border and pinned in a Sylgard®-lined petri dish. The mucosal surface (~2 cm) was removed using a sharp scalpel. Following the muscularis mucosa, the submucosal plexus, submucosa and circular muscle layer were dissected away using fine-tipped forceps. The resulting whole mount preparation containing the myenteric plexus, longitudinal muscle and serosa (LMMP) was fixed in 4% paraformaldehyde overnight at 2-8˚C. The next day tissues were washed 3 X 10 min in 0.01 M PBS with 0.5% Triton X-100. Tissues were then incubated in 4% normal donkey serum in 0.01 M PBS with 0.1% Triton X-100 for 1 h at room temperature. Tissues were incubated with primary antibodies made in 4% normal donkey serum in 0.01M PBS with 0.1% Triton X-100 overnight at 2-8˚C. The following primary antibodies were used: rabbit anti-5-HT at 1:2000 dilution (Sigma Aldrich) and anti-Human neuronal protein HuC/HuD at 1:200 dilution (Molecular Probes). The following morning, tissues were washed 3 X 10 min in 0.01 M PBS

with 0.5% Triton X-100. Secondary antibodies prepared in 0.01 M PBS in 0.1% Triton X-100 were incubated for 2 h at room temperature. The following secondary antibodies were used: Cy^{TM}3-conjugated AffiniPure Donkey Anti-Rabbit IgG at a 1:200 dilution (Jackson Immuno Research Laboratories, Inc.) and Alexa Fluor® 488-conjugated streptavidin at a 1:200 dilution (Jackson Immuno Research Laboratories, Inc.). Negative controls lacking the primary antibodies were performed. Tissues were then washed 3 X 10 min in 0.01 M PBS with 0.5% Triton X-100, mounted on slides and visualized using Nikon TE2000-U inverted microscope with the Cy3 and FITC filter to visualize 5-HT and Hu, respectively.

4.3.9 Statistical analysis

All data analysis was done using GraphPad Prism software. Two group comparisons were made using an unpaired Student's *t*-test. Two group comparisons were made to determine diet effects in each genotype (e.g. CD-fed WT vs. HFD-fed WT and CD-fed TPH1 KO vs. HFD-fed TPH1 KO) and to determine genotype effects in each diet group (e.g. CD-fed WT vs. CD-fed TPH1 KO and HFD-fed WT vs. HFD-fed TPH1 KO). This was done for male and female mice. Lastly, two group comparisons were made to determine sex differences in each matched diet/genotype group (e.g. male CD-fed WT vs. female CD-fed WT). For data not normally distributed, a log transformation of the data or a Mann-Whitney test was performed. For fraction of fluorescence vs. intestinal segment number plots, comparisons were made using a two-way ANOVA. For all comparisons, $P < 0.05$ was considered statistically significant. Data are reported as mean $\pm$ S.E.M.

4.4 RESULTS

4.4.1 Male and female WT and TPH1 KO mice develop DIO on HFD

Male and female WT mice on a HFD (60 kcal %) developed an obese phenotype compared to WT mice placed on a CD (10 kcal %). Male HFD-fed mice developed greater body

weights compared to CD-fed mice (HFD: 44.5 ± 1.6 g, CD: 30.3 ± 1.1 g, n = 8, P < 0.05). Female HFD-fed mice developed greater body weights compared to CD-fed females (HFD: 29.0 ± 2.4 g, CD: 20.5 ± 1.0 g, n = 8, P < 0.05). In addition, the abdominal fat pad mass weight encompassing both the epididymal and retroperitoneal fat pads was used as an index of obesity. Male HFD-fed mice had greater abdominal fat pad weights compared to CD-fed mice (HFD: 2.3 ± 0.2 g, CD: 0.9 ± 0.8 g, n = 8, P < 0.05). Female HFD-fed mice had greater abdominal fat pad weights compared to CD-fed mice (HFD: 1.4 ± 0.3 g, CD: 0.3 ± 0.1 g, n = 8, P < 0.05).

Male and female TPH1 KO mice on a HFD (60 kcal %) developed an obese phenotype compared to TPH1 KO mice placed on a CD (10 kcal %). Male HFD-fed mice developed greater body weights compared to CD-fed mice (HFD: 35.3 ± 2.3 g, CD: 26.5 ± 1.8 g, n = 8, P < 0.05). Female HFD-fed mice had similar body weights compared to CD-fed mice (HFD: 24.9 ± 1.5 g, CD: 20.0 ± 0.8 g, n = 8, P < 0.05). Male HFD-fed mice had greater abdominal fat pad weights compared to CD-fed mice (HFD: 2.1 ± 0.3 g, CD: 0.5 ± 0.2 g, n = 8, P < 0.05). Despite similar body weights, female HFD-fed mice had greater abdominal fat pad weights compared to CD-fed mice (HF: 0.9 ± 0.2 g, C: 0.2 ± 0.0 g, n = 8, P < 0.05).

When comparing WT and TPH1 KO animals on matched diets, male HFD-fed WT mice had greater body weights compared to male HFD-fed TPH1 KO mice (P < 0.05). There were no differences in abdominal fat pad weights regardless of sex when comparing WT and TPH1 KO animals on matched diets.

4.4.2 *In vivo* GI transit

For male mice, gastric emptying was similar among WT and TPH1 KO regardless of diet (Figure 19). For female mice, gastric emptying was increased in HFD-fed WT and CD-fed TPH1 KO compared to CD-fed WT (P < 0.05, Figure 19). Female HFD-fed WT gastric emptying was greater than male HFD-fed WT gastric emptying (P < 0.05).

For male mice, the GC was similar between WT CD-fed and HFD-fed mice, but was slightly increased in HFD-fed TPH1 KO mice compared to CD-fed TPH1 KO mice; however, this did not reach significance (P = 0.08, Figure 20). For female mice, the GC was similar between WT and TPH1 KO regardless of diet (Figure 20). The GC of male HFD-fed TPH1 KO was greater compared to the GC of female HFD-fed TPH1 KO mice. To visualize the pattern of FITC-dextran distribution along the small intestine, I plotted the fraction of fluorescence as a function of intestinal segment number. The pattern of FITC-dextran was similar in WT CD-fed and HFD-fed male (Figure 21A) and female (Figure 22A) mice. Similarly, the pattern of FITC-dextran was similar in TPH1 KO CD-fed and HFD-fed male (Figure 21B) and female (Figure 22B) mice. No effect of genotype was observed in the pattern of FITC-dextran in CD-fed male (Figure 21C) and female (Figure 22C) mice.

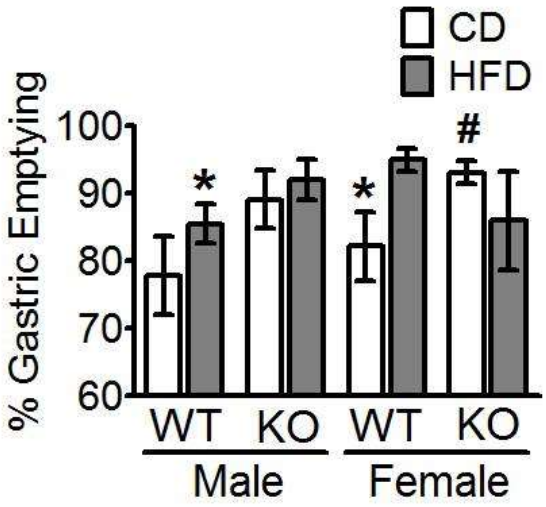

Figure 19. Comparison of *in vivo* gastric emptying in male and female WT and TPH1 KO fed a CD or HFD. Gastric emptying was assessed as the emptying of FITC-dextran delivered through gastric gavage after 30 min. In females, gastric emptying was greater in HFD-fed WT and CD-fed TPH1 KO compared to CD-fed WT. Female HFD-fed WT gastric emptying was greater than male HFD-fed WT gastric emptying. Data are mean ± SEM. *P < 0.05 compared to female HFD-fed WT, $^{\#}P$ < 0.05 compared to female CD-fed WT N = 7-8.

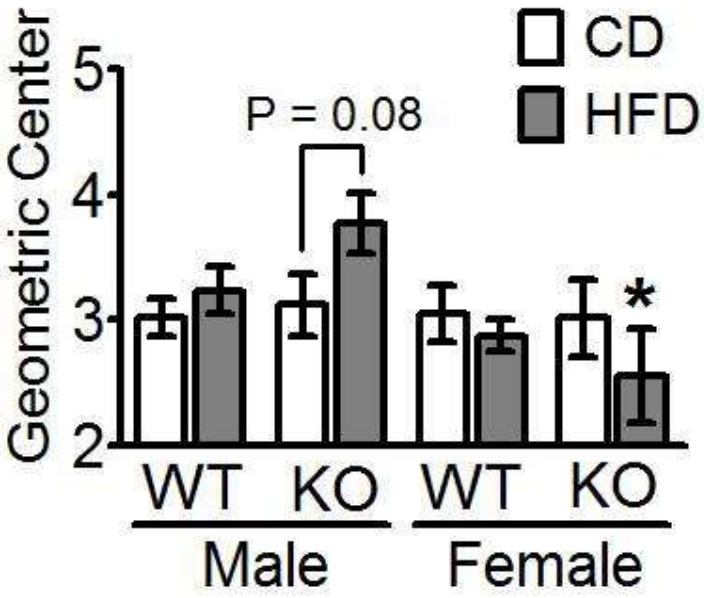

Figure 20. Comparison of *in vivo* small intestinal transit in male and female WT and TPH1 KO fed a CD or HFD. Transit was assessed by the traverse of FITC-dextran along the length of the small intestine delivered through gastric gavage after 30 min. The GC was greater in male HFD-fed TPH1 KO compared to female HFD-fed TPH1 KO mice. Data are mean ± SEM. **P* < 0.05 compared to male HFD-fed TPH1 KO mice, N = 7-8.

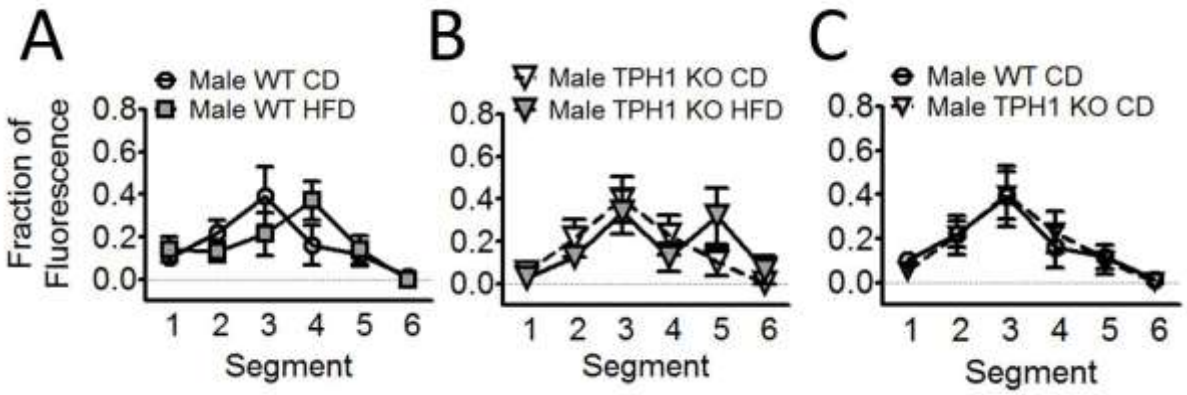

Figure 21. FITC-dextran distribution along the small intestine in male WT and TPH1 KO fed CD or HFD. FITC-dextran distribution as described by the fraction of fluorescence plotted as a function of segment number. (A) The pattern of FITC-dextran was similar in CD-fed and HFD-fed WT mice. (B) The pattern of FITC-dextran was similar in CD-fed and HFD-fed TPH1 KO mice. (C) The pattern of FITC-dextran was similar in CD-fed WT and TPH1 KO mice. Data are mean ± SEM, N = 7-8.

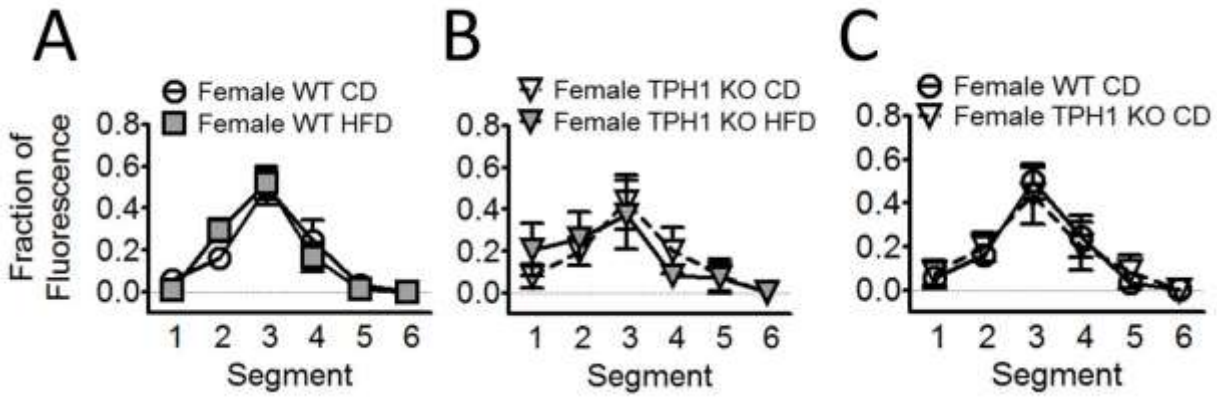

Figure 22. FITC-dextran distribution along the small intestine in female WT and TPH1 KO fed CD or HFD. FITC-dextran distribution as described by the fraction of fluorescence plotted as a function of segment number. (A) The pattern of FITC-dextran was similar in CD-fed and HFD-fed WT mice. (B) The pattern of FITC-dextran was similar in CD-fed and HFD-fed TPH1 KO mice. (C) The pattern of FITC-dextran was similar in CD-fed WT and TPH1 KO mice. Data are mean ± SEM, N = 7-8.

4.4.3 TNFα was under the limit of detection in the majority of mucosal scrapes

Six to eight samples were collected for each animal group totaling 62 samples. Out of the 62 samples, 16 samples had a TNF-α concentration above the limit of detection (L.O.D.) for the ELISA (8.0 pg mL^{-1}). For the samples above the L.O.D, the TNF-α concentration ranged from 8.3 – 17.5 pg mL^{-1}. Samples above the L.O.D. had similar tissue weight and protein concentration to samples below the L.O.D. The range of tissue weights was 11.6 – 53.5 mg depending on the volume of Krebs buffer in the mucosal scrape. The range of protein concentrations was 2.2 - 6.2 μg μL^{-1}.

4.4.4 Mast cell number was greater in the jejunum from HFD-fed females

To quantify the number of mast cells, I used IHC to label 5-HT positive cells in the lamina propria. The distinction of the lamina propria from the epithelial layer was possible using paraffin-embedded sections of 4-5 μm in thickness. Hence, 5-HT positive cells in the epithelial layer (EC cells) were distinguished from 5-HT positive cells in the lamina propria (mast cells).

This is shown in Figure 23A. Female HFD-fed jejunum had a greater number of mast cells compared to female CD-fed jejunum and male HFD-fed jejunum ($P < 0.05$, Figure 23B).

4.4.5 Neuronal 5-HT is unchanged in DIO

IHC was used to visualize 5-HT in the myenteric plexus. In Figure 24A, 5-HT staining is shown in red and Hu staining used to label cell bodies is presented in green. This image shows that the majority of 5-HT staining in the myenteric plexus was found in varicosities in the ganglia and in nerve fiber bundles (e.g. internodal strands) and that 5-HT positive cell bodies were not observed. In some tissues, 5-HT positive varicosities encircled Hu positive cell bodies. Whole tissue levels of 5-HT in whole mount LMMP/SP preparations were similar between CD-fed and HFD-fed jejunum (Figure 24B). No sex differences were observed. Likewise, whole tissue levels of 5-HIAA were similar between CD-fed and HFD-fed jejunum and sex differences were not observed (Figure 24C).

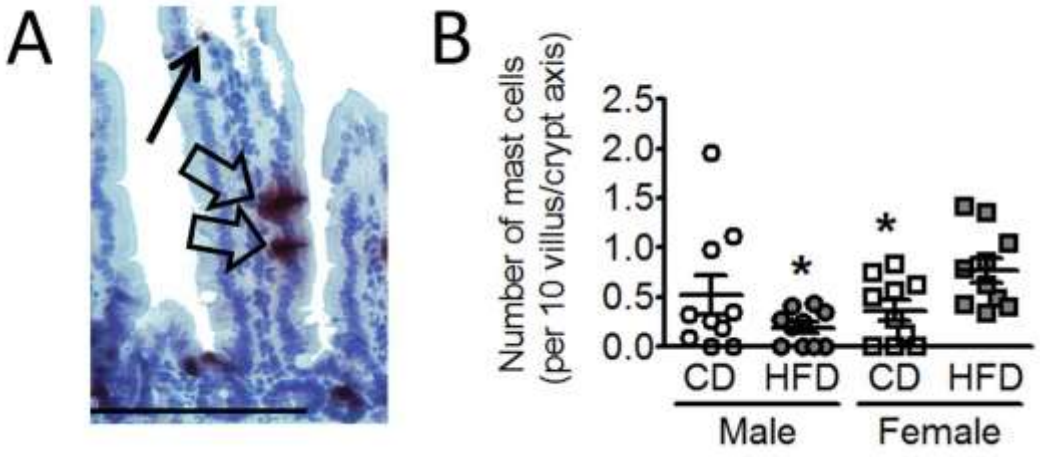

Figure 23 Mast cell number was increased in the lamina propria of HFD-fed female mice. (A) Mast cell (solid black arrow) identified as 5-HT positive cells located in lamina propria and EC cells (open black arrows) identified as 5-HT positive cells in epithelial layer. Mast cells are circular in shape and smaller than EC cells. (B) Mast cell number was greater in HF-fed female compared to control-fed female and HF-fed male jejunum. Scale bar is 200 μm. Data are mean ± SEM, *$P < 0.05$ from HFD-fed fed female, N = 10.

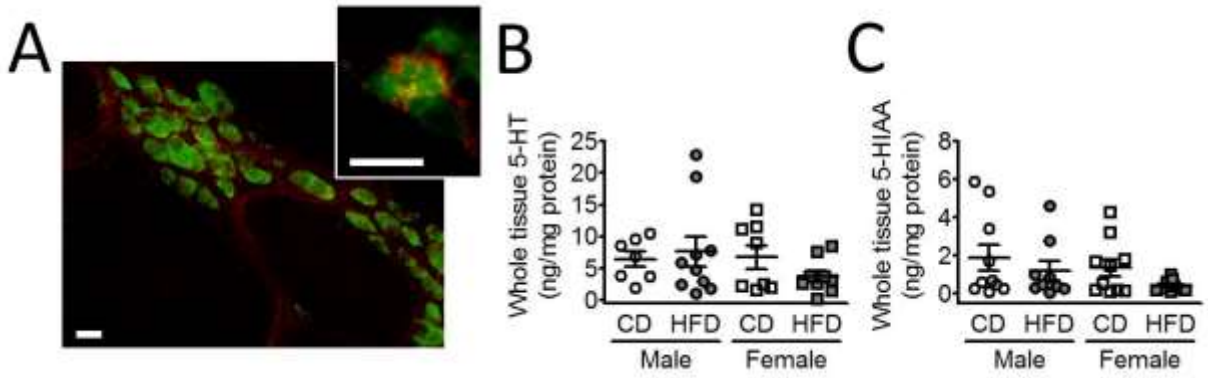

Figure 24 Neuronal 5-HT and 5-HIAA whole tissue levels were similar in CD-fed and HFD-fed WT mice. (A) 5-HT positive staining (red) in whole mount myenteric plexus preparation was present in varicosities in the ganglia, in nerve fiber bundles (internodal strands) and encircling cell bodies. 5-HT positive cell bodies were not observed. Hu was used to label cell bodies (green). (B) 5-HT whole tissue levels from LMMP/SP tissues were similar in CD-fed and HFD-fed WT mice. (C) 5-HIAA whole tissue levels from LMMP/SP tissues were similar in CD-fed and HFD-fed WT. There were no sex differences in (B) or (C). Scale bars are 50 μm. Data are mean ± SEM, N = 7-10.

4.5 DISCUSSION

4.5.1 DIO effects on GI transit in WT and TPH1 KO male and female mice

The role of mucosal 5-HT in initiating peristaltic reflexes is controversial. The role has been hypothesized to be essential for initiation of peristaltic reflexes;[8] however, studies demonstrate that mucosal 5-HT is non-essential.[11, 45] It was demonstrated that CD-fed TPH1 KO and WT littermates have similar transit in both male and female mice. I did not observe any genotype effect in the GC or the pattern of FITC-dextran distribution in the fraction of fluorescence plots vs. intestinal segment number. These plots likely represent the interdigestive migrating motor complex (MMC) of the fasting state.[46] My results are in agreement with those published by Li and colleagues.[11] The authors demonstrated that total transit time assessed by the first observance of carmine red dye in fecal pellets, gastric emptying and the GC were similar in TPH1 KO and WT littermates. The authors used both male and female mice in their studies and combined results of either sex. Measurements of gastric emptying and GC were similar to those results reported herein. The results from this work, together with Li and

colleagues[11] suggest that mucosal 5-HT may not be essential in propulsive MMC generation but may be necessary in the regulation of normally propagating MMCs.

Despite evidence demonstrating that 5-HT is not essential in the initiation of peristalsis, I wanted to determine if mucosal 5-HT plays a role in altered GI motility in DIO. In Chapter 3, I hypothesized that greater mucosal 5-HT concentrations may be necessary for the observed increased small intestinal transit in male HFD-fed mice compared to male CD-fed mice. Therefore, I predicted that if mucosal 5-HT is critical in altered transit in HFD-fed mice then mice that lack mucosal 5-HT should not demonstrate altered transit when fed a HFD. However, in the present study, small intestinal transit was similar in HFD-fed and CD-fed WT littermates. Inconsistencies in my transit studies likely result from differences between Jackson Laboratory mice and our mice breed in-house. This includes the type of cage used to house mice. It is unknown what cage was used in the Jackson Laboratory, but our cages allow minimal climbing (e.g. exercise). In agreement with this, our in-house breed male mice weighed significantly more than the Jackson Laboratory mice for both CD-fed and HFD-fed groups. Regardless, in male TPH1 KO mice, HFD-fed mice had a slightly greater GC compared to CD-fed mice, but this result did not reach significance ($P = 0.08$). This is likely the result of a type II error since there was a significant difference between male HFD-fed TPH1 KO and male CD-fed WT littermates. Male CD-fed WT mice had a similar GC compared to male CD-fed TPH1 KO littermates. Male HFD-fed TPH1 KO mice had a greater GC value compared to female HFD-fed TPH1 KO littermates. This increase in GC observed in males is likely multi-factorial, but may involve sex-related differences in gut microbiota composition. For example, the gut microbiome can regulate the immune system[47] that, in turn, can modulate MMC.[46] This microbiome-immune system axis may differ in both sexes because sex differences in gut microbiome composition exist.[48] In conclusion, mucosal 5-HT is not essential in small intestinal transit in control fed mice, but its absence with the addition of a HFD revealed opposite effects in transit in male and female mice.

The percentage of gastric emptying in males regardless of genotype or diet was similar. In contrast, I found that both female HFD-fed WT and CD-fed TPH1 KO mice had an increase in gastric emptying compared to CD-fed WT littermates. In comparison to female CD-fed WT mice, female HFD-fed WT mice had reduced 5-HT availability as determined in Chapter 3. Hence, a reduction or absence of mucosal 5-HT may result in increased gastric emptying. For instance, glucose-induced 5-HT activation of 5-HT receptors on vagal afferents reduces gastric emptying by a vagovagal reflex.[49] With reduced 5-HT as in the female HFD-fed WT mice, the 5-HT signal to reduce gastric emptying is minimal and hence an increase in gastric emptying is observed. The absence of mucosal 5-HT in the CD-fed TPH1 KO mice means there is no glucose-induced 5-HT activation of 5-HT receptors on vagal afferents to reduce gastric emptying and hence an increase in gastric emptying is observed. The source of glucose from my studies likely comes from FITC-dextran that would be metabolized to glucose by intestinal dextranases. The regulation of gastric emptying involves more than mucosal 5-HT vagovagal signaling since female TPH1 KO mice fed a HFD had similar gastric emptying compared to CD-fed WT littermates. This result suggests that the HFD itself plays a role in modulating gastric emptying. For example, lipids decrease gastric emptying by a vagovagal reflex in rats.[50] Therefore, the HFD fed to female TPH1 KO mice decreases gastric emptying compared to female TPH1 KO littermates fed the CD. However, all mice were fasted overnight before the gastric gavage and so few residual lipids remain in the intestine. Based on the likelihood that few residual lipids are in the intestine during the gastric gavage, 5-HT-dependent effects on gastric emptying will override the HF-diet-dependent regulation of gastric emptying. This is observed by the increase in gastric emptying in female TPH1 KO mice compared to female WT mice both fed the HFD. The predicted roles of mucosal 5-HT and a HFD on the regulatory pathways of gastric emptying are illustrated in Figure 25. Overall, mucosal 5-HT may play an important role in the nutrient vagovagal reflex that regulates gastric emptying, particularly in females.

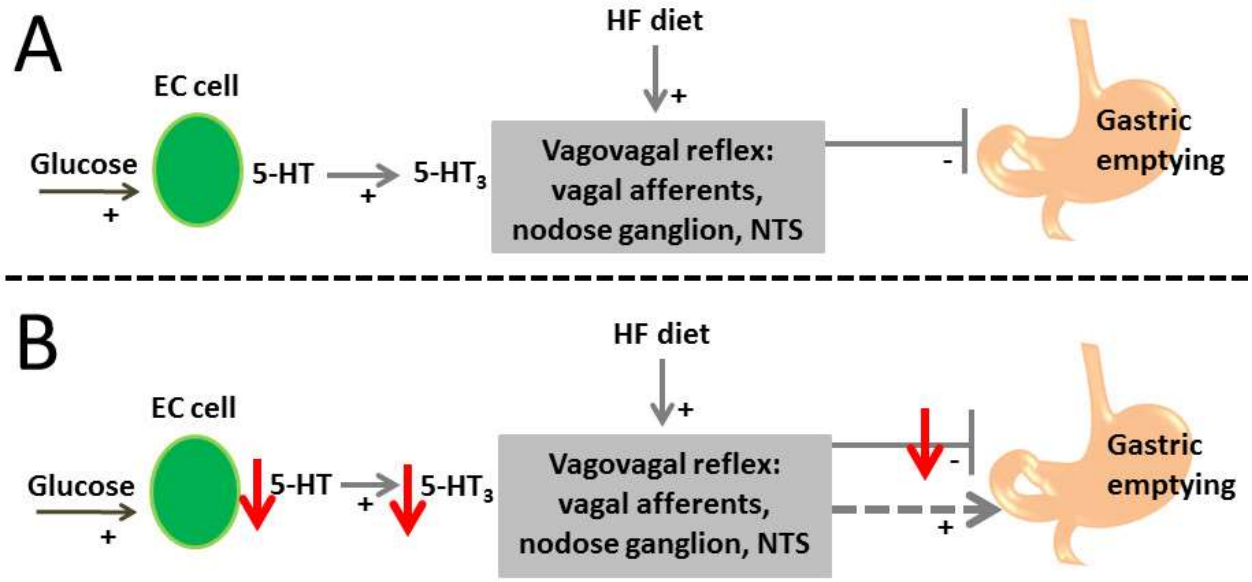

Figure 25 Predicted 5-HT and HFD modulation of gastric emptying. (A) Glucose-driven 5-HT release from EC cells activates 5-HT_3 receptors that are located in the vagovagal reflex either at vagal afferents, nodose ganglion or the NTS to inhibit gastric emptying. Lipids from a HFD can activate the vagovagal reflex to inhibit gastric emptying as well. (B) A reduction or loss of mucosal 5-HT results in lack of 5-HT_3 receptor activation of the vagovagal reflex and in turn removes gastric emptying inhibition revealing and increase in gastric emptying.

4.5.2 Major neuronal 5-HT loss is absent in DIO

I hypothesized that intestinal inflammation in DIO resulted in serotonergic neuron loss caused from the production of a neurotoxic agent by the reaction of 5-HT and MPO. Therefore, the goal of this study was to determine serotonergic neuronal cell death by counting serotonergic neuron number in whole mount LMMP preparations from control and HF-fed mice. However, I did not observe 5-HT positive cell bodies in any preparation. This may be accounted for by the small percentage of serotonergic cell bodies (~2%) in the myenteric plexus.[51] I did observe 5-HT positive varicosities that encircled Hu positive cell bodies and were present on intermodal strands. These observations are in agreement with studies performed by Furness and Costa.[51, 52]

To determine if reductions in neuronal 5-HT concentrations were present in HFD-fed mice, whole tissue levels of 5-HT in LMMP/SP preparations was measured. To prevent any 5-HT degradation that is likely to result from a timely dissection for a preparation that only contains the myenteric plexus, I only removed the mucosa. It has been shown that serotonergic cell bodies in the myenteric plexus send projections to the submucosal plexus.[51, 52] Thus, whole tissue levels combine 5-HT concentrations in the myenteric and submucosal plexus. I did not observe any difference in whole tissue 5-HT or 5-HIAA concentrations between jejunal tissues from CD-fed and HFD-fed males or females. These results suggest that a HFD causes negligible 5-HT neuronal loss. In these preparations, neuronal 5-HT and resulting 5-HIAA concentrations may be confounded by mucosal-derived 5-HT taken up at nerve terminals within the submucosal plexus. Any changes in neuronal concentrations could be masked by this. However, no sex differences in neuronal 5-HT or 5-HIAA concentrations were observed. In contrast, females had greater mucosal whole tissue 5-HT and 5-HIAA levels regardless of diet, as discussed in Chapter 3. This sex difference in mucosal 5-HT and 5-HIAA concentrations demonstrates that little EC cell derived 5-HT contributes to the neuronal concentrations in myenteric plexus preparations. My results suggest that while there may be a sex difference in mucosal 5-HT, neuronal 5-HT concentrations in either diet group were similar across sexes. In conclusion, HFD does not induce major 5-HT neuronal loss and neuronal 5-HT concentrations are similar across sexes.

4.5.3 Mast cell numbers were increased in females fed a HFD

Mast cell numbers were increased in HFD-fed females compared to CD-fed females and to HFD-fed males. Mast cells contain 5-HT in rodents,[53] but the increase in mast cell contributed little 5-HT to whole tissue 5-HT levels because females had similar whole tissue 5-HT levels regardless of diet as demonstrated in Chapter 3. This result confirms that the amount of 5-HT that mast cells contain is negligible compared to that contained in EC cells. The

importance of the increase in mast cell number is not clear. However, this increase does appear to be sex and diet dependent. I determined the number of mast cells in the lamina propria called mucosal mast cells. These cells compromise 2-3% of cells in the lamina propria in healthy individuals.[54] Mast cells react to bacterial, allergenic and parasitic antigens but may also regulate barrier function. Thus, the reason and outcome of an increase in number of mast cells should be further studied.

4.5.4 Conclusions

In conclusion, the present study demonstrated that mucosal 5-HT is not essential for small intestinal transit in CD-fed mice, but may modulate transit in HFD-fed male mice. In female mice, mucosal 5-HT is important in regulating gastric emptying. Neuronal 5-HT is not significantly affected by a HFD in either males or females. Lastly, the concentration of TNFα was too low to detect in the mucosa, but the number of mast cells was increased in HFD-fed female mice. Overall, HFD-dependent alterations in transit are not the direct result of changes in mucosal 5-HT homeostasis or neuronal 5-HT loss.

REFERENCES

REFERENCES

1. Erspamer V. Occurrence of indolealkylamines in nature. In: Erspamer V, ed. 5-Hydroxytryptamine and Related Indolealkylamines. Volume 19: Springer Berlin Heidelberg, 1966:132-181.

2. Bulbring E, Lin RC. The effect of intraluminal application of 5-hydroxytryptamine and 5-hydroxytryptophan on peristalsis; the local production of 5-HT and its release in relation to intraluminal pressure and propulsive activity. J Physiol 1958;140:381-407.

3. Bulbring E, Crema A. The action of 5-hydroxytryptamine, 5-hydroxytryptophan and reserpine on intestinal peristalsis in anaesthetized guinea-pigs. J Physiol 1959;146:29-53.

4. Kidd M, Modlin IM, Gustafsson BI, et al. Luminal regulation of normal and neoplastic human EC cell serotonin release is mediated by bile salts, amines, tastants, and olfactants. Am J Physiol Gastrointest Liver Physiol 2008;295:G260-72.

5. Chin A, Svejda B, Gustafsson BI, et al. The role of mechanical forces and adenosine in the regulation of intestinal enterochromaffin cell serotonin secretion. Am J Physiol Gastrointest Liver Physiol 2012;302:G397-405.

6. Bertrand PP, Kunze WA, Furness JB, et al. The terminals of myenteric intrinsic primary afferent neurons of the guinea-pig ileum are excited by 5-hydroxytryptamine acting at 5-hydroxytryptamine-3 receptors. Neuroscience 2000;101:459-69.

7. Furness JB, Callaghan BP, Rivera LR, et al. The enteric nervous system and gastrointestinal innervation: integrated local and central control. Adv Exp Med Biol 2014;817:39-71.

8. Heredia DJ, Dickson EJ, Bayguinov PO, et al. Localized release of serotonin (5-hydroxytryptamine) by a fecal pellet regulates migrating motor complexes in murine colon. Gastroenterology 2009;136:1328-38.

9. Jin JG, Foxx-Orenstein AE, Grider JR. Propulsion in guinea pig colon induced by 5-hydroxytryptamine (HT) via 5-HT4 and 5-HT3 receptors. J Pharmacol Exp Ther 1999;288:93-7.

10. Viramontes BE, Camilleri M, McKinzie S, et al. Gender-related differences in slowing colonic transit by a 5-HT3 antagonist in subjects with diarrhea-predominant irritable bowel syndrome. Am J Gastroenterol 2001;96:2671-6.

11. Li Z, Chalazonitis A, Huang YY, et al. Essential roles of enteric neuronal serotonin in gastrointestinal motility and the development/survival of enteric dopaminergic neurons. J Neurosci 2011;31:8998-9009.

12. Walther DJ, Peter JU, Bashammakh S, et al. Synthesis of serotonin by a second tryptophan hydroxylase isoform. Science 2003;299:76.

13. Oshima S, Fujimura M, Fukimiya M. Changes in number of serotonin-containing cells and serotonin levels in the intestinal mucosa of rats with colitis induced by dextran sodium sulfate. Histochem Cell Biol 1999;112:257-63.

14. Mushref MA, Srinivasan S. Effect of high fat-diet and obesity on gastrointestinal motility. Ann Transl Med 2013;1:14.

15. Ouchi N, Parker JL, Lugus JJ, et al. Adipokines in inflammation and metabolic disease. Nat Rev Immunol 2011;11:85-97.'

16. Spagnuolo MI, Cicalese MP, Caiazzo MA, et al. Relationship between severe obesity and gut inflammation in children: what's next? Ital J Pediatr 2010;36:66.

17. Cani PD, Bibiloni R, Knauf C, et al. Changes in gut microbiota control metabolic endotoxemia-induced inflammation in high-fat diet-induced obesity and diabetes in mice. Diabetes 2008;57:1470-81.

18. de La Serre CB, Ellis CL, Lee J, et al. Propensity to high-fat diet-induced obesity in rats is associated with changes in the gut microbiota and gut inflammation. Am J Physiol Gastrointest Liver Physiol 2010;299:G440-8.

19. Ding S, Chi MM, Scull BP, et al. High-fat diet: bacteria interactions promote intestinal inflammation which precedes and correlates with obesity and insulin resistance in mouse. PLoS One 2010;5:e12191.

20. Coombes JL, Powrie F. Dendritic cells in intestinal immune regulation. Nat Rev Immunol 2008;8:435-46.

21. Bertola A, Ciucci T, Rousseau D, et al. Identification of adipose tissue dendritic cells correlated with obesity-associated insulin-resistance and inducing Th17 responses in mice and patients. Diabetes 2012;61:2238-47.

22. Idzko M, Panther E, Stratz C, et al. The serotoninergic receptors of human dendritic cells: identification and coupling to cytokine release. J Immunol 2004;172:6011-9.

23. Kidd M, Gustafsson BI, Drozdov I, et al. IL1beta- and LPS-induced serotonin secretion is increased in EC cells derived from Crohn's disease. Neurogastroenterol Motil 2009;21:439-50.

24. Ghia JE, Li N, Wang H, et al. Serotonin has a key role in pathogenesis of experimental colitis. Gastroenterology 2009;137:1649-60.

25. Neal KB, Parry LJ, Bornstein JC. Strain-specific genetics, anatomy and function of enteric neural serotonergic pathways in inbred mice. J Physiol 2009;587:567-86.

26. Gershon MD, Tack J. The serotonin signaling system: from basic understanding to drug development for functional GI disorders. Gastroenterology 2007;132:397-414.

27. Costa M, Brookes SJ, Steele PA, et al. Neurochemical classification of myenteric neurons in the guinea-pig ileum. Neuroscience 1996;75:949-67.

28. Galligan JJ, LePard KJ, Schneider DA, et al. Multiple mechanisms of fast excitatory synaptic transmission in the enteric nervous system. Journal of the Autonomic Nervous System 2000;81:97-103.

29. Monro RL, Bertrand PP, Bornstein JC. ATP and 5-HT are the principal neurotransmitters in the descending excitatory reflex pathway of the guinea-pig ileum. Neurogastroenterology and Motility 2002;14:255-264.

30. Lakhan SE, Kirchgessner A. Neuroinflammation in inflammatory bowel disease. J Neuroinflammation 2010;7:37.

31. Linden DR, Couvrette JM, Ciolino A, et al. Indiscriminate loss of myenteric neurones in the TNBS-inflamed guinea-pig distal colon. Neurogastroenterol Motil 2005;17:751-60.

32. Ximenes VF, Maghzal GJ, Turner R, et al. Serotonin as a physiological substrate for myeloperoxidase and its superoxide-dependent oxidation to cytotoxic tryptamine-4,5-dione. Biochem J 2010;425:285-93.

33. Chen JC, Fine RE, Squicciarini J, et al. Neurotoxicity of free-radical-mediated serotonin neurotoxin in cultured embryonic chick brain neurons. European Journal of Pharmacology 1996;303:109-114.

34. Jiang XR, Wrona MZ, Dryhurst G. Tryptamine-4,5-dione, a putative endotoxic metabolite of the superoxide-mediated oxidation of serotonin, is a mitochondrial toxin: possible implications in neurodegenerative brain disorders. Chem Res Toxicol 1999;12:429-36.

35. Wrona MZ, Jiang XR, Kotake Y, et al. Stability of the putative neurotoxin tryptamine-4,5-dione. Chem Res Toxicol 2003;16:493-501.

36. Rivera LR, Poole DP, Thacker M, et al. The involvement of nitric oxide synthase neurons in enteric neuropathies. Neurogastroenterol Motil 2011;23:980-8.

37. Surendran S, Kondapaka SB. Altered expression of neuronal nitric oxide synthase in the duodenum longitudinal muscle-myenteric plexus of obesity induced diabetes mouse: implications on enteric neurodegeneration. Biochem Biophys Res Commun 2005;338:919-22.

38. Walther DJ, Bader M. A unique central tryptophan hydroxylase isoform. Biochem Pharmacol 2003;66:1673-80.

39. Miller MS, Galligan JJ, Burks TF. Accurate measurement of intestinal transit in the rat. J Pharmacol Methods 1981;6:211-7.

40. McLean AC, Valenzuela N, Fai S, et al. Performing vaginal lavage, crystal violet staining, and vaginal cytological evaluation for mouse estrous cycle staging identification. J Vis Exp 2012:e4389.

41. Byers SL, Wiles MV, Dunn SL, et al. Mouse estrous cycle identification tool and images. PLoS One 2012;7:e35538.

42. Caligioni CS. Assessing reproductive status/stages in mice. Curr Protoc Neurosci 2009;Appendix 4:Appendix 4I.

43. Chen TS, Doong ML, Chang FY, et al. Effects of sex steroid hormones on gastric emptying and gastrointestinal transit in rats. Am J Physiol 1995;268:G171-6.

44. Wood GA, Fata JE, Watson KL, et al. Circulating hormones and estrous stage predict cellular and stromal remodeling in murine uterus. Reproduction 2007;133:1035-44.

45. Keating DJ, Spencer NJ. Release of 5-hydroxytryptamine from the mucosa is not required for the generation or propagation of colonic migrating motor complexes. Gastroenterology 2010;138:659-70 670 e1-2.

46. Romanski KW. Migrating motor complex in biological sciences: characterization, animal models and disturbances. Indian J Exp Biol 2009;47:229-44.

47. Koboziev I, Reinoso Webb C, Furr KL, et al. Role of the enteric microbiota in intestinal homeostasis and inflammation. Free Radic Biol Med 2014;68:122-33.

48. Markle JG, Frank DN, Mortin-Toth S, et al. Sex differences in the gut microbiome drive hormone-dependent regulation of autoimmunity. Science 2013;339:1084-8.

49. Raybould HE, Glatzle J, Robin C, et al. Expression of 5-HT3 receptors by extrinsic duodenal afferents contribute to intestinal inhibition of gastric emptying. Am J Physiol Gastrointest Liver Physiol 2003;284:G367-72.

50. Holzer HH, Turkelson CM, Solomon TE, et al. Intestinal lipid inhibits gastric emptying via CCK and a vagal capsaicin-sensitive afferent pathway in rats. Am J Physiol 1994;267:G625-9.

51. Costa M, Furness JB, Cuello AC, et al. Neurons with 5-hydroxytryptamine-like immunoreactivity in the enteric nervous system: their visualization and reactions to drug treatment. Neuroscience 1982;7:351-63.

52. Furness JB, Costa M. Neurons with 5-hydroxytryptamine-like immunoreactivity in the enteric nervous system: their projections in the guinea-pig small intestine. Neuroscience 1982;7:341-9.

53. Theoharides TC, Bondy PK, Tsakalos ND, et al. Differential release of serotonin and histamine from mast cells. Nature 1982;297:229-31.

54. Bischoff SC, Wedemeyer J, Herrmann A, et al. Quantitative assessment of intestinal eosinophils and mast cells in inflammatory bowel disease. Histopathology 1996;28:1-13.

CHAPTER 5

OTHER ELECTROACTIVE SPECIES CONTRIBUTE TO OXIDATION CURRENTS IN ADDITION TO 5-HT IN CONTINUOUS AMPEROMETRIC MEASUREMENTS IN GUT MUCOSA

5.1 ABSTRACT

Continuous amperometry (CA) is now a common technique used to study 5-HT release and clearance in healthy or diseased intestinal tissues. In CA, a microelectrode is positioned near to 5-HT release sites at the intestinal mucosal surface and used to detect 5-HT as an oxidation current. Our study revealed that other electroactive species, besides 5-HT, contributed to the measured oxidation current in CA measurements. We measured oxidation currents near to the mucosal surface using CA in small and large intestine from tryptophan hydroxylase 1 knockout (TPH1 KO) (the enzyme necessary for intestinal 5-HT production) and wildtype (WT) mice. Results showed that oxidation currents measured in tissues from TPH1 KO mice are only slightly decreased compared to tissues from wildtype (WT) mice. The selective serotonin reuptake inhibitor (SSRI) fluoxetine or cocaine did not increase oxidation currents measured in TPH1 KO small intestine, suggesting the measured current is not from 5-HT oxidation. Fluid sampled near to the mucosa contained similar concentrations of the 5-HT metabolite, 5-hydroxyindole acetic acid (5-HIAA) and uric acid. The peak oxidation potential (E_p^{ox}) of 5-HIAA (0.58 V) and uric acid (0.61) overlap that of 5-HT (0.35 - 0.72 V). The E_p^{ox} of tryptophan was ~+1 V, but produced a significant current when flowed through the CA system at +0.855 V. Our results demonstrate that other electroactive molecules contribute to the oxidation currents measured using CA in addition to 5-HT. Use of this method is appropriate to study 5-HT release and uptake using pharmacological methods; however, determining absolute 5-HT concentrations from the measured oxidation current can be subject to error.

5.2 INTRODUCTION

Continuous amperometry (CA) is the analytical method often used to measure 5-hydroxytryptamine (5-HT, serotonin) from the gut mucosa using animal intestinal specimens *ex vivo*.[1-13] CA is ideal in studying real-time 5-HT concentration changes because of its high temporal resolution in contrast to enzyme-linked immunoassays (ELISA) that measure steady state levels. Typically, microelectrodes are used because measurements can be made very close to 5-HT release sites on villi of the gut mucosa. In CA, the potential of a recording electrode is poised at a fixed potential sufficient to oxidize or reduce a redox analyte at a mass transport-limited rate. In the present work, the potential is selected based on the peak oxidation potential (E_p^{ox}) for 5-HT. Any electroactive species that can be oxidized at or below the E_p^{ox} for 5-HT will contribute to the measured current. Thus, CA may not be selective for 5-HT or any one redox analyte. However, the major electroactive species present in the gut mucosa is 5-HT. Our lab determined in whole tissue mucosal scrapes that dopamine (DA) and norepinephrine (NE), their precursors and metabolites are ~100 fold lower than the 5-HT concentration measured with HPLC using electrochemical detection (unpublished data). Others determined with voltammetry that other possible electroactive molecules present in the mucosa are not detected at the potentials used to measure 5-HT oxidation. These include melatonin and tyramine.[1] This led researchers to use calibration plots in which standard concentrations are run through the system and plotted against the measured oxidation current in order to convert the experimental current made in intestinal preparations to a 5-HT concentration.[1, 2, 5, 6, 11-14] By this method, 5-HT concentrations in the gut mucosa are in the micromolar range while 5-HT concentrations in the nanomolar range were measured with ELISA.[15] Discrepancies in 5-HT concentration result from the differences in the sampled volume in each technique. In addition, other electroactive

species likely present near to the gut mucosa could contribute to the oxidation current thereby over estimating the 5-HT concentration.

In the gut mucosa, 5-HT is synthesized, stored and released from enterochromaffin (EC) cells. EC cells are a specialized enteroendocrine cell that represent 1-3% of the epithelial population[16] and are located within the epithelial layer that covers the finger-like villi. In the EC cell, tryptophan is converted to the 5-HT precursor 5-hydroxytrytophan (5-HTP) by the rate-limiting and EC cell specific enzyme tryptophan hydroxylase 1 (TPH1).[17] 5-HTP is then converted to 5-HT by L-amino acid decarboxylase (L-AADC) and transported by the vesicular transporter VMAT1 into secretory granules localized to the basolateral and apical side of the EC cell.[18] EC cells sense and respond to certain nutrients and chemicals present in the luminal content[15] by releasing 5-HT in a calcium-dependent manner.[19] In addition, mechanical stimulation of the mucosa by an adenosine-dependent pathway stimulates 5-HT release.[20] Thus, amperometric measurements oxidize luminally released 5-HT and 5-HT overflow following its release into the lamina propria.[2] In these measurements, the stress of the flowing buffer mechanically activates 5-HT release. Following its release it can encounter the electrode and become oxidized.

The aim of my study was to determine if 5-HT was the major contributor to the oxidation current in CA measurements made near to the gut mucosa. To accomplish this, I 1) compared amperometric measurements in intestinal tissues from TPH1 knockout (KO) and wildtype (WT) mice, 2) used pharmacological methods to block 5-HT uptake in these tissues, 3) measured 5-HT, 5-HIAA and uric acid in the Krebs buffer fluid sampled in the region where the electrode is positioned during CA recordings and 4) determined if tryptophan could potentially contribute to the measured oxidation current.

5.3 METHODS AND MATERIALS

5.3.1 Mice

All animal use protocols were approved by the Institutional Animal Care and Use Committee at Michigan State University. Homozygous breeder TPH1 KO mice were obtained from Dr. Michael Bader, Max-Delbrück-Center for Molecular Medicine (MDC) at Berlin, Germany.[17, 21] Homozygous TPH1 KO mice were then bred with C57BL/6J WT from Jackson Laboratories (Bar Harbor, ME, USA) in house to produce heterozygous. The colony was maintained by breeding heterozygous mice. Male WT and TPH1 KO littermates were used for the studies. Littermates were housed in cages (max. 5 per cage) and allowed food and water *ad libitum* on a 12 h light dark cycle. Mice were studied at 10-12 wk of age. Mice were euthanized using isoflurane anesthesia followed by cervical dislocation. For CA studies, a segment of the jejunum or distal colon was excised and placed in oxygenated (95% O_2, 5% CO_2) Krebs buffer (pH 7.4). The jejunum was excised just distal to the ligament of Treitz. The distal colon was removed ~ 0.5 cm proximal to the rectum.

5.3.2 Boron-doped diamond microelectrode fabrication

Details of the preparation and characterization of the diamond microelectrodes have been reported elsewhere.[8, 22-24] Pt wire (99.99%, Sigma-Aldrich Chemical, 76 μm diam.) was cut into a 1.3 cm long segment. Both ends were sharpened electrochemically in 1 M KOH into a conical shape. The sharpened Pt wires were then ultrasonically cleaned in acetone for 10 min and then ultrasonically seeded in a diamond powder suspension (3–6 nm particles, ca. 20 mg in 100 ml of ethanol, Tomei Diamond Co., Tokyo, Japan) for 30 min. During the ultrasonic treatments, the Pt wire laid flat on the bottom of a glass beaker. Next, a boron-doped diamond thin film was deposited on the Pt wire using microwave-assisted chemical vapor deposition (CVD). It was common practice to deposit boron-doped diamond onto 3 Pt wires simultaneously. The deposition was achieved using a commercial CVD system (1.5 kW, 2.54 GHz, ASTeX, Woburn,

MA, USA) in which the source gas mixture was 1% CH_4/H_2 (v/v) and 10 ppm of diborane (0.1% B_2H_6 diluted in H_2) was used for doping. The parameters were as follows: microwave power was 600 W, system pressure was 35 Torr, and an estimated substrate temperature in the range of 700 - 800 °C. The temperature was estimated using a single filament optical pyrometer. The deposition time was typically 6 - 7 h. During the deposition, the seeded Pt wires were positioned horizontally sandwiched between two small pieces of quartz such that the fibers were a couple of millimeters above the substrate stage. At the end of the deposition period, the diamond-coated wires were slowly cooled in the presence of atomic hydrogen by lowering the power and pressure over a 30 min period. This cool down, which is critical for maintaining sp^3 carbon bonding and hydrogen termination at the surface, was performed with only an H_2 gas flow and the plasma ignited. After this post-growth hydrogen plasma treatment, the diamond-coated wires were cooled to room temperature under a flow of H_2.

After growth, the diamond-coated wire was cut in the center producing two conically-shaped diamond microelectrodes. The cut end of each wire was connected to a copper wire using a dab of super glue to enhance the mechanical strength and then with conducting silver epoxy for electrical connection. The end of the diamond-coated wire was then sealed by carefully melting the end of a polypropylene pipette tip using the heating coil of a micropipette puller. The resulting exposed diamond microelectrode was conical in shape with a tip diameter of about 10 μm and an exposed length of 300 - 700 μm. In this preparation, the exposed length is difficult to reproducibly control.

5.3.3 Cyclic voltammetry

Cyclic voltammetry was then used to determine which microelectrodes are suitable for the CA measurements. This was done with several aqueous redox systems, including a 10 μmol L^{-1} 5-HT standard solution, using a CH Instruments electrochemical workstation (Model 600D, Austin, TX). All measurements were made in a single-compartment glass electrochemical cell. A Pt

wire served as the counter electrode and a commercial, no-leak, Ag/AgCl electrode (3 M KCl) was used as the reference. The cyclic voltammetric peak oxidation potential (E_p^{ox}) and peak current (i_p^{ox}) for 5-HT (10 µmol L^{-1}) prepared in Krebs buffer (pH 7.4) were measured before and after the CA measurements to assess the stability of the microelectrode response. The cyclic voltammetric E_p^{ox} was also used to determine the fixed potential to use for detection in the CA measurements. For most diamond microelectrodes, there was very little change in either the E_p^{ox} or i_p^{ox} for the 5-HT standard solution after CA measurements (data not shown). This confirmed the excellent response stability of diamond in this complex biological environment.

5.3.4 Continuous amperometric (CA) measurements of 5-HT uptake

Segments of jejunum or distal colon were stretched gently (ca. 1 cm^2) and pinned (stainless steel, 0.2 mm diameter, 26002-20, Fine Science Tools, Foster City, CA) in a Sylgard® lined flow bath (ca. 6 mL) with the mucosal surface turned upwards. A schematic of the diamond microelectrode and the mucosal preparation used in CA measurements was shown in Chapter 3 (Figure 14). Oxygenated Krebs buffer solution, kept at room temperature, flowed over the tissue at a rate of 2 mL min^{-1} using a peristaltic pump (Minipuls 2, Gilson, Middleton, WI). Precise positioning of the diamond microelectrode was accomplished using a micromanipulator (MM33, Fine Scientific Tools, Foster City). Villi and diamond microelectrode positioning were visualized using an upright microscope (Model SMZ1000, Nikon, USA). Experiments commenced after a 30-min equilibration period. Measurements were made in a Faraday cage to minimize electrical noise.

5-HT detection was accomplished at +0.855 V vs. Ag/AgCl (3 M KCl) using a ChemClamp potentiostat (Dagan Corp., Minneapolis, MN, USA). The analog current from the potentiostat was captured and digitally converted with an e-corder hardware unit (eDAQ Inc., Colorado Springs, CO, USA) at a sampling rate of 200 points s^{-1}. The current was low-pass filtered (1

kHz filter) prior to digitization. Current recordings were generated on-line using Chart software. A home-made Ag/AgCl electrode served as the counter and reference in a two-electrode measurement configuration. The reference electrode was positioned in the flow bath somewhat removed from the position of the working electrode and tissue. CA measurements consisted of current approach curves in which the electrode distance in relation to the mucosal surface was decreased in a step-wise fashion. Electrode distances used were 750, 500, 250, 100, 50 and 10 μm away from the mucosal surface. In order to determine the electrode distance from the mucosal surface, the electrode was first positioned such that it gently touched the villus, then it was retracted to a distance of 2000 μm that served as the distance for the background current measurements. The background current was measured at 2000 μm as at this distance the current was unaffected by 5-HT release due to dilution effects. When the background current was stable, the recording of current-approach curves commenced. For each current measurement, the electrode was positioned at a calibrated distance for ca. 40 - 60 s. Within this time window, a stable current was reached. The current magnitude at each electrode distance was recorded by averaging the current over the last 20 - 30 s of the period and subtracting from this the average background current measured at the 2000 μm distance. The natural log (*ln*) of the current at each electrode distance was plotted as a function of the distance. A linear fit of the data was performed and the slope was determined in order to assess 5-HT uptake as previously described. [10, 25] Fluoxetine and citalopram (1 μmol L^{-1}), selective 5-HT reuptake inhibitors (SSRI), and cocaine (10 μmol L^{-1}), a SERT, norepinephrine (NET) and dopamine transport (DAT) inhibitor, were used to assess SERT function. Fluoxetine, citalopram and cocaine are not electroactive at the potential used for detecting 5-HT (data not shown). A solution containing any of the drugs used was flowed across the tissue for 5 min before a current approach curve was recorded. The drug was also present during the measurement. Measurements were made before (Krebs buffer), during application, and after washout (20 min) of the drug. All drugs evoked a reversible increase in the 5-HT oxidation

current due to an increase in the 5-HT extracellular concentration. In our studies, SERT function was assessed by comparing the slope of the *In* current vs. the electrode distance plots with and without drug addition.[10] A decrease in the slope indicated reduced 5-HT uptake.[10]

5.3.5 HPLC measurements of molecules in fluid sampled near to gut mucosa

For extracellular levels, a Hamilton syringe was used to sample the Krebs buffer (150 µL) near to the mucosa surface (ca. 500 µm away) in jejunal preparations used for CA experiments. The syringe was positioned using a micromanipulator. Extracellular fluid was added to ice cold 0.1 M perchloric acid (50 µL), centrifuged (4 ˚C) at 14,000 RPM for 10 min. Supernatant was removed and stored at -80 ˚C until analysis. Supernatant (20 µL) samples were injected using an autosampler (ESA 542, Thermo-Fisher) maintained at 35 ˚C onto a ESA guard column (70-1972) in-line with a Thermo MD column (150 mm x 3.2 mm, 3 µm particle size) for separation and detected using a ESA 5011A analytical cell set to a potential of + 200 mV. The mobile phase consisted of the following composition (mmol L^{-1}): 90 sodium phosphate, 50 citrate, 1.94 sodium octyl sulfate, 0.05 EDTA and 10 % acetonitrile and flowed at a rate of 0.6 mL min^{-1} (ESA 582). Representative retention times for 5-HT and 5-HIAA were around 15 and 5 min, respectively. Uric acid, hypoxanthine and xanthine were separated using a Phenomenex's Luna C-18 column (250 mm x 4.6 mm, 5 µm particle size) and detected using a photo diode array. The mobile phase consisted of 0.02 M sodium acetate (pH 4.5) with acetic acid and flowed at 1 mL min^{-1}. Uric acid, hypoxanthine and xanthine were detected at 284, 248 and 266 nm, respectively. All results are presented as nM.

5.3.6 Reagents and drugs

The Krebs buffer used in the measurements consisted of the following composition (mmol L^{-1}): 117 NaCl, 4.7 KCl, 2.5 $CaCl_2$, 1.2 $MgCl_2$, 1.2 NaH_2PO_4, 25 $NaHCO_3$, and 11 glucose. All drugs

and reagents were obtained from Sigma Aldrich (St. Louis, MO, USA). For CA studies, drugs were stored as aliquots at -20 ˚C and were freshly prepared in Krebs buffer for each experiment.

5.3.7 Statistical analysis

All data analysis was performed using GraphPad Prism software. For CA experiments, comparisons between measurements made in Krebs buffer and measurements made in the presence of a drug were made using a paired Student's *t*-test. Two-way ANOVA was used to determine the effect of genotype (WT vs. TPH1 KO) and electrode distance (750 - 10 µm) on the measured oxidation current from current approach curves. For all comparisons, $P < 0.05$ was considered statistically significant. Data are reported as mean $\pm$ S.E.M.

5.4 RESULTS

5.4.1 Large oxidation currents from TPH1 KO intestinal tissues are not from 5-HT oxidation

Figure 26A shows current approach curves made before (Krebs buffer, pH = 7.4), during application and after washout of fluoxetine (1 µmol L^{-1}, 5 min) in jejunum from WT mice. Two consecutive current approach curves (only one of which is shown) were made under control conditions where only Krebs buffer flowed over the tissue. Fluoxetine (1 µmol L^{-1}) applied for 5 min caused in increase in the oxidation current at all electrode distances. Two consecutive curves were made in the presence of fluoxetine and both traces were reproducible in terms of the current magnitudes. Fluoxetine was washed from the tissue (20 min) and oxidation currents returned to Krebs buffer only levels. Similar current approach curves were achieved in the presence of cocaine. Figure 26B shows current approach curve made before (Krebs buffer, pH = 7.4) and during application of fluoxetine (1 µmol L^{-1}, 5 min) in jejunum from TPH1 KO mice. The current magnitudes at each distance in the approach curve recorded in the jejunum from TPH1 KO mice were smaller in magnitude compared to WT mice. Fluoxetine and cocaine did

not increase the current magnitude at any electrode distances in current approach curves in made TPH1 KO jejunum. Due to the lack of a drug effect, a washout step was not performed. Data for the current approach curves made in Krebs buffer, fluoxetine and during washout are summarized in Figure 26C for WT and Figure 26D for TPH1 KO jejunal tissues.

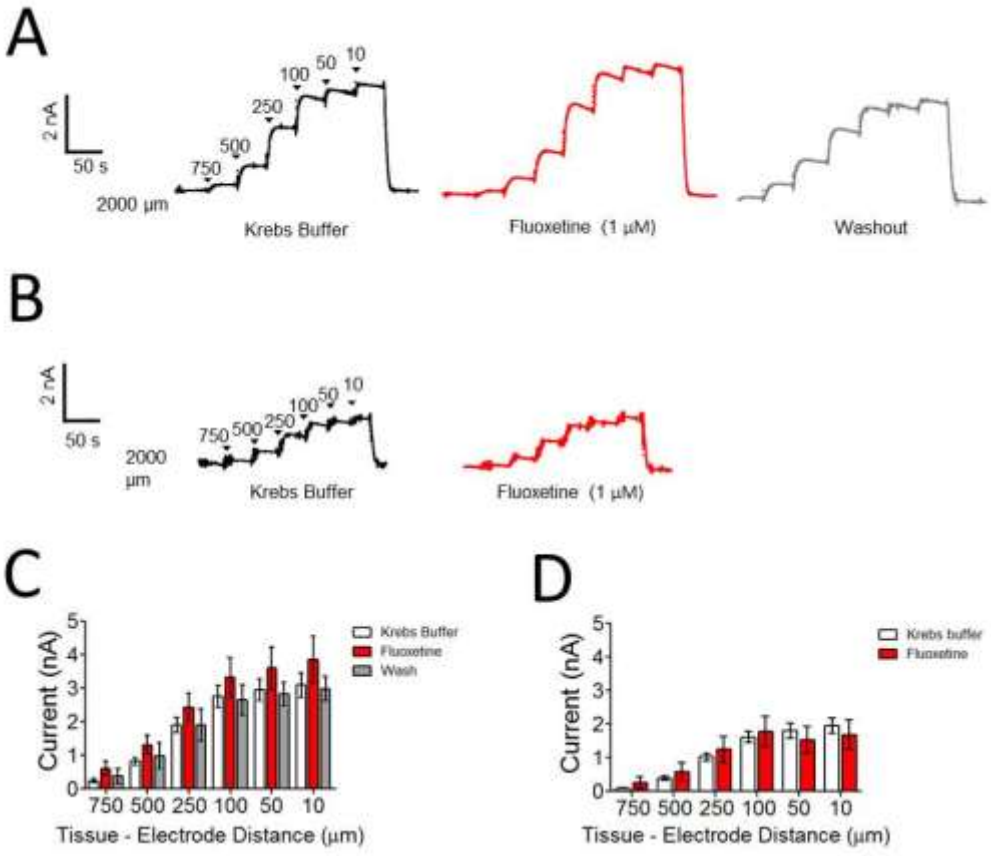

Figure 26. Comparison of oxidation currents made in WT and TPH1 KO jejunal tissues presented as current approach curves. (A) Representative current approach curve made in the jejunum from WT mice made from current measurements obtained at varying electrode distances (750 – 10 µm) before (Krebs buffer, pH 7.4), during and after (washout) application of fluoxetine (1 µmol L^{-1}; 5 min). Background current was measured in the bulk media at 2000 µm. Fluoxetine produced a reversible increase in 5-HT oxidation currents. (B) Representative current approach curve made in the jejunum from TPH1 KO mice. Fluoxetine did not change current measurements at any electrode distance. (C) Bar graph summarizing measured oxidation current from WT jejunal current approach curves (*n* = 4) made in Krebs buffer (control, white bars), in presence of fluoxetine (red bars) and after fluoxetine was washed out (grey bars). (D) Bar graph summarizing oxidation current from TPH1 KO jejunal current approach curves (*n* = 4) made in Krebs buffer (control, white bars) and in presence of fluoxetine (red bars). Scale is 2 nA and 50 s. Data are mean ± S.E.M.

Current magnitudes were plotted as a function of tissue-electrode distance (data not shown) and the best-fit line to the *ln* current vs. electrode distance plot was used to obtain the slope; a measure of 5-HT uptake. The x-axis is in reverse compared to Figure 26. In the jejunum from WT mice, fluoxetine and cocaine reduced the slope of the best-fit line to the *ln* current vs. electrode distance plot compared to measurements in Krebs buffer (fluoxetine: 0.0026 ± 0.0002 μm^{-1}; cocaine: 0.0023 ± 0.0003 μm^{-1}; Krebs buffer: 0.0036 ± 0.0002 μm^{-1}; n = 4; $P < 0.05$, Figure 27A). In contrast, fluoxetine and cocaine did not change the slope of the best-fit line to the ln current vs. electrode distance plot compared to measurements in Krebs buffer in jejunum from TPH1 KO mice (fluoxetine: 0.0043 ± 0.0002 μm^{-1}; cocaine: 0.0044 ± 0.0004 μm^{-1}; Krebs buffer: 0.0046 ± 0.0003 μm^{-1}; n = 4, $P > 0.05$, Figure 27B). The data for the two animal groups are summarized in the bar graph shown in Figure 27C.

Figure 28 shows current approach curves made in distal colonic tissues from WT (A) and TPH1 KO (B) mice in Krebs buffer. Fluoxetine, citalopram and cocaine did not increase the measured current in WT distal colon preparations (data not shown). Regardless of genotype, oxidation current magnitudes from distal colonic tissues were much reduced compared those from jejunal tissues.

I next compared WT and TPH1 KO oxidation currents from current approach curves in jejunal (Figure 29A) and distal colonic (Figure 29B) tissues. In jejunal tissues, oxidation currents from TPH1 KO mice are roughly 1/2 to 2/3 of the oxidation currents from WT mice at electrode distances close to the mucosal surface (250 - 10 µm). In distal colonic tissues, the oxidation currents from TPH1 KO mice overlap those from WT mice at all electrode distances. Table 1 provides the measured oxidation current ± S.E.M at each electrode distance for WT and TPH1 KO jejunal and distal colonic tissues. Two-way ANOVA analysis with Bonferroni *post-hoc* test revealed that genotype (P <0.05) and electrode distance (P <0.05) had an effect on the oxidation current measured in both jejunal and distal colonic tissues.

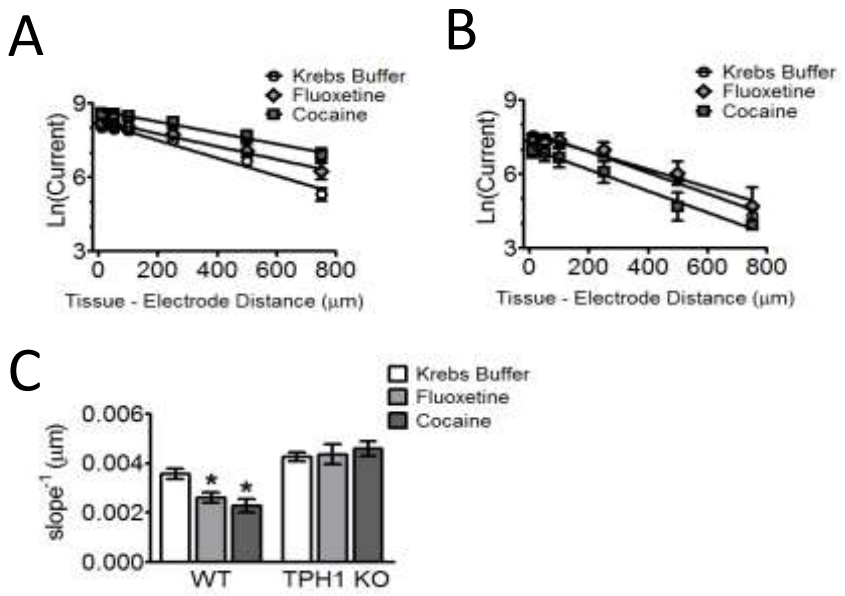

Figure 27. Effect of fluoxetine and cocaine in the jejunum of WT and TPH1 KO mice. The natural log (*ln*) of the current magnitude was plotted as a function of tissue-electrode distances in which the slope was a measure of 5-HT uptake. Measurements were made in Krebs buffer (control; open circle, pH 7.4), fluoxetine (1 μmol L^{-1}, grey diamond) and cocaine (10 μmol L^{-1}, dark grey square). (A) Fluoxetine and cocaine reduced the slope (i.e. reduced 5-HT uptake) in measurements made in the jejunum from WT mice (*n* = 4). (B) Fluoxetine and cocaine did not change the slope in measurements made in the jejunum from TPH1 KO mice (*n* = 4). (C) Bar graph summarizing fluoxetine and cocaine effects on the slope in WT and TPH1 KO jejunal preparations. Data are mean ± S.E.M., **P* < 0.05 vs. WT Krebs buffer.

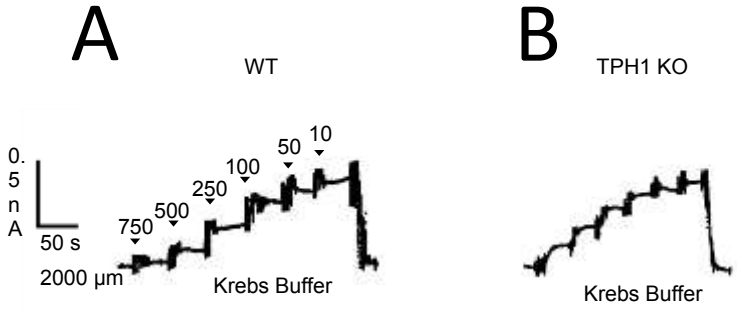

Figure 28. Comparison of WT and TPH1 KO distal colonic current approach curves. Representative current approach curves (750 – 10 μm) made in distal colonic preparations from WT (A) and TPH1 KO (B) mice in Krebs buffer (pH 7.4). Fluoxetine, citalopram and cocaine did not increase 5-HT oxidation currents in WT distal colons (not shown). Scale is 0.5 nA and 50 s.

There was no interaction of genotype or electrode distance on the measured oxidation current in jejunal and distal colonic preparations. Oxidation currents measured at electrode distances of 250-10 µm were different between WT and TPH1 KO jejunal tissues. Oxidation currents measured at all electrode distances were similar between WT and TPH1 KO distal colonic tissues.

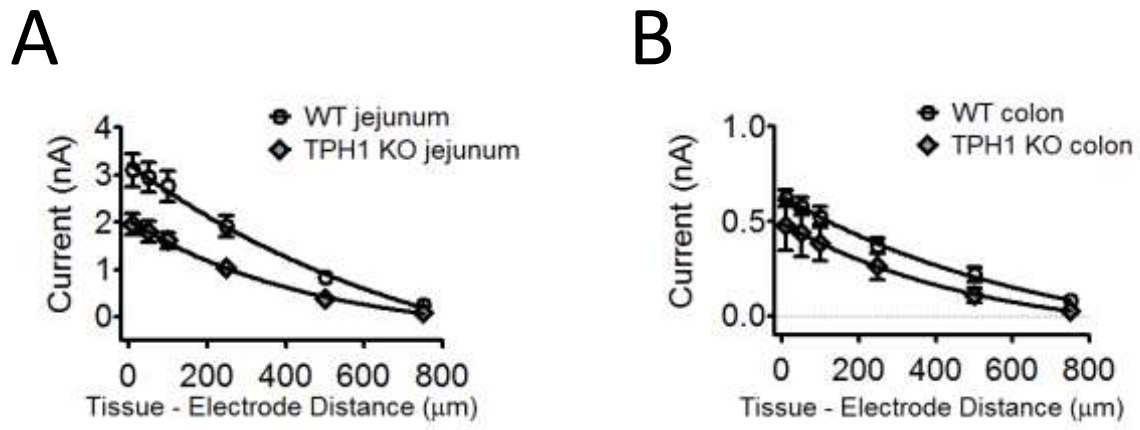

Figure 29. Comparison of current vs. tissue-electrode distance curves in WT and TPH1KO jejunal and distal colonic tissues. Current vs. tissue-electrode distance plots were generated by plotting the current magnitude as a function of the tissue-electrode distances. Current magnitudes were calculated from the difference in current magnitude from an individual tissue-electrode distance and the current measured within the bulk media (2000 µm). (A) Oxidation currents measured at electrode distances near to the mucosa (250-10 µm) were greater in WT (open circle) compared to TPH1 KO (grey diamond) jejunal tissues. (B) Oxidation currents measured at all electrode distances were similar in WT and TPH1 KO distal colonic preparations. A significant oxidation current was measured in jejunal and distal colonic tissues from TPH1 KO mice. This current was not due to 5-HT oxidation. Scales are different in A and B. Data are mean ± S.E.M.

Electrode distance (μm)	Oxidation current magnitude (nA)			
	WT jejunum (*n* = 4)	**TPH1 KO jejunum (*n* = 4)**	**WT distal colon (*n* = 4)**	**TPH1 KO distal colon (*n* = 6)**
750	0.24 ± 0.06	0.09 ± 0.02	0.08 ± 0.02	0.03 ± 0.02
500	0.82 ± 0.12	0.38 ± 0.06	0.22 ± 0.04	0.11 ± 0.04
250	1.91 ± 0.23	1.02 ± 0.11*	0.37 ± 0.04	0.26 ± 0.07
100	2.76 ± 0.33	1.61 ± 0.17*	0.52 ± 0.06	0.39 ± 0.10
50	2.95 ± 0.32	1.80 ± 0.22*	0.58 ± 0.05	0.44 ± 0.13
10	3.09 ± 0.35	1.96 ± 0.22*	0.62 ± 0.05	0.48 ± 0.13

Table 1. Oxidation current magnitudes from intestinal tissues of WT and TPH1 KO mice. Comparisons of oxidation current magnitudes (nA) measured at different electrode distances (μm) from current approach curves were made between WT jejunal, TPH1 KO jejunal, WT distal colonic and TPH1 KO distal colonic tissues. Data are mean ± S.E.M., *P < 0.05 vs. WT jejunum, two-way ANOVA with Bonferroni's *post hoc* test.

5.4.2 Uric acid is present near to jejunal mucosa

Jejunal extracellular hypoxanthine and xanthine concentrations were similar in WT (n = 2) and TPH1 KO (n = 4) mice, respectively (WT: 0.23 ± 0.08 nM, 0.41 ± 0.04 nM; TPH1 KO: 0.13 ± 0.03 nM, 0.25 ± 0.06 nM, P > 0.05, Figure 30A). The jejunal extracellular uric acid concentration was greater than both precursors in WT and TPH1 KO mice (P < 0.05) and was greater in WT(n = 2) compared to TPH1 KO (n = 4) mice (1.23 ± 0.09 nM vs. 3.19 ± 0.42 nM, P < 0.05, Figure 30A). Similar jejunal extracellular 5-HT and 5-HIAA concentrations were observed in WT mice (3.25 ± 0.68 nM vs. 3.55 ± 0.44 nM, P > 0.05, Figure 30B).

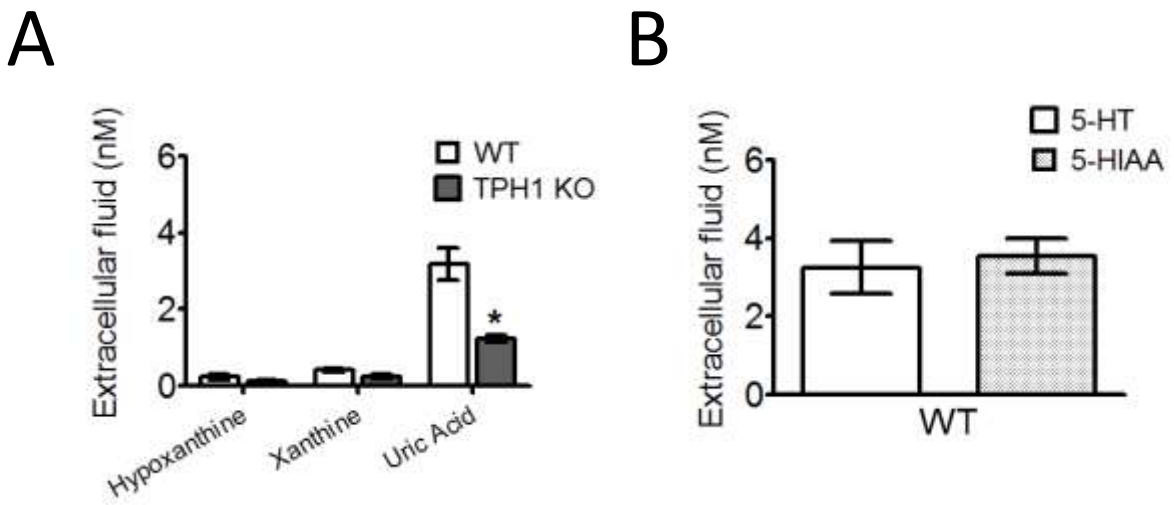

Figure 30. Other electroactive analytes present near the jejunal mucosa are similar in concentration to 5-HT. (A) Hypoxanthine, xanthine and uric acid were present in extracellular fluid from WT (n = 2) and TPH1 KO (n = 4) jejunal tissues. Extracellular uric acid concentration was greater in WT compared to TPH1 KO mice. (B) Extracellular 5-HT and 5-HIAA concentrations were similar in fluid sampled from WT jejunal tissues. 5-HT and 5-HIAA were not detected in the extracellular fluid from TPH1 KO jejunal tissues. Data are mean ± S.E.M., *P < 0.05 vs. WT uric acid extracellular fluid concentration.

5-HT and 5-HIAA were not detected in fluid from TPH1 KO jejunal tissues (data not shown). 5-HT and 5-HIAA extracellular concentrations were similar to extracellular uric acid concentrations in fluid sampled from WT jejunal tissues (P > 0.05).

5.4.3 5-HT, 5-HIAA and uric acid are oxidized at similar potentials

Figure 31 shows the cyclic voltammogram of Krebs buffer, 5-HT, 5-HIAA and uric acid on a diamond microelectrode. The cyclic voltammetric E_p^{ox} of 5-HT was +0.35 V for this electrode. It is common for the E_p^{ox} of analytes to vary slightly from electrode to electrode. The cyclic voltammetric E_p^{ox} of 5-HIAA and uric acid were +0.58 and +0.61 V, respectively.

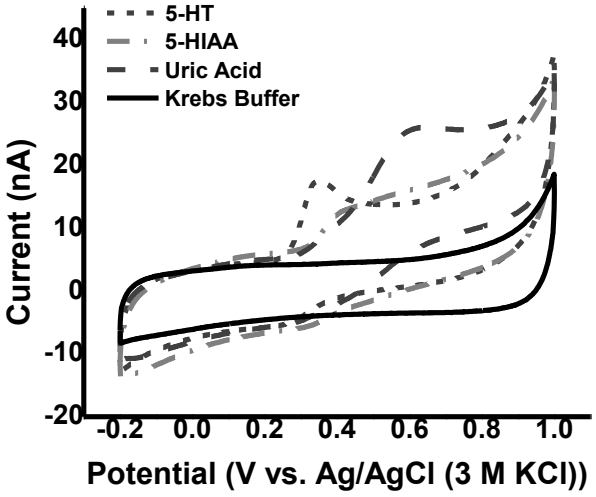

Figure 31. Cyclic voltammograms of 5-HT, 5-HIAA and uric acid at a diamond microelectrode. All analytes (10 μmol L^{-1}) were prepared in Krebs buffer (pH 7.4). The cyclic voltammetric E_p^{ox} of 5-HT (short dash dark grey), 5-HIAA (dash dot light grey) and uric acid (long dash dark grey) were 0.35, 0.58 and 0.61 V, respectively. The cyclic voltammogram of Krebs buffer is the solid black line. Cyclic voltammograms are not background subtracted. Scan rate was 0.1 V s^{-1}.

5.4.4 Tryptophan is oxidized at fixed potential used in CA measurements

Tryptophan (10 μmol L^{-1}) was oxidized ca. +1 V on a diamond microelectrode (Figure 32A) and generated current when flowing through the system used for CA experiments (Figure 32B). The oxidation current grew larger when the concentration of tryptophan (100 μmol L^{-1}) was increased and returned to baseline when replaced with flowing Krebs buffer (Figure 32B).

5.5 DISCUSSION

5.5.1 Oxidation interferences in brain electrochemistry

The problem of contributing interferences to oxidation currents was first identified in the 1980's when measuring dopamine oxidation with carbon electrodes in the brain in anesthetized rats and in brain slices.[26-28] Particularly, the measured current, assumed to be from dopamine

oxidation, was reduced to a great extent when ascorbic acid oxidase was injected near to the recording site.[28] Ascorbic acid oxidase oxidizes ascorbic acid to a non-electroactive molecule.

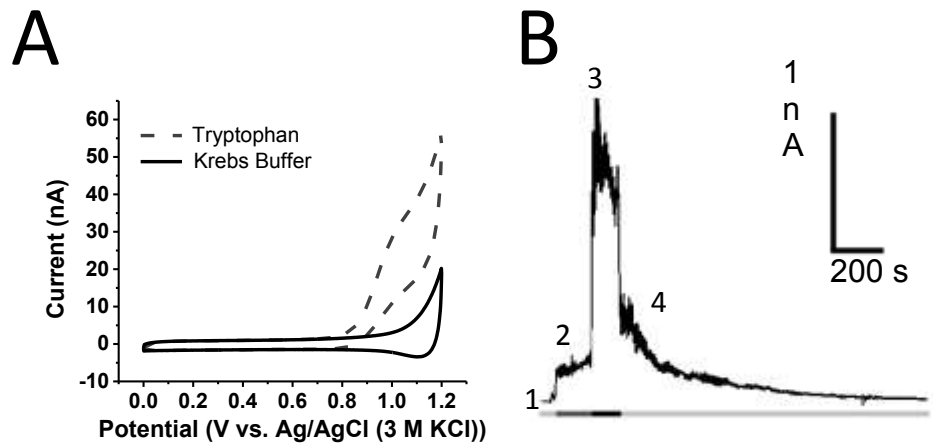

Figure 32. Oxidation of tryptophan at a diamond microelectrode. (A) Cyclic voltammogram of tryptophan (10 µmol L^{-1}) prepared in Krebs buffer (pH 7.4, solid black line). The cyclic voltammetric E_p^{ox} of tryptophan (dash dark grey) was ca. +1 V. Scan rate was 0.1 V s^{-1}. (B) An oxidation current was measured when tryptophan ((2) 10 µmol L^{-1}, dark grey line; (3) 100 µmol L^{-1}, black line) flowed continuously through the same system used for CA experiments. Krebs buffer ((1 & 4) light grey) ran through the system before and after tryptophan. Oxidation current approaches the initial baseline current when Krebs buffer flowed through the system following tryptophan. The same fixed potential applied for CA experiments (+0.855 V) was used.

Not long after, it was recognized that oxidation of uric acid confounded the oxidation peak assumed to be from indole oxidation in the striatum of anesthetized rats. For instance, as the injection of uric acid near to the working electrode increased the measured peak current, injection of uricase (0.1 - 0.2 units) reduced the peak current by 30 to 100 % using carbon fiber and carbon paste electrodes, respectively.[29, 30] Uricase is an enzyme that converts uric acid to the non-electroactive molecule allantoin. The presence of uric acid in brain tissue was confirmed using HPLC with UV detection.[30] Voltammetric measurements using carbon fiber electrodes demonstrated that the peak oxidation potentials of uric acid and ascorbic acid were similar to those of indoleamines and catecholamines.[30, 31] Hence, biogenic amine characterization by early voltammetry studies was confounded by ascorbic acid and uric acid

oxidation. To improve analyte selectivity, electrode surfaces were modified with the cation-exchange material Nafion and cyclic voltammograms were scanned at much greater speeds (e.g. 100 V s^{-1}). At physiological pH, catecholamines are cationic with protonation occurring at the amine side chain whereas ascorbic acid and uric acid are anionic. Nafion is a polyanionic electrode coating that functions to draw in cations while repelling anions. Fast scan cyclic voltammetry (FSCV) with scan rates >100 V s^{-1} can be used to generate voltammograms subtracted from the background current that reveal separate peaks for the analytes of interest (e.g. catecholamines and indoleamines) from interferences (e.g. metabolites, ascorbic acid and uric acid) because the peaks are kinetically controlled. For example, DA has much faster electron transfer kinetics at carbon fiber microelectrodes compared to DOPAC and ascorbic acid.[31] Despite knowledge of electroactive interferences in the brain, a comprehensive analysis of electroactive species present near to the gut mucosa where amperometric measurements are made has not been performed.

5.5.2 CA used to measure 5-HT release from gut mucosa

CA was first reported for the detection of 5-HT near to the gut mucosa in 2004.[1] To date most measurements are made with a carbon fiber microelectrode (CFM) (1) held at a fixed distance[22] or (2) placed in contact with the mucosa for the duration of the measurement.[5, 6] Before the birth of applying amperometry to study gut 5-HT, it was known that 5-HT oxidation caused robust electrode fouling. Studies performed by Wrona and Dryhurst showed that 5-HT oxidation was complex and generated many oxidation products[32, 33] that readily adhered to the carbon electrode surface at pH 7.2.[34] These oxidation products interact with oxygen functional groups present on sp^2-carbon surfaces.[35] To prevent CFM fouling in studies in which the electrode touched the mucosa, electrodes have been coated with Nafion.[4, 6] However, electrodes treated with Nafion require a greater time to respond to rapidly changing concentrations of 5-HT *in vitro* [36] and are still at risk for electrode fouling under *in vitro*

experimental conditions.[37] Moreover, some studies do not coat CFM with Nafion.[5, 12, 13] Diamond microelectrodes, rather than a CFM, have been employed because the material affords resistance to electrode fouling in the presence of relatively high concentrations of 5-HT.[8, 22-24] Absence of electrode fouling at diamond microelectrodes eliminated the need for any electrode pretreatment including Nafion coating. Regardless of electrode material used, often the current magnitude measured in the biological experiment is converted to a concentration.[1-3, 5, 6, 11-13] In this method, an oxidation current is measured for various standard concentrations either in an electrochemical cell or in the system used for CA biological measurements. A calibration plot is generated from these measurements and used to determine the unknown 5-HT concentration in the gut mucosa. A limitation in analyzing measurements this way is that the diffusion layer in an electrochemical cell (or the CA system) does not recapitulate the diffusion layer near to the mucosal surface.[38] The diffusion layer, described as the length of the concentration gradient, is critical to the measured current magnitude. Moreover, mucosal surface variations tissue to tissue and mucosal layer thickness likely alters the diffusion layer. It was hypothesized that this concentration gradient formed from the flux of analyte to the electrode surface contributed to the 10^3 difference in concentration measured by amperometry compared to ELISAs.[19] With the knowledge of the electroactive interferences in voltammetric brain measurements and the discrepancies in 5-HT concentration, I hypothesized that 5-HT oxidation current was confounded by other electroactive molecules present in the gut mucosa.

5.5.3 Large oxidation currents are measured in intestinal tissues from TPH1 KO mice

My first approach to determine if the current measured in amperometric measurements was mainly from 5-HT oxidation was to use intestine from mice that lacked the enzyme required for 5-HT production in the EC cell (TPH1). TPH1 KO mice show a 96% reduction in intestinal 5-HT.[17, 21] The remainder of 5-HT present is speculated to be from the enteric 5-HT stores. Despite the extremely low mucosal 5-HT concentrations, the oxidation current measured in

jejunal tissues from these mice was roughly 2/3 of that measured in intestinal tissues from WT mice. Oxidation currents measured from distal colonic tissues from TPH1 KO mice were similar in magnitude to distal colonic tissues from WT mice. I found that oxidation currents were much greater in the jejunum than in the distal colon regardless of genotype. This oxidation current gradient along the intestine was described previously.[14] The oxidation currents measured in TPH1 KO jejunal tissues were not generated from 5-HT oxidation because 5-HT was not detected in the fluid sampled close to the mucosal surface and the oxidation current was unchanged by fluoxetine and cocaine. The distance of the syringe from the mucosal surface used to sample fluid was the same distance used in CA measurements. The present results provide strong evidence that the greater majority of measured current in small and large intestine from mice is due to electroactive molecules other than 5-HT present at the gut mucosa.

5.5.4 Uric acid, 5-HIAA and tryptophan likely contribute to the oxidation current in CA measurements of 5-HT in the gut mucosa

Like the brain, ascorbic acid and uric acid are present in the mucosal layer of the intestine[39, 40] and functional transport mechanisms for uric acid excretion are present on enterocytes.[41] The extracellular fluid data demonstrate that uric acid as well as its precursors are present near to the mucosal surface. Ascorbic acid in the fluid was not measured using HPLC with electrochemical detection. The concentration of uric acid present in the fluid is similar to that of 5-HT. Since the E_p^{ox} for uric acid is below the potential used for CA experiments, uric acid oxidation contributes equally with 5-HT to the measured current. This is also true of experiments using CFM. For CFM experiments a lower fixed potential is applied (e.g. +0.4 V) compared to experiments that employ diamond microelectrodes. The difference in fixed potential is due to differences in the rate of electron transfer at CFM and diamond microelectrodes. Electron transfer rates are faster at CFM compared to diamond microelectrodes allowing the fixed potential to be smaller. Regardless, the E_p^{ox} for uric acid is

similar to the E_p^{ox} for 5-HT at CFM.[41] Thus, it is very likely that studies that use CFM not coated with Nafion are oxidizing uric acid as well as ascorbic acid. While Nafion coating may increase the sensitivity for DA, NE and 5-HT oxidation, it does not completely block the oxidation of anionic species at the electrode surface. For example, ascorbic acid and DOPAC were still detected in chronoamperometry experiments using Nafion-coated glassy carbon electrodes[42] and at Nafion-coated CFM using voltammetry.[43] Together, these results demonstrate the Nafion treatment does not fully block confounding anionic oxidation at the electrode surface. Our studies using diamond microelectrode and others using Nafion-coated or untreated CFM are likely oxidizing uric acid in CA measurements performed in gut mucosa.

Similar to uric acid, 5-HIAA and 5-HT are present at similar concentrations in the extracellular fluid sampled near to the gut mucosa from WT mice. I found that the E_p^{ox} for 5-HIAA is below the potential used for our CA experiments at diamond microelectrodes. Again, suggesting that 5-HIAA contributes equally with 5-HT to the measured oxidation current in CA experiments. Like uric acid, 5-HIAA is an anion at physiological pH and will be partially repelled by Nafion. As discussed above, it is unlikely that zero current is contributed by 5-HIAA oxidation in CA measurements using Nafion-coated electrodes. A cation that would not be repelled by Nafion is tryptophan. Tryptophan is electroactive and is likely present at the gut mucosa. In contrast to uric acid and 5-HIAA, the E_p^{ox} for tryptophan is close to 1 V at our diamond electrode. Such a positive E_p^{ox} suggests that tryptophan would not be oxidized at the potential used for CA experiments and would not contribute to the measured current. However, I measured an oxidation current when tryptophan flowed through our CA system when using the same fixed potential for CA experiments. The tryptophan oxidation current magnitude measured at +0.8 V in the cyclic voltammogram appeared negligible; however, the tryptophan oxidation current in the cyclic voltammogram and the measured current made in intestinal tissues were similar in magnitude. This evidence suggests that even though the fixed potential used for CA measurements is below that of the E_p^{ox} for tryptophan, the applied fixed potential

oxidizes tryptophan to an extent that matches the current magnitudes measured in biological experiments.

5.5.5 5-HT concentration is likely in the nM range in CA measurements

The extracellular fluid data suggests that 5-HT concentration is in the nanomolar and not the micromolar range as predicted by CA. Studies in support of a nanomolar 5-HT concentration used mathematical models to predict 5-HT release from EC cells based on *in vitro* single EC cell measurements using CA[19] and ELISAs that measure 5-HT in the media of dissociated EC cells.[15] Similar to 5-HT, concentrations of DA in the nanomolar range were observed in the extracellular fluid of rodent brains using no net flux method with microdialysis probes.[44, 45] Using the same no net flux method, extracellular fluid ascorbic acid concentrations were in the micromolar range.[46] The much smaller DA concentration compared to ascorbic acid contributed to the difficulty in isolating DA oxidation currents in brain voltammetry. It is not impossible that ascorbic acid in the intestine is in the micromolar range. Ascorbic acid is an essential vitamin and therefore must be absorbed by the intestine. Therefore, like the brain, ascorbic acid may account for some of the oxidation current in CA measurements in the gut mucosa.

5.5.6 Conclusions

The results presented herein provide evidence that oxidation currents measured in CA experiments in gut mucosa may not be exclusively attributable to 5-HT oxidation. Therefore, it is not appropriate to use a standard calibration plot to calculate the unknown 5-HT concentration in the gut mucosa. For this type of analysis, it is likely that the current is an exaggeration of the true 5-HT concentration. The discrepancies between calculated 5-HT concentrations calculated in CA experiments and those measured by ELISA are likely the result of interferences of other electroactive molecules. The results herein do not mean that using CA measurements to

understand 5-HT uptake are not appropriate. For all electrochemical techniques, pharmacological methods help assist in selectivity. CA measurements in 5-HT gut mucosa are appropriate when SSRIs are used to generate increases in oxidation current. This increase in oxidation current in the presence of a SSRI demonstrates selectivity for 5-HT. Hence, CA measurements can be used to study SERT function. In addition to using SSRIs, enzymes that target ascorbic acid and uric acid may be useful in eliminating their contribution to the current more effectively than coating the electrode with Nafion. For example, tissues could be incubated with uricase prior to CA measurements. Besides amperometry, FSCV may provide adequate selectivity to study 5-HT oxidation. In conclusion, a more targeted approach to understand amperometric measurements in gut mucosa should be made including making necessary precautions to isolate 5-HT oxidation currents. In conclusion, CA can be used to understand the function of SERT and that quantitative work relating a measured current to a local concentration should be carried out with caution.

REFERENCES

REFERENCES

1. Bertrand PP. Real-time detection of serotonin release from enterochromaffin cells of the guinea-pig ileum. Neurogastroenterol Motil 2004;16:511-4.

2. Bertrand PP. Real-time measurement of serotonin release and motility in guinea pig ileum. J Physiol 2006;577:689-704.

3. Bertrand PP, Barajas-Espinosa A, Neshat S, et al. Analysis of real-time serotonin (5-HT) availability during experimental colitis in mouse. Am J Physiol Gastrointest Liver Physiol 2010;298:G446-55.

4. Bertrand PP, Hu X, Mach J, et al. Serotonin (5-HT) release and uptake measured by real-time electrochemical techniques in the rat ileum. Am J Physiol Gastrointest Liver Physiol 2008;295:G1228-36.

5. Bertrand RL, Senadheera S, Markus I, et al. A Western diet increases serotonin availability in rat small intestine. Endocrinology 2011;152:36-47.

6. Bertrand RL, Senadheera S, Tanoto A, et al. Serotonin availability in rat colon is reduced during a Western diet model of obesity. American Journal of Physiology-Gastrointestinal and Liver Physiology 2012;303:G424-G434.

7. Bertrand PP, Paranavitane UT, Chavez C, et al. The effect of low estrogen state on serotonin transporter function in mouse hippocampus: a behavioral and electrochemical study. Brain Res 2005;1064:10-20.

8. Bian X, Patel B, Dai X, et al. High mucosal serotonin availability in neonatal guinea pig ileum is associated with low serotonin transporter expression. Gastroenterology 2007;132:2438-47.

9. Galligan JJ, Patel BA, Schneider SP, et al. Visceral hypersensitivity in female but not in male serotonin transporter knockout rats. Neurogastroenterology and Motility 2013;25:e373-e381.

10. Marcelli G, Patel BA. Understanding changes in uptake and release of serotonin from gastrointestinal tissue using a novel electroanalytical approach. Analyst 2010;135:2340-7.

11. Patel BA. Continuous amperometric detection of co-released serotonin and melatonin from the mucosa in the ileum. Analyst 2008;133:516-24.

12. Keating DJ, Spencer NJ. Release of 5-hydroxytryptamine from the mucosa is not required for the generation or propagation of colonic migrating motor complexes. Gastroenterology 2010;138:659-70 670 e1-2.

13. Spencer NJ, Nicholas SJ, Robinson L, et al. Mechanisms underlying distension-evoked peristalsis in guinea pig distal colon: is there a role for enterochromaffin cells? Am J Physiol Gastrointest Liver Physiol 2011;301:G519-27.

14. Bertrand PP, Bertrand RL. Serotonin release and uptake in the gastrointestinal tract. Auton Neurosci 2010;153:47-57.

15. Kidd M, Modlin IM, Gustafsson BI, et al. Luminal regulation of normal and neoplastic human EC cell serotonin release is mediated by bile salts, amines, tastants, and olfactants. Am J Physiol Gastrointest Liver Physiol 2008;295:G260-72.

16. Furness JB, Costa M. Neurons with 5-hydroxytryptamine-like immunoreactivity in the enteric nervous system: their projections in the guinea-pig small intestine. Neuroscience 1982;7:341-9.

17. Walther DJ, Peter JU, Bashammakh S, et al. Synthesis of serotonin by a second tryptophan hydroxylase isoform. Science 2003;299:76.

18. Nilsson O, Ahlman H, Geffard M, et al. Bipolarity of duodenal enterochromaffin cells in the rat. Cell Tissue Res 1987;248:49-54.

19. Raghupathi R, Duffield MD, Zelkas L, et al. Identification of unique release kinetics of serotonin from guinea-pig and human enterochromaffin cells. J Physiol 2013;591:5959-75.

20. Chin A, Svejda B, Gustafsson BI, et al. The role of mechanical forces and adenosine in the regulation of intestinal enterochromaffin cell serotonin secretion. Am J Physiol Gastrointest Liver Physiol 2012;302:G397-405.

21. Walther DJ, Bader M. A unique central tryptophan hydroxylase isoform. Biochem Pharmacol 2003;66:1673-80.

22. Patel BA, Bian X, Quaiserova-Mocko V, et al. In vitro continuous amperometric monitoring of 5-hydroxytryptamine release from enterochromaffin cells of the guinea pig ileum. Analyst 2007;132:41-7.

23. Zhao H, Bian X, Galligan JJ, et al. Electrochemical measurements of serotonin (5-HT) release from the guinea pig mucosa using continuous amperometry with a boron-doped diamond microelectrode. Diam Relat Mater 2010;19:182-185.

24. Park J, Show Y, Quaiserova V, et al. Diamond microelectrodes for use in biological environments. Journal of Electroanalytical Chemistry 2005;583:56-68.

25. Marcelli G, Patel BA. Theoretical modelling to understand the neurotransmission mechanism in the gastrointestinal tract. Conf Proc IEEE Eng Med Biol Soc 2008;2008:5548-51.

26. Dayton MA, Ewing AG, Wightman RM. Evaluation of amphetamine-induced in vivo electrochemical response. Eur J Pharmacol 1981;75:141-4.

27. Gonon FG, Buda MJ. Regulation of dopamine release by impulse flow and by autoreceptors as studied by in vivo voltammetry in the rat striatum. Neuroscience 1985;14:765-74.

28. Schenk JO, Miller E, Rice ME, et al. Chronoamperometry in brain slices: quantitative evaluations of in vivo electrochemistry. Brain Res 1983;277:1-8.

29. Crespi F, Sharp T, Maidment N, et al. Differential pulse voltammetry in vivo--evidence that uric acid contributes to the indole oxidation peak. Neurosci Lett 1983;43:203-7.

30. Mueller K, Palmour R, Andrews CD, et al. In vivo voltammetric evidence of production of uric acid by rat caudate. Brain Res 1985;335:231-5.

31. Kovach PM, Ewing AG, Wilson RL, et al. In vitro comparison of the selectivity of electrodes for in vivo electrochemistry. J Neurosci Methods 1984;10:215-27.

32. Wrona MZ, Dryhurst G. Oxidation Chemistry of 5-Hydroxytryptamine .2. Mechanisms and Products Formed at Millimolar Concentrations in Acidic Aqueous-Solution. Journal of Electroanalytical Chemistry 1990;278:249-267.

33. Wrona MZ, Dryhurst G. Further Insights into the Oxidation Chemistry of 5-Hydroxytryptamine. Journal of Pharmaceutical Sciences 1988;77:911-917.

34. Wrona MZ, Dryhurst G. Electrochemical Oxidation of 5-Hydroxytryptamine in Aqueous-Solution at Physiological Ph. Bioorganic Chemistry 1990;18:291-317.

35. McCreery RL. Advanced carbon electrode materials for molecular electrochemistry. Chemical Reviews 2008;108:2646-87.

36. Jackson BP, Dietz SM, Wightman RM. Fast-scan cyclic voltammetry of 5-hydroxytryptamine. Anal Chem 1995;67:1115-20.

37. Singh YS, Sawarynski LE, Michael HM, et al. Boron-Doped Diamond Microelectrodes Reveal Reduced Serotonin Uptake Rates in Lymphocytes from Adult Rhesus Monkeys Carrying the Short Allele of the 5-HTTLPR. ACS Chem Neurosci 2010;1:49-64.

38. Michael DJ, Wightman RM. Electrochemical monitoring of biogenic amine neurotransmission in real time. J Pharm Biomed Anal 1999;19:33-46.

39. Oelrichs BA, Kratzing CC. Effect of barbiturate on the distribution of ascorbic acid in the gastrointestinal tract. Biochem Pharmacol 1980;29:1839-41.

40. Oelrichs BA, Kratzing CC. Ascorbic acid in intestinal tissues. Aust J Exp Biol Med Sci 1980;58:515-20.

41. Hosomi A, Nakanishi T, Fujita T, et al. Extra-renal elimination of uric acid via intestinal efflux transporter BCRP/ABCG2. PLoS One 2012;7:e30456.

42. Gerhardt GA, Oke AF, Nagy G, et al. Nafion-coated electrodes with high selectivity for CNS electrochemistry. Brain Res 1984;290:390-5.

43. Wiedemann DJ, Basse-Tomusk A, Wilson RL, et al. Interference by DOPAC and ascorbate during attempts to measure drug-induced changes in neostriatal dopamine with Nafion-coated, carbon-fiber electrodes. J Neurosci Methods 1990;35:9-18.

44. Birbeck JA, Khalid M, Mathews TA. Potentiated striatal dopamine release leads to hyperdopaminergia in female brain-derived neurotrophic factor heterozygous mice. ACS Chem Neurosci 2014;5:275-81.

45. Bosse KE, Maina FK, Birbeck JA, et al. Aberrant striatal dopamine transmitter dynamics in brain-derived neurotrophic factor-deficient mice. J Neurochem 2012;120:385-95.

46. Miele M, Fillenz M. In vivo determination of extracellular brain ascorbate. J Neurosci Methods 1996;70:15-9.

CHAPTER 6

CONCLUSIONS, SIGNIFICANCE AND FUTURE DIRECTIONS

6.1 CONCLUSIONS

GI motility is regulated by many factors. I investigated the roles of the BK channel and 5-HT in GI motility in health and DIO. Novel to this work were the observations of sex differences in GI transit and in the effects of DIO on intestinal 5-HT. Lastly, through careful analysis of 5-HT oxidation currents in CA measurements used to understand intestinal 5-HT concentration dynamics, I provide evidence for the presence of electroactive substances in addition to 5-HT from the intestinal mucosa.

6.1.1 BK channels are necessary for propulsion in the distal colon in normal mice

I demonstrated that elimination of the β1-subunit of the BK channel causes functional impairments in propulsion in the distal colon, but not the small intestine or the proximal colon. *In vivo* studies showed that β1-subunit KO mice had reduced pellet output and longer bead expulsion times. Our *in vitro* data demonstrated a heightened sensitivity to the muscarinic agonist bethanechol in the distal colon of β1-subunit KO mice compared to WT distal colon. In addition, impaired CMMC coordination in β1-subunit KO excised colons was observed as a greater number of contractions first occurring in the oral end before the aboral end compared to WT distal colons. Our overall conclusion was that smooth muscle cells in the distal colon were hyperexcitable due to the absence of the β1-subunit such that any stimulus-driven muscle contraction would occur to a greater extent than in WT. This is because the BK channel sensitivity to intracellular Ca^{2+} is dampened by the loss of the β1-subunit so K^+ efflux presented as STOCs occurs less often. Since less K^+ leaves the cell, the membrane potential remains at a more depolarized state thereby increasing smooth muscle cell excitability. This is illustrated in Figure 33.

The present study reveals a prominent role for the BK channel in the distal colon. The function of the distal colon is to store feces and to do so the muscle must be at a relaxed state to accommodate large luminal volumes. Loss of the β1-subunit results in increased smooth

muscle tone thereby causing constipation. I propose that β1-subunit KO mice are a model of slow transit constipation in humans. To date, there is no evidence that BK channel dysfunction exists in the human colon.

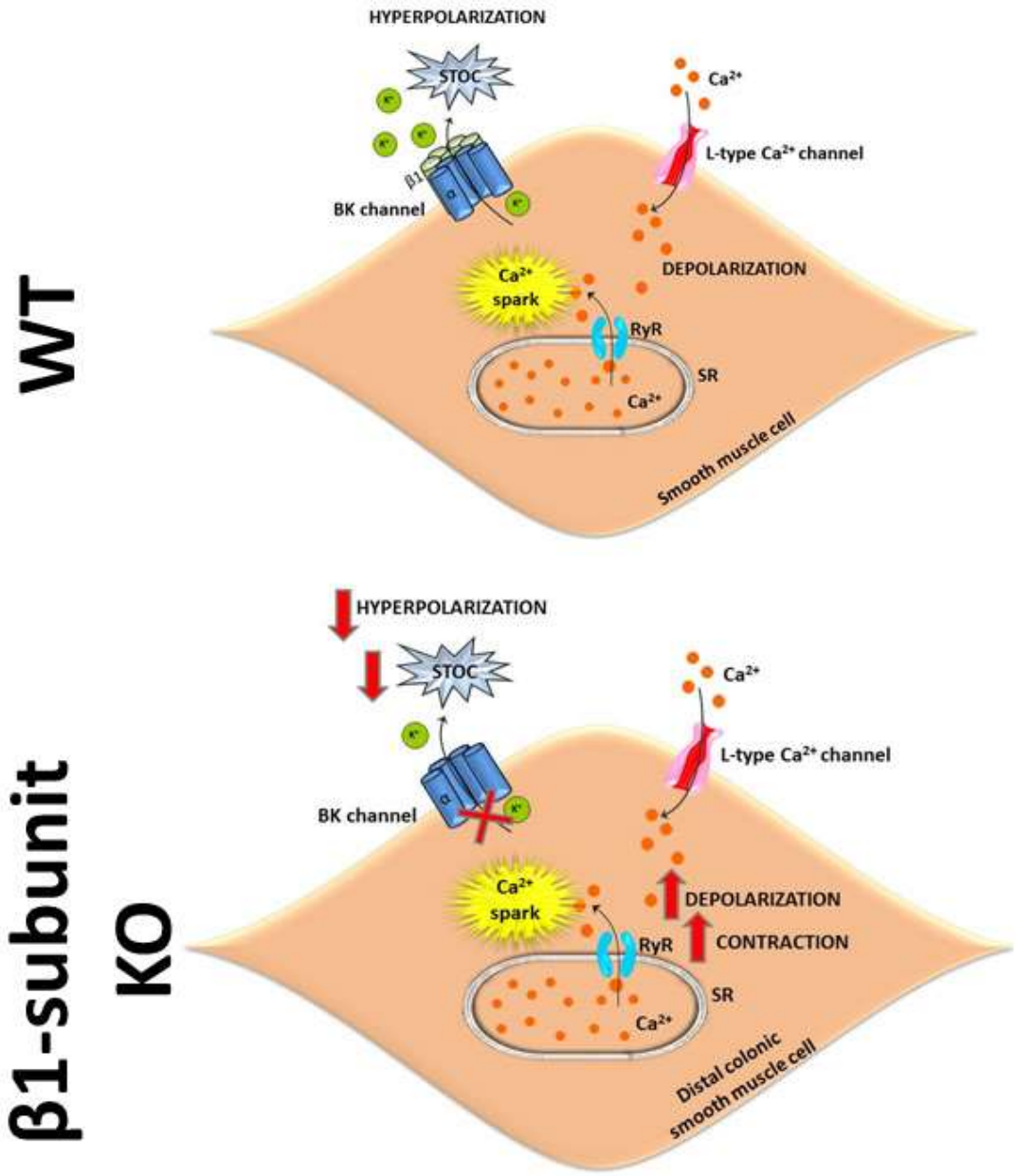

Figure 33. BK channel function in distal colonic smooth muscle cells in WT and β1-subunit KO mice. Normal smooth muscle hyperpolarization occurs due to BK channel function. Smooth muscle cells from β1-subunit KO mice are hyperexcitable from the loss of the β1-subunit.

6.1.2 A HFD in DIO differentially affects 5-HT and GI motility in male and female mice

In this work, I demonstrated that DIO affects small intestinal transit in male, but not female HFD-fed mice. Moreover, DIO impaired jejunal SERT function in male, but not female HFD-fed mice. In male HFD-fed mice, impaired SERT function likely generated greater local 5-HT concentrations that, once reached a concentration threshold, were cleared by the low affinity transporter DAT. Novel to this work is the identification of DAT in the lamina propria and along the apical border of enterocytes. In contrast, female HFD-fed mice had greater SERT protein levels compared to CD-fed female mice. SERT protein was likely functional at the plasma membrane because HFD-fed female jejunum was sensitive to fluoxetine, had decreased extracellular 5-HT and increased whole tissue 5-HIAA levels. Based on these results, male HFD-fed jejunum had increased 5-HT availability while female HFD-fed jejunum had decreased 5-HT availability. While I could not directly measure local 5-HT concentrations due to the lack of specificity in amperometry experiments, I can predict changes in local 5-HT concentrations by the function and protein availability of SERT.

I found that DIO did not alter the number of EC cells or the whole tissue 5-HT concentrations. This is in contrast with previous reports that a Western diet-fed rat had increased EC cell numbers and 5-HT concentrations.[1] These discrepancies are likely the result of a combination of DIO model, species and intestine region. Moreover, these authors quantified the 5-HT concentration using amperometry. I found that the fixed potential used in amperometry allowed for the oxidization of 5-HIAA, uric acid and tryptophan, in addition to 5-HT. Therefore, amperometry without the use of pharmacological methods cannot be used to quantify mucosal 5-HT concentrations. Moreover, my studies using TPH1 KO intestine demonstrate that the greater majority of measured current is not due to 5-HT oxidation.

I hypothesized that any change in 5-HT availability would result in small intestinal transit changes. In male HDF-fed mice, an increase in 5-HT availability caused by impaired SERT function would then increase 5-HT_3 receptor activation, increase IPAN activation and ultimately

lead to increased muscle contraction. I did not investigate this entire pathway. I did find that 5-HT_3 receptor function was not altered in male or female HFD-fed mice. I demonstrated that the GC and transit pattern of male HFD-fed mice differ from CD-fed male mice and revealed that intestinal transit was increased in male HFD-fed mice. Transit patterns described in the fraction of fluorescence vs. segment number plot resemble what is described in the literature as the interdigestive MMC.[2, 3] The pattern of FITC-dextran in CD-fed males is consistent with a bolus being propelled by a phase III migrating contraction wave. While I did not directly measure MMCs, I can speculate that DIO likely affects the MMC pattern based on the fluorescence vs. segment number plots. I predict that this increase in local 5-HT concentrations in HFD-fed males resulted in faster transit given evidence that increasing exogenous 5-HT concentrations (10-20 nmol/kg/min) shortened the interval of phase III contraction occurrences[4] such that a greater number of phase III contraction occurrences would propel FITC-dextran much quicker. Moreover, the bimodal curve in the HFD-fed males may also be explained by a shortened MMC cycle length.

In female HFD-fed mice, I saw the opposite; greater functional SERT protein levels decreased 5-HT availability. I would then predict based on the predictions in male HFD-fed mice that a decrease in 5-HT availability would then decrease 5-HT_3 receptor activation, decrease IPAN activation and ultimately lead to slower intestinal transit. However, this prediction is likely more complicated. For example, female CD-fed mice have greater extracellular 5-HT levels compared to HFD-fed females. Normally occurring greater 5-HT concentrations in CD-fed female mice would generate a desensitized state such that 5-HT_3 receptors are not activated to the same extent as they would when exposed to reduced 5-HT concentrations. The present data suggest that this is true. For example, I observed diminished 5-HT-dependent increases in longitudinal muscle contraction at 5-HT_3 receptor activating doses in female CD-fed mice. It is likely that a normal desensitized state in CD-fed females driven by greater 5-HT levels is lost in the females fed a HFD. Greater 5-HT sensitivity in HFD-fed

females may arise from reduced extracellular 5-HT levels that are driven by greater SERT levels compared to CD-fed females. This was observed in our organ bath studies where 5-HT produced greater contraction amplitudes in HFD-fed compared to CD-fed females at 5-HT concentrations that would activate 5-HT_3 receptors. With increased sensitivity to 5-HT in female HFD-fed mice, it is possible that the MMC is disrupted. For example, greater exogenous concentrations of 5-HT (40 nmol/kg/min)[4] or the 5-HT precursor, 5-hydroxytryptophan (5-HTP; 4-8 mg/kg),[5] resulted in a loss of coordinated MMC. In my study, the increase in 5-HT sensitivity in HFD-fed females likely mirrors what is observed with greater concentrations of 5-HT or 5-HTP. This prediction for HFD-fed females is visualized in the fraction of fluorescence vs. segment number plot where the FITC-dextran distribution was more uniform along the entire length of the small intestine suggesting that phase III episodes were either absent or occurred less frequently.

I predicted that this difference in transit where MMC is likely disrupted in HFD-fed females and shortened in HFD-fed males occurs from differences in 5-HT levels. The present results demonstrate that females have roughly 2 times greater whole-tissue 5-HT levels compared to males that could translate to greater 5-HT being released. With the methods used in this study, I was not able to directly measure 5-HT release. In the studies described previously,[4, 5] increasing exogenous 5-HT and 5-HTP levels shortened the MMC by decreasing the interval of phase III contractions, but when 5-HT and 5-HTP concentrations were doubled, the MMC was disrupted. My predictions for how a HFD differentially affects 5-HT and GI motility in male and female mice are illustrated in Figure 34.

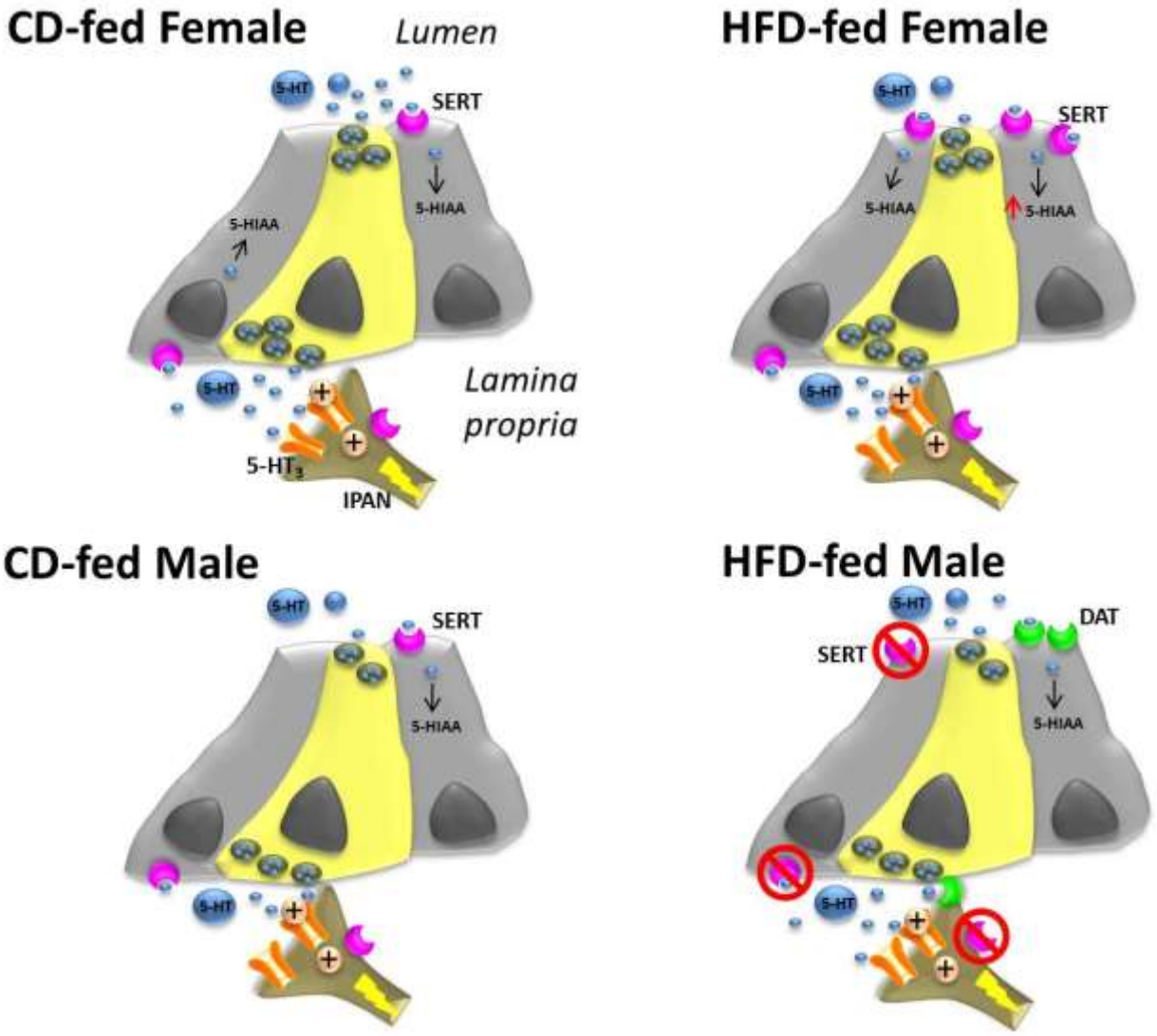

Figure 34. Proposed DIO effects on jejunal 5-HT dynamics in CD-fed and HFD-fed male and female mice. HFD affects SERT function in a sex-dependent manner that leads to differences in local 5-HT levels. Differences in local 5-HT levels influence 5-HT_3 receptor activation and ultimately small intestinal transit. Sex differences exist in 5-HT levels in the EC cell and likely contribute to the changes in transit between males and females.

The foundation for all of my predictions is that mucosal 5-HT is necessary for GI dysfunction in DIO. However, the transit studies performed in TPH1 KO mice suggest that mucosal 5-HT is not necessary for small intestinal transit. This evidence was demonstrated by similar GC and transit patterns in the fraction of fluorescence vs. segment number plot in TPH1 KO and WT littermates. My results are in agreement with those of Li and colleagues.[6] This

result suggests that mucosal 5-HT is not directly involved with the initiation of reflexes necessary for transit. However, mucosal 5-HT can greatly influence the mechanisms governing transit when 1) the intestine is more sensitive to 5-HT as in HFD-fed females and 2) the local 5-HT concentrations are increased as in HFD-fed males. As discussed previously, there is an ongoing controversy about the necessity for 5-HT in propulsive motility. Smith and colleagues argue that mucosal 5-HT is essential in propulsive MMCs[7] whereas Spencer and colleagues provide evidence that mucosal 5-HT is not necessary for propulsive MMCs, but the lack of mucosal 5-HT decreased MMC frequency.[8] Hence, mucosal 5-HT may not be essential in propulsive MMC generation, but may be necessary in the regulation of normally propagating MMCs. My data are in line with this general hypothesis.

Similar to mucosal whole tissue levels, whole tissue LMMP/SP 5-HT and 5-HIAA levels were similar in HFD-fed and CD-fed mice. These results suggest that there was no major loss of neuronal 5-HT in DIO.

6.2 SIGNIFICANCE

6.2.1 Sex differences in 5-HT and alosetron sensitivity

The significance of my work is revealed in the sex differences both in CD-fed mice and in HFD-dependent DIO effects. The major goal of this work was to identify existing sex differences in the intestinal serotonergic system.

My study is the first to offer a comprehensive study of the intestinal 5-HT system in female mice. In striking contrast to males fed a HFD, SERT remained functional in females where SERT function was impaired in males. In addition, I found that CD-fed females had greater whole tissue 5-HT levels and EC cell numbers compared to CD-fed males. A functional consequence of greater 5-HT in females was likely the observed increased transit compared to CD-fed males.

Alosetron decreased GI transit only in female CD-fed mice. Alosetron sensitivity observed only in females mimics what is seen in clinical research where alosetron provides adequate relief of IBS symptoms including a decrease in transit in women patients.[9] Similar to our study, Bush and colleagues demonstrated *in vitro* that female mouse ileum was more sensitive to alosetron-dependent decreases in the frequency of the MMC compared to male mouse ileum.[10] Together, this result suggests that alosetron in females, but not males, may be an adequate treatment of intestinal dysmotility in obesity.

My results suggest that sex hormones likely modulate the intestinal serotonergic system. These results are relevant to therapeutic approaches to treat GI disorders. Future therapeutic approaches that target the serotonergic system to treat intestinal dysfunctions should be more personalized with consideration of sex and weight.

6.3 FUTURE DIRECTIONS

6.3.1 SERT expression and function

The present results suggest that jejunal SERT function is impaired in HFD-fed males, but not HFD-fed females. I concluded this based on my fluoxetine CA studies. However, it may be that HFD-fed males are insensitive to fluoxetine, but sensitive to other SSRIs. The conclusion that SERT is dysfunctional can be strengthened by using several SSRIs in the CA studies. However, I've found that citalopram could not be easily washed from the tissue and paroxetine was not water soluble. In addition, SERT function can be addressed using the [^{3}H] 5-HT radioligand to more directly assess SERT function. The idea is less [^{3}H] 5-HT will be taken up in HFD-fed male tissues compared to CD-fed male tissues and similar [^{3}H] 5-HT will be taken up in HFD-fed female compared to CD-fed female tissues.

The mechanisms underlying SERT dysfunction in HFD-fed males and increased SERT protein in HFD-fed females need to be identified. In HFD-fed males, the change in SERT function independent of total protein levels could result from changes in SERT plasma

membrane surface expression or protein activity. For example, in the HFD-fed male more SERT may be phosphorylated (e.g. by PKC/PKG) internalized and sequestered in endosomes/secretory granules[11] such that less protein is available at the plasma membrane. Secondly, it is also possible that in HFD-fed male jejunum, SERT remains present at the plasma membrane but is rendered inactive independent of internalization. For example, the inflammatory cytokines interferon gamma (IFNɣ) and tumor necrosis factor alpha (TNFα) decreased SERT function in a human intestinal epithelial cell line.[12] Greater SERT protein levels were observed in HFD-fed female jejunum compared to CD-fed females. Here, SERT may not be internalized in HFD-fed females since SERT was sensitive to fluoxetine and extracellular 5-HT levels were reduced. To understand the location of SERT in HFD-fed males and females, we could use confocal microscopy in conjunction with apical border markers such as villin. To identify mechanisms underlying SERT regulation, we would remove gonadal hormones by gonadectomy to determine if sex hormones play a role is this observed sex difference.

The present results demonstrate that jejunal SERT protein levels were increased in HFD-fed compared to CD-fed female mice. It is possible the increase in SERT protein levels is a result of increased enterocyte number. Pilot studies suggested that villus height was similar between males and females regardless of diet. A better approach to address this question would be to count the number of enterocytes per villus.

6.3.2 Obesity or HFD-dependent effects?

The present results demonstrate differences in HFD-fed mice that develop obesity. However, these results do not clarify whether the results obtained are caused by the HFD or by obesity. To investigate this, a number of experiments can be performed. For example, we can feed animals the HFD for a shorter length of time where BW is similar between HFD-fed and CD-fed groups and then determine if these differences between the HFD-fed and CD-fed

groups exist. Secondly, we can feed animals as we did in the present studies, but then allow the HFD-fed mice exercise (e.g. running wheel) so that their BW is similar to CD-fed mice yet they remain on the HFD. The idea here is that if HF feeding is crucial to these differences, the differences will be observed when the HFD is continued in the HFD-fed group despite similar BW compared to CD-fed mice. If the obesity phenotype is essential in the observed differences, then the differences will be absent when BW is normalized to CD-fed mice despite the continuation of the HFD.

6.3.3 Causes of sex differences in CD-fed mice

The goal of this work was to identify sex differences and so one of the future directions would be to address why these sex differences occur specifically in CD-fed mice. The main sex differences between CD-fed female and male mice were females had greater EC cell number, whole tissue and extracellular 5-HT levels. In these studies, female mice were not staged and so the observed sex differences may be dependent on female hormonal cyclicity. As suggested by McCarthy and colleagues, cycle stage dependence can be identified if the intragroup variability in females is greater than males.[13] Computing the variance for male and female mice showed that the variance in females was 10-fold greater but was only observed in the extracellular 5-HT levels. This suggests that female cycle may be important in 5-HT release. Moreover, the variance in females was 10-fold greater compared males in 5-HT uptake and SERT/LDH, despite similar means. Together, it is likely that female hormonal cyclicity is important in the intestinal 5-HT system. Therefore, the first step would be to determine the role of gonadal hormones in the adult mice. To do this, mice would be placed on diets at weaning and gonadectomized in adulthood (e.g. 14 wks of age). Following, hormonal replacement would be performed during continuation of respective diets. In this experiment, comparisons between mice with and without hormone replacement will be made. The goal of this study would be to

identify if gonadal hormones in adulthood are necessary for the observed sex differences and if so, which gonadal hormones.

6.3.4 Gonadal hormone role in HFD-fed female mice

As mentioned in the paragraph above, the intragroup variability was greater in CD-fed females than males in extracellular 5-HT, 5-HT uptake and the ratio of SERT/LDH. However, the greater intragroup variability was lost in the HFD-fed females and was similar to CD-fed males. This suggests that if female hormonal cyclicity is important, this importance is lost when females are fed the HFD. It has been demonstrated that irregular cyclicity was observed in DIO rats.[14] However, the steady state plasma levels of estradiol and progesterone were similar in the present study. This same result was demonstrated by Haslam and colleagues using a very similar mouse model.[15] Haslam and colleagues determined that the HFD-fed females were less responsive to estradiol effects. Thus, an appropriate next step in our research would be to determine if the HFD-fed females are less responsive to gonadal hormones. The study suggested in the paragraph above would first identify if gonadal hormones modulate the intestinal serotonergic system and specifically what parts of the system are influenced by what gonadal hormones. For example, if estradiol was important in modulating extracellular 5-HT levels, ovariectomized control and HFD-fed females would have similar extracellular levels. With estradiol administration to ovariectomized CD-fed and HFD-fed females, extracellular levels would increase in control but not HFD-fed females. This result would suggest that HFD-fed females are less responsive to estradiol effects on extracellular 5-HT levels. In obese women patients, menstrual cycle irregularities and ovulation disorders are more prevalent than in lean women patients.[16, 17]

6.3.5 Targeted approach for inflammation

The analysis of TNFα in mucosal scrapes was inconclusive. This is likely the result of low TNFα protein in the mucosal layer. To gain a better understanding of TNFα levels in the intestine, the next step would be to measure TNFα levels in the entire intestine. In addition, we need a more targeted approach to study 5-HT role in intestinal inflammation. Instead of investigating the role of one inflammatory maker we can focus on a few. A second inflammatory marker we could focus on is IL-12p40. For example, when mucosal 5-HT was absent in TPH1 KO mice treated with dextran sulfate sodium (DSS) to induce colitis, dendritic cell culture supernatant contained significantly less of the proinflammatory mediator, IL-12p40, compared to WT.[18] Further, exogenous 5-HT addition to naïve dendritic cells obtained from TPH 1 KO mice significantly up-regulated IL-12p40 production.[18] Intestinal IL-12p40 levels are elevated in DIO.[19] Therefore, by investigating TNFα and IL-12p40 levels, we can address more thoroughly the role of mucosal 5-HT in intestinal inflammation in DIO.

REFERENCES

REFERENCES

1. Bertrand RL, Senadheera S, Markus I, et al. A Western diet increases serotonin availability in rat small intestine. Endocrinology 2011;152:36-47.

2. Takahashi T. Mechanism of interdigestive migrating motor complex. J Neurogastroenterol Motil 2012;18:246-57.

3. Romanski KW. Migrating motor complex in biological sciences: characterization, animal models and disturbances. Indian J Exp Biol 2009;47:229-44.

4. Lordal M, Hellstrom PM. Serotonin stimulates migrating myoelectric complex via 5-HT3-receptors dependent on cholinergic pathways in rat small intestine. Neurogastroenterol Motil 1999;11:1-10.

5. Sagrada A, Brancaccio N, Schiavone A. 5-Hydroxytryptamine affects rat migrating myoelectric complexes through different receptor subtypes: evidence from 5-hydroxytryptophan administration. Life Sci 1990;46:1207-16.

6. Li Z, Chalazonitis A, Huang YY, et al. Essential roles of enteric neuronal serotonin in gastrointestinal motility and the development/survival of enteric dopaminergic neurons. J Neurosci 2011;31:8998-9009.

7. Heredia DJ, Dickson EJ, Bayguinov PO, et al. Localized release of serotonin (5-hydroxytryptamine) by a fecal pellet regulates migrating motor complexes in murine colon. Gastroenterology 2009;136:1328-38.

8. Keating DJ, Spencer NJ. Release of 5-hydroxytryptamine from the mucosa is not required for the generation or propagation of colonic migrating motor complexes. Gastroenterology 2010;138:659-70 670 e1-2.

9. Viramontes BE, Camilleri M, McKinzie S, et al. Gender-related differences in slowing colonic transit by a 5-HT3 antagonist in subjects with diarrhea-predominant irritable bowel syndrome. Am J Gastroenterol 2001;96:2671-6.

10. Bush TG, Spencer NJ, Watters N, et al. Effects of alosetron on spontaneous migrating motor complexes in murine small and large bowel in vitro. Am J Physiol Gastrointest Liver Physiol 2001;281:G974-83.

11. Blakely RD, Ramamoorthy S, Schroeter S, et al. Regulated phosphorylation and trafficking of antidepressant-sensitive serotonin transporter proteins. Biol Psychiatry 1998;44:169-78.

12. Foley KF, Pantano C, Ciolino A, et al. IFN-gamma and TNF-alpha decrease serotonin transporter function and expression in Caco2 cells. Am J Physiol Gastrointest Liver Physiol 2007;292:G779-84.

13. McCarthy MM, Arnold AP, Ball GF, et al. Sex differences in the brain: the not so inconvenient truth. J Neurosci 2012;32:2241-7.

14. Balasubramanian P, Jagannathan L, Mahaley RE, et al. High fat diet affects reproductive functions in female diet-induced obese and dietary resistant rats. J Neuroendocrinol 2012;24:748-55.

15. Olson LK, Tan Y, Zhao Y, et al. Pubertal exposure to high fat diet causes mouse strain-dependent alterations in mammary gland development and estrogen responsiveness. Int J Obes (Lond) 2010;34:1415-26.

16. Castillo-Martinez L, Lopez-Alvarenga JC, Villa AR, et al. Menstrual cycle length disorders in 18- to 40-y-old obese women. Nutrition 2003;19:317-20.

17. Wilkes S, Murdoch A. Obesity and female fertility: a primary care perspective. J Fam Plann Reprod Health Care 2009;35:181-5.

18. Li N, Ghia JE, Wang H, et al. Serotonin activates dendritic cell function in the context of gut inflammation. Am J Pathol 2011;178:662-71.

19. Li H, Lelliott C, Hakansson P, et al. Intestinal, adipose, and liver inflammation in diet-induced obese mice. Metabolism 2008;57:1704-10.